The Effect of Mesenchymal Stromal Cells, Platelet-Rich Plasma, and Collagen on Rat Achilles Tendon Repair

By

Dragan Juzbasich

Submitted in Partial Fulfillment of the Requirements

for the Degree of

Master of Science

in the Biological Sciences

Youngstown State University

December 2021

The Effect of Mesenchymal Stromal Cells, Platelet-Rich Plasma, and Collagen on Rat Achilles Tendon Repair

Dragan Juzbasich

I hereby release this thesis to the public. I understand that this thesis will be made available from the OhioLINK ETD Center and the Maag Library Circulation Desk for public access. I also authorize the University or other individuals to make copies of this thesis as needed for scholarly research.

Signature:

_____

Dragan Juzbasich, Master's Student Date

Approvals:

_____

Dr. Diana L. Fagan, Thesis Advisor Date

_____

Dr. Gary R. Walker, Committee Member Date

_____

Dr. Carmen Panaitof, Committee Member Date

_____

Dr. Salvatore A. Sanders, Dean of Graduate Studies Date

Abstract

The calcaneal (Achilles) tendon is capable of handling tremendous tensile loads during locomotion. However, cases of Achilles tendon ruptures have increased in recent years, requiring long healing times. Repaired tendons are more prone to re-rupture after healing, which may negatively impact patient quality of life. Thus, there exists a need for new methods of treatment aimed to improve and accelerate tendon healing. We studied the effect a combination of collagen, platelet-rich plasma (PRP), and mesenchymal stromal cells (MSC) on healing a complete Achilles tendon rupture in a Lewis rat model. The PRP was produced from rat blood collected during exsanguination procedures. MSCs from rat bone marrow met the criteria to be considered stem cells in a rat model, as they were seen to be plastic adherent and capable of tri-lineage differentiation. Rupture was surgically simulated by a full-thickness transection of the tendon, followed by surgical repair. All treatments included a strip of CollaTape™ wrapped around the repair, acting as a vehicle for the biologics prior to closure of the wound. A single, 100µL subcutaneous injection of MSCs, PRP, or both were administered adjacent to the incision and assigned 1- or 2-week recovery periods before harvesting the operated and unoperated tendons. We observed promising trends which show an increase in gene expression activity in the treated tendons and differences in the expression of Col1a1 and Col3a1 which align with our predicted response to the treatments. However, due to contamination of the GAPDH RT-PCR results, the collagen analysis results remain inconclusive. The biomechanical properties of the tendons were determined using force-extension analysis. When normalized as a percent of the unoperated tendon, a significant improvement was seen in the strain at failure and in ultimate tensile strength after only one week of recovery in the rats who received any biological treatments used in this study, when compared to a surgical control. Compared to the vehicle control, using all three biologics together shows a significant improvement over adding just MSCs or PRP alone. These results suggest that this treatment yields an accelerated healing response and may reduce occurrence of re-rupture after healing.

Acknowledgement

I would like to express my immense gratitude to my thesis advisor and mentor, Dr. Diana Fagan, for allowing me to pursue this project, which felt less like a thesis research assignment, but for me, felt more like a passion project since day one. It was worth every early morning, late night, weekend, and over-night stay invested the lab. Words cannot express my thanks or appreciation for sharing your invaluable advice, expertise, and skills. Your patience and encouragement have allowed me to develop confidence in the lab and my research skills, providing a strong foundation for me to build upon throughout life. I would like to thank my committee members, Dr. Gary Walker and Dr. Carmen Panaitof, for agreeing to take part in the project and providing useful insights while planning our collagen analysis. To Thywill Ettey and Brittany Austin, thank you both so much for allowing me to become so deeply invested in the work while I was an undergrad and laying the foundation for the project I would later continue. I'd like to thank Dr. Stewart Drew for his work performing the surgeries for our project and for his insightful conversations. To Errek Pham (or "the machine" as I call him), I cannot thank you enough for all of your assistance with the surgeries, your (almost machine-like) efficiency during harvests, perfecting the office coffee, but above all, thank you for your friendship and the lasting memories. Thank you to Dr. Hazel Marie, Nancy Boulos, Jack Farrell, Jane Casto, Megan McCloskey, and the Department of Mechanical Engineering at YSU for performing the biomechanical testing. From the Department of Biological Sciences faculty at YSU, I'd like to thank Dr. Caguiat for allowing me to use your lab, and whose guidance was instrumental in performing, optimizing, and interpreting the collagen analysis results. Also, thank you Dr. Butcher, for sharing your insights and expertise in biomechanics which aided in interpreting the tensile testing data. To my peers as an undergrad (Jared Vanasdale, Katie Platt) and the students who helped with the project (Vi-Trinh Luu, Chris Economus, Georgia Weatherman, and the others), I'd like to say thank you all for your valued work. Finally, I'd like to give special thanks to friends (Jordan Fain, Andrew Zack, Issac "Ike" Gadzekpo, Alex Huber) for a memorable time here at YSU and to my family for their loving support.

Table of Contents

List of Abbreviations

Ag - Antigen

Ang-1 – Angiopoietin 1

ANOVA – Analysis of Variance

bFGF – Basic Fibroblast Growth Factor

BLAST – Basic Local Alignment Sequencing Tool

bp – Base Pairs

CD – Cluster of Differentiation

cDNA – Complementary Deoxyribonucleic Acid

Col – CollaTape ("Collagen Only" when referring to study group)

Col1a1 – Collagen Type I α-Chain 1

Col3a1 – Collagen Type III α-Chain 1

CSA – Cross-Sectional Area

DMSO – Dimethyl Sulfoxide

ECM – Extracellular Matrix

EDTA – Ethylenediaminetetraacetic acid

EtOH – Ethanol

FCS – Fetal Calf Serum

g – gravitational acceleration

GAPDH – Glyceraldehyde 3-Phosphate Dehydrogenase

IGF – Insulin-Like Growth Factor

IL – Interleukin

ISCT – International Society for Cellular Therapy

MCL – Medial Collateral Ligament

MEM – Minimal Essential Media

MHC – Major Histocompatibility Complex

MMP – Metalloproteinase

mRNA – Messenger Ribonucleic Acid

MSC – Mesenchymal Stromal/Stem cell

NCBI – National Center for Biotechnology Information

NF-H_2O – Nuclease-Free Water

PBS – Phosphate Buffered Saline

PCR – Polymerase Chain Reaction

PDGF – Platelet-Derived Growth Factor

PPP – Platelet-Poor Plasma

PRP – Platelet-Rich Plasma

RefSeq – Reference Sequence

rER – Rough Endoplasmic Reticulum

RT-PCR – Reverse-Transcriptase Polymerase Chain Reaction

TBE – Tris-Borate-EDTA

TGF-β – Transforming Growth Factor β

TIMP – Tissue Inhibitor of Metalloproteinases

UTS – Ultimate Tensile Strength

VEGF – Vascular Endothelium Growth Factor

"X" – RT-PCR Control (Collagen Analysis)

List of Figures

List of Tables

Introduction:

The calcaneal tendon, otherwise known as the Achilles tendon, serves to transmit the forces generated by the muscles of the posterior lower leg to the heel of the foot, making it a key component of the musculoskeletal system, due to its involvement in locomotion. However, the frequency of rupture of this tendon is increasing, often requiring long healing times with varying rates of re-rupture based upon treatment. Due to the impact on the quality of life of patients who experience Achilles tendon rupture, as well as the large annual healthcare cost of treating the injury, it is of great interest to develop impactful therapeutic treatments that can be used in combination with the current methods of treating tendon injuries that can both accelerate and improve the healing quality. Currently, research has been conducted on the use of biologics such as collagen scaffolding, platelet-rich plasma, and stem cell therapies to accelerate and improve the healing of ruptured tendons. Promising results have been observed in the use of one, or a combination of two of the previously mentioned biologics and are being considered for use in clinical settings. However, little is known about how a combination of all three of these biologics will affect the healing of Achilles tendon ruptures. Identifying the effect of using a combination of collagen, platelet-rich plasma, and mesenchymal stromal cells may show further improvement to the healing rate and quality of ruptured Achilles tendons.

Problem – Rupture of the Achilles/Calcaneal Tendon

Tearing or rupture of the calcaneal tendon, also known as the Achilles tendon, accounts for 35% of all tendon injuries (Chiodo at al. 2006, Yuksel et al, 2016). According to recent reports, the occurrence of rupture of the Achilles tendon has been increasing in frequency, being seen by orthopedists in 18 of every 100,000 patients annually (Chiodo et al. 2006, Aktas et

al. 2016, Yuksel et al. 2016, Shamrock and Varacallo 2020). Patients who experience tendon rupture present with significant pain, localized edema caused by inflammation, and the formation of a hematoma around the posterior ankle near the site of the damaged tendon as common clinical symptoms (Zabrynski et al. 2018). These symptoms result in severely reduced or complete loss of mobilization of the ankle joint as well as hindering an individual's ability to bear weight on the affected lower limb. Due to the structure of tendons, in order to properly heal the damaged tendon requires long recovery times. In addition, this healing of the tendon is often limited due to the healing ability of the tendon itself. In almost all cases, the biomechanical properties of the healed tendon are not optimal compared to that of an uninjured tendon. The sub-optimal healing leads to reduced strength and stiffening of the tendon, which not only makes the tendon more susceptible to re-rupture (Schneider et al. 2018) but can potentially have a negative impact on an individual's quality of life. There are many extrinsic and intrinsic factors that may cause rupture of the Achilles tendon. The most common causes are factors such as age and sports-related activities. Achilles tears are more frequently seen in male patients between 30 and 50 years of age and athletes (Yuksel et al. 2016, Schneider et al. 2018, Zabrynski et al. 2018). Part of the reason that an increase in the occurrence of Achilles tendon rupture is occurring is because the world's population of elderly individuals is increasing, and many in this population are choosing to continue an active lifestyle. The age of an individual plays a large part in the structure and mechanical properties of tendons. As we age, degenerative changes in collagen and changes the non-collagen components of the tendons such as in the extracellular matrix, the cells within the extracellular called tenocytes (Cury et al., 2016), and changes in gene expression (Kostrominova and Brooks 2013, Zabrynski et al. 2018) are seen. In addition, the accumulation of microinjuries that we experience throughout life, and the subsequent healing of those microinjuries, progressively serve to further weaken

the tendon structure. With increased age, tendons become susceptible to tendon injuries (Cury et al. 2016, Zabrynski et al. 2018). In addition, those who live more active lifestyles may be at a higher risk for Achilles tendon rupture, depending on the activity being performed. This is due to the high amount of load that can be experienced by the tendon in a relatively short amount of time. For example, during running the Achilles tendon can experience forces up to 12.5 times one's own body weight (Zabrynski et al. 2018). Sudden or forced plantar flexion of the foot as well as direct trauma to the Achilles tendon during athletic activities may cause the rupture of tendons even in young healthy individuals. In many cases, improper "warming" of the muscles and tendons prior to exercise as well as low experience level of the individual performing the exercise or improper conditioning further increases the risk of tendon rupture (Shamrock and Varacallo, 2020).

Several additional factors such as use of corticosteroids, Vitamin C deficiencies, fluoroquinolone antibiotics, or long-standing and untreated degenerative tendinopathies such as tendinitis/tendinosis may contribute or be the causative factor for rupture of the Achilles tendon by affecting its mechanical properties (Yuksel et al. 2016, Schneider et al. 2018, Zabrynski et al. 2018, Shamrock and Varacallo 2020). These factors affect collagen, which is the main structural and functional component of tendons. Deficiencies in vitamin C is best known to be the cause of scurvy, which is characterized by inadequate collagen production. Low vitamin C levels in an individual can lead to low levels of collagen production (Zabrynski et al. 2018). This is because vitamin C is required for the enzymes 3-hydroxylase, prolyl 4-hydroxylase, and lysyl hydroxylase, which are involved in posttranslational modifications of the collagen precursor molecule, procollagen (Gelse et al, 2003). Fluoroquinolone antibiotics inhibit the extracellular peptidase (Zabrynski et al. 2018), procollagen peptidase, which is involved in the formation of tropocollagen from the procollagen precursor molecule.

The use of corticosteroid medications may also increase an individual's susceptibility to tendon injuries. Corticosteroids decrease the general production of collagen. However, corticosteroids are used to relieve the symptoms of tendinopathy, which can play a causative role in tendon rupture (Mishra et al. 2009; Schneider et al. 2018; Zabrynski et al. 2018). Tendinopathy indicates a tendon pathology that encompasses tendinitis and tendinosis (Mishra et al. 2009), with the difference these two mentioned pathologies being time, duration, and severity. Tendinitis is the acute, short-term condition that is caused by a direct injury to the tendon and is characterized by the infiltration of inflammatory cells which cause inflammation of the tendon. Tendinosis is the chronic, long-lasting condition that results from multiple traumas to the tendon or the improper healing of a previous tendon injury. Tendinosis leads to progressive intratendinous degeneration (Schneider et al. 2018). Due to the degeneration of the tendon tissue, type I collagen is broken down and replaced with type III collagen, causing the formation of scar tissue. Incorporation of type III collagen into the type I collagen fibrils of tendons produces shorter and less organized fibrils within the tendon (Xu et al. 2018), leading to the restricted movement of joints and potentially rupture of the tendon as the tendon becomes stiffer. For untreated cases of chronic tendinopathies, particularly tendinosis, rupture of tendons can be seen as the end stage progression of tendinopathy where the tendon itself fails.

Current treatments for Achilles tendon rupture include surgical and non-surgical options, with both options having advantages and disadvantages, resulting in debate over which treatment method is better (Yuksel et al. 2016). Non-surgical treatments, or conservative treatments, are generally recommended to older patients, patients who tend to be less active, or those who are more at risk of developing surgery related complications (Moller et al. 2001). This method of treatment involves eliminating mechanical loading by immobilizing and casting the lower leg (Yang et al. 2018). By not undergoing a surgical procedure to repair the ruptured

tendon, this significantly lowers the chance of infection and eliminates the possibility of damage that may be experienced during the repair procedure, such as sural nerve lesions (Moller et al. 2001; Yuksel et al. 2016). In addition, a non-surgical treatment leaves a better cosmetic appearance after healing, due to the lack of scar formation after a surgical incision. However, patients that undergo non-surgical treatment to heal the tendon, often have high rates of re-rupture. In a prospective randomized multicenter study by Moller et al. (2001), one fifth of the patients who underwent non-surgical treatment (20.8%) experienced re-rupture. When compared to the re-rupture rate experienced in surgical treatments (1.7%), many consider non-surgical treatments as an unacceptable option for patients over 65 years of age who live typically active lifestyles. However, they also report that if re-rupture did not occur, the long-term healing quality equals that of surgically treated tendons (Moller et al. 2001). Additionally, further disadvantages of non-surgical treatment options include longer recovery times, increased muscle atrophy, and decreased range of motion in the ankle joint due to the immobilization (Moller et al. 2001; Aspenburg, 2007; Yuksel et al. 2016; Kanchanatawan et al. 2018).

Assuming that they are fit to undergo the surgical procedure, surgical treatments are often favored by young athletes or by those who seek a faster recovery time than what would be expected with conservative, non-surgical treatments, either due to occupational or muscle atrophy concerns (Kanchanatawan et al. 2018; Yang et al. 2018). Though there are numerous variations in the exact procedures performed and innovations in surgical procedures and methods, surgical treatments can be categorized as either open or percutaneous surgical treatments (Yuksel et al. 2016). In open surgical treatments, a relatively large single incision is made to fully expose the injured region of the tendon and the tendon is sutured back together. If an Achilles tendon rupture leaves a deficit of over 3 cm between the superior and inferior

ends of the rupture, tendon grafts or transplantation can be performed using this method to repair the tendon. In percutaneous repair methods multiple small incisions are made, and the suturing of the tendon is done through the incisions, resulting in lower risk of infection, less soft tissue damage, and less scar tissue than is seen in open surgical treatments (Yang et al. 2018). Depending upon the patient and situation, each type of surgical treatment presents their own advantages and disadvantages. However, both surgical treatments share the same advantages and disadvantages in comparison to non-surgical treatments. Surgical treatment has lower re-rupture rates and shorter recovery times, leading to less muscle atrophy and better range of motion after healing than seen in non-surgical treatments (Moller et al. 2001; Yuksel et al. 2016; Kanchanatawan et al. 2018). However, surgery increases the chance of infection and cosmetic scarring at the site of the incision as well as allowing the possibility of generating additional damage, such as nerve damage, during the surgery (Yuksel et al. 2016; Yang et al. 2018).

Regardless of the treatment method, the healing process of the calcaneal tendon remains a lengthy, and often expensive process. In combination with the rate of re-rupture and the debilitating effect of Achilles tendon rupture has on people's quality of life, this creates a need to develop new treatment methods. These methods include developing new anti-inflammatory medications for pain relief, improved surgical techniques to reduce the chances of infection and shorten recovery times, and research into the use of biologics. The biologics being tested to improve the healing quality and accelerate the healing rate of ruptured tendons include platelet-rich plasma (PRP) injections and mesenchymal stem cell (MSC) therapies (Yuksel et al. 2016).

Calcaneal Tendon: Functions, Composition, and Structure

Tendons serve to transmit the mechanical force generated by muscle to bone as well as to stabilize joints (Xu et al. 2017). The calcaneal tendon, commonly referred to as the Achilles tendon, is the largest and strongest tendon in the human body (Cury et al., 2016). It originates from the three superficial muscles of the posterior leg (the gastrocnemius, the soleus, and the plantaris muscles). These three originating muscles are also collectively referred to as the triceps surae, and the regions where they become tendinous merge together to form the calcaneal tendon. After fusion of the tendinous regions, the calcaneal tendon runs inferiorly on the posterior leg as a single tendon, crossing the posterior portion of the ankle joint to insert into the calcaneus bone of the foot. The primary function of the calcaneal tendon is to transmit the force generated by the triceps surae to cause movement of the calcaneus bone. More specifically, it transmits the forces responsible for plantar flexion of the foot at the ankle joint as its primary action and prevents dorsiflexion of the foot at the ankle joint. This transmission of force makes the calcaneal tendon a crucial link in the musculoskeletal system (Yuksel et al., 2016).

Structurally, the Achilles tendon consists of two generalized layers of organization. Zabrynski et al. (2018) describes the organization and structure of large tendons, such as the Achilles tendon, as being similar to a synthetic climbing rope in that they have many thin, load transferring inner fibers contained within an outer covering which contains the fibers. The outer covering of large tendons is known as the epitenon and surrounds the entire structure. Contained with the epitenon are a collection of smaller chords lined by a layer of connective tissue called the endotenon which serves to provide a vascular supply to the tendon. The endotenon also contains lymphatics and nerves (Cury et al., 2016). Tendons are characteristically poorly vascularized (Fedato et al. 2019). Within the endotenon, numerous

collagen fibers are arranged and organized into bundles called fascicles, which run longitudinally along the length of the tendon (Zabrzynski et al. 2018).

To discuss tendon structure on a histological level, collagen must first be defined and discussed. Gelse, Poschl, and Aigner (2003) define collagen as a generic term used to describe a characteristic right-handed polypeptide triple helix consisting of three collagen family peptide α-chains. The peptide chains are rich in glycine, which is found every third residue, followed by proline and hydroxyproline. Collagens are the most abundant extracellular proteins in the body, with several genetically and structurally distinct types being identified (Heinriksen et al. 2010). The different types, with slight variations in the α-chain sequence, are found in all parts of the body with differing functions.

All collagen serves to provide structural support for body tissues, mediate certain biomechanical properties within the extracellular matrix (ECM) and provide connective tissues with their specific mechanical properties. Though collagen can be synthesized by various cells (Kadler et al., 2008), this discussion will focus on the fibroblasts that produce fibril-forming collagens, such as type I and type III collagens (Gelse et al., 2003).

Synthesis of collagen fibrils can be separated into two stages; an intercellular process that produces and secretes the collagen precursor molecule procollagen, and the extracellular processing of procollagen to form the collagen fibers and the subsequent fibrillogenesis that arranges the fibers into fibrils. Collagen synthesis begins within the cell nucleus, as the procollagen genes are transcribed, undergo alternative splicing, and are translated at the rough endoplasmic reticulum (rER). Procollagen is then released into the luminal space of the rER (Gelse et al., 2003; Kadler et al. 2007). The procollagen molecule undergoes post-translational modifications, in which glycosylation and hydroxylation of the α-chain region occurs. The

hydroxylation enzymes prolyl 3-hydroxylase, prolyl 4-hydroxylase, and lysyl hydroxylase in the presence of Fe^{2+}, O_2, 2-oxogluterate, and ascorbate (Vitamin C) cofactors convert certain proline residues to hydroxyproline, depending on the collagen type being produced. This conversion of proline to hydroxyproline is essential to the structure and stability of the finished collagen fibril (Gelse et al., 2003). After post-translational modification, the procollagen molecule is transferred to the Golgi apparatus where additional carbohydrates are added, the molecule is packaged into secretory vesicles, and then exocytosed into the extracellular space. In the extracellular space, the non-helical N- and C-propeptides are cleaved by procollagen peptidase to form tropocollagen, which subsequently "self-assemble" and polymerize into collagen fibrils and fibers. This is due to the non-reducable covalent cross-links formed from the interactions between the hydroxylated regions of the tropocollagen molecules in a process called fibrillogenesis (Gelse et al., 2003; Kadler et al. 2007; Kadler et al., 2008; Heinriksen et al. 2010).

Tendons can be histologically characterized as dense regular connective tissues by having a relatively low number of cells in an extensive extracellular matrix. In this extracellular matrix, there is an extensive network of collagen fibers, in which the predominant fibers are collagen types I and type III. Of these two, collagen type I is the most common, accounting for roughly 90% of the collagen content (Xu et al. 2018). Type I collagen is attributed to providing tendons the ability to transmit the mechanical force from muscle to bone, as the dense parallel arrangement of the fibers allows for high resistance to tensile forces (Gelse et al., 2003; Xu et al, 2018). Type III collagen, usually a component of reticular fibers which support soft organs, is often found in elastic tissues mixed in abundance with type I collagen (Gelse et al., 2003). In tendons, incorporation of type III collagen into the type I collagen fibers during events such as wound healing produces smaller and less organized fibrils, causing a decrease in tendon

strength leading to a higher risk of developing tendinopathies and rupture (Xu et al. 2018; Xu1 et al. 2018; Aspenburg and Virchenko, 2004).

Wound Healing

Enoch and Leaper (2005) define a wound as a break or damage of the skin's epithelial integrity that may disrupt the structure and function of underlying tissues. However, this definition can be expanded to encompass several non-integumentary types of tissues. The body's ability to heal itself plays an important role in maintaining homeostasis by restoring function to a damaged tissue such as skin, bone, muscle, or connective tissues. The process of wound healing is a complex, dynamic process that involves a series of events in order to occur. The outcome of the healed wound can be affected by the type of wound healing that occurs, as well as the nature, structure, and type of tissue that is damaged (Ehrlich and Krummel, 1996; Enoch and Leaper, 2005; Wu et al. 2007; Schneider et al., 2018; Zabrynzki et al. 2018). Healing requires the recruitment of several types of cells, including immune cells, fibroblasts, and platelets. Additionally, there are several growth factors that serve to initiate certain events and activate cells during the process (Enoch and Leaper, 2005).

As stated previously, there are different types of wound healing. In cutaneous wounds, healing by first intention, also called primary healing, is usually seen in injuries that involve a clean cut, such as a surgical incision. Healing of these wounds may be immediate or delayed, depending upon the time at which the wound edges are approximated. Wounds that heal by first intention usually heal quickly with relatively minimal loss in strength (Ehrlich and Krummel, 1996; Enoch and Leaper, 2005). Ehrlich and Krummel (1996) cite a study by Edwards and Dunphy (1958) which tested the breaking strength of healing incisional wounds in animal skin

and reported that the final breaking strength of these wounds reached 80% of intact skin. Healing by second intention, or secondary healing, occurs in wounds that experience loss in soft tissues, leaving a deep open wound whose edges are too large to approximate, such as in severe burns or some surgical procedures. In healing by second intention, there is an ingrowth of granular tissues and an accumulation of collagen within the wound. The wound is thought to be closed by wound contraction caused by myofibroblasts, followed by epithelization. This type of wound healing is slower and may lead to functional restriction (Enoch and Leaper, 2005). To explain the basic principles of typical wound healing in cutaneous wounds and to compare it to the healing process of tendons, this review will look at wounds that heal by first intention.

In cutaneous wounds, healing begins with immediate homeostasis (lag phase) in which damage to small blood vessels cause them to contract and cause platelet aggregation to form a clot, which will serve to stop bleeding (Ehrlich and Krummel, 1996). The clot also acts as a scaffold for migrating cells (Enoch and Leaper, 2005). In addition to clot formation, platelets release alpha granules which secrete growth factors such as platelet-derived growth factor (PDGF), insulin-like growth factor (IGF), transforming growth factor beta (TGF-β), and vascular endothelial growth factor (VEGF), along with several others that influence wound healing.

Platelet growth factors serve to attract and activate fibroblasts, endothelial cells, bone marrow derived cells, and macrophages, as well as activating the classical and alternate complement cascades (Badivas et al. 2003). Complement activation begins the next phase of wound healing, the inflammatory phase. Activation of the compliment cascade brings neutrophils to the wound, monocytes differentiate into macrophages, and the phagocytic immune cells remove dead and foreign material, debriding the wound by releasing proteolytic enzymes such as collagenase (Enoch and Leaper, 2005). In addition, the neutrophils and macrophages secrete inflammatory cytokines to increase the immune response (Ehrlich and

Krummel, 1996). At the same time, basal cells along the wound edges migrate and proliferate, depositing components of the basement membrane (Enoch and Leaper, 2005).

The next phase of wound healing is the proliferation phase, which is characterized by the migration and proliferation of fibroblasts (Ehrlich and Krummel, 1996). Once at the wound site, fibroblasts produce the components needed to form the extracellular matrix, such as collagen, as well as needed to form granulation tissue (Ehrlich and Krummel, 1996; Enoch and Leaper, 2005). Characteristic of this phase is newly formed granulation tissue, the heightened level of neovascularization, and high numbers of fibroblasts (Ehrlich and Krummel, 1996). Studies by Badivas et al. (2003) and Wu et al. (2007) suggest that during this phase, the bone marrow derived stem cells differentiate and begin to form cutaneous structures such as blood vessels and sebaceous glands, as well as contributing to angiogenesis by releasing growth factors such as Ang-1 and VEGF. At the end of the proliferation phase epithelialization occurs with a thin layer of epithelial cells migrating from the wound edges to form a covering over the wound. This prepares the wound for the final stage of healing (Enoch and Leaper, 2005).

During the remodeling phase the extracellular matrix is degraded, re-synthesized, and remodeled. Influenced by cytokines, such as TGF-β, fibroblasts and the extracellular matrix may undergo wound contraction. Substantial changes in the granular tissue occur during this phase as the tissue changes to avascular scar tissue and the collagen fibrils of the granular tissue is replaced by fibers that are more dense. This results in the formation of scar tissue (Ehrlich and Krummel, 1996). As this scar tissue matures and the collagen bundles become thicker, the scar tissue becomes more resistant to tensile forces. However, the tensile strength of repaired tissue remains less than that of undamaged tissue (Enoch and Leaper, 2005)

Wound healing in tendons follows a similar process to that described for cutaneous wounds, but with some key differences. One difference is in the vascularity of the tissues. Dermal tissues are well vascularized, while tendon tissues, are characteristically poorly vascularized (Al-Ani et al., 2015; Fedato et al. 2019). There is also a large difference in the cellular composition between the tissues of the integument and in tendons. Tendons, histologically classified as dense regular connective tissue (Schneider et al. 2018), have few fibroblast-like cells (tenocytes) within the tissue with a large, highly organized extracellular matrix. These cells have a slow metabolic rate when compared to other types of cells, such as skeletal muscle or epithelial tissues. The low metabolism of the tenocytes allows them to endure the stress of loading and a more anaerobic environment resulting from the low vascularization of the tissue. However, the slower metabolism results in slower healing rates, taking about one to two years depending on the individual's age and general condition (Schneider et al. 2018; Zabrynski et al., 2018). In addition, the extracellular matrix in tendons is primarily type I collagen fibers that are arranged along the direction of stress experienced by the tendon. The composition and organization of these fibers are important to the function of the tendon. The disruption of this organized structure during wound healing affects the mechanical properties, and therefore the functionality of tendons and increases the chance of re-injuring the tendon (Kostrominova and Brooks, 2013; Fedato et al. 2019).

The exact healing mechanism is not completely understood in human tendons due to the lack of a suitable animal model that accurately mimics the features of human tendons (Schneider et al. 2018). However, it is agreed that the process of tendon healing passes through only three phases; the inflammatory, proliferative, and remodeling phases of wound healing, in which there may be some overlap between the phases (Schneider et al., 2018; Zabrynski et al., 2018). The initial inflammatory phase of tendon healing is heavily influenced by the platelets

and inflammatory immune cells present after the formation of a hematoma around the site of the tendon injury. The growth factors released from platelets, such as platelet-derived growth factor (PDGF) stimulate the production of other growth factors (Zabrynski et al, 2018) by the surrounding cells. The growth factor VEGF stimulates angiogenesis to form the vascular plexus at the site of the poorly vascularized tissue and increases capillary permeability (Yuksel et al. 2016; Schneider et al, 2018). TGF-β, also secreted by the platelets, promotes the migration of tenocytes and immune cells into the tissue. There are several other contributing growth factors derived from platelets, some of which will be discussed later. However, in addition to VEGF, inflammatory cytokines released by invading immune cells also serve to increase capillary permeability. The immune cells also produce cytokines, such as IL-2 and IL-6, that serve to both modulate the immune response and to influence the proliferation of tendon derived stem cells, called tenoblasts (Yuksel et al. 2016; Chen et al. 2018). The tenocytes, recruited from the endotenon, synthesize and deposit temporary fibrous tissue that consists of fibronectin and type III collagen, as well as components of the extracellular matrix (ECM) such as proteoglycans. This new tissue lacks the organization seen in undamaged tendon tissues, and therefore must later be remodeled for the tendon to regain function and durability (Schneider et al, 2018; Zabrynski et al. 2018).

The proliferative phase in tendon healing is characterized by the high cellularity of the tendon tissue resulting from the cells moving into the injured area, in addition to proliferation of the cells and increased water absorption from the proteoglycans and other components in the formed ECM. During this phase, the newly produced type III collagen begins to be replaced by the much stronger type I collagen as the proliferating tenocytes begin production of type I collagen (Schneider et al. 2018). The newly formed type I collagen fibers undergo fibrillogenesis in which they self-assemble into parallel fibrils (Gelse et al., 2003; Xu1 et al. 2018; Zabrynski et

al. 2018) which is facilitated by the proteoglycans and fibronectin (Kadler et al., 2008; Xu et al. 2018; Xu1 et al. 2018). The tenocytes also secrete matrix metalloproteinases (MMPs), such as collagenases, which degrade collagen as well as tissue inhibitor of metalloproteinases (TIMPS) (Madden and Peacock, 1971; Heinriksen et al. 2010; Xu et al. 2018; Xu1 et al. 2018). The actions of the growth factors VEGF and TGF-β1 play key roles in this phase by further stimulating angiogenesis and stimulating further cell migration, proliferation, and differentiation, respectively. It has been reported that these growth factors produce a feedback loop resulting in further increases in the production of the cytokines. These growth factors have paracrine and autocrine effects that result in the stimulation of stem cells to rapidly differentiate into fibroblasts, thus increasing the type I collagen synthesis (Yuksel et al. 2016). PDGF and TGF-β1 also stimulate proliferation of the activated cells and stimulate the production of the ECM by tenocytes. This process continues, gradually improving tendon strength as more type III collagen is converted to type I collagen. This can take up to 6 to 8 weeks (Schneider et al. 2018).

Following the proliferative phase is the remodeling phase in tendon healing, which can last up to two years, depending on the individual. During this phase, there is a reduction in the vascularity and cellularity of the tendon, but an increase in organization of the collagen fibers and a restoration in the tensile strength and stiffness of the tendon. The remodeling phase of healing can be divided into two stages, the consolidation stage and the maturation stage. During the consolidation stage, there is a characteristic change in the tendon tissue, going from high cellularity to a more fibrous tissue as the synthesis of type III collagen is replaced with the type I collagen. The collagen also begins to align in the direction of stress. Fibroblasts begin to differentiate into myofibroblasts which then undergo wound contraction. The maturation stage results in the formation of scar tissue within the tendon and is characterized by a reduction in tenocyte metabolism and reduced vascularity within the tendon (Schneider et al. 2018).

There have been several studies investigating whether applying stress to the tendon during healing improves the quality of healing in the tendon. Some studies suggest that applying a stress, or loading a tendon, may help in the healing process of tendons after tendon elasticity has been re-established (Aspenburg, 2007). A study by Eliasson, Andersson, and Aspenberg (2012) investigated changes in gene expression in healing tendons after a single loading event. In their study they observed several changes in gene expression (Eliasson et al., 2012). Their data suggested that mechanical loading of tendons may decrease excessive angiogenesis, protect cells from oxidative stress, and improve the mechanical properties in healing tendons. Studies by Xu et al. (2018) looked at the effects of loading Achilles tendons through varying intensities via treadmill running. In both studies, they found that when the tendon is under a moderate level of loading, it caused an equilibrium in MMP and TIMP expression which allowed for a significant increase in type I collagen production. This resulted in an improvement in the mechanical properties of tendons (Xu et. al, 2018; Xu1 et al., 2018). However, further research is required to investigate the effect of loading on healing tendons.

Platelet-Rich Plasma

Platelet-rich plasma has been investigated for its effect upon healing wounds. Blood is classified as a connective tissue, in which plasma is the liquid ground substance which holds the cells of this connective tissue. The cells that are carried by plasma are known as the formed elements of blood, which includes erythrocytes, leukocytes, and thrombocytes. Thrombocytes, more commonly known as platelets, are most often known for producing fibrinogen which contributes to the formation of a clot to stop bleeding in the case of wounding. When platelets are activated, they also produce a multitude of growth factors, cytokines, and other molecules

that are believed to have advantageous effects in wound healing. These factors are chemotactic for cells of the immune system and the mesenchyme, as well as also being anti-inflammatory (Mishra et al. 2009; Aspenberg and Virchenko 2004). In the production of platelet-rich plasma (PRP), platelets are concentrated into a smaller volume of plasma than the normal physiological concentration of platelets found in the blood. When this elevated concentration of platelets in PRP are activated, this yields a higher level of growth factors and cytokines per volume when compared to the platelet-poor plasma (PPP) of whole blood (Yuskel et al. 2016).

Yuksel and co-workers (reviewed in Yuksel et al. 2016) refer to several studies which suggest that PRP may be useful in processes such as tissue repair and wound healing due to the production of growth factors. These include platelet-derived growth factor (PDGF), transforming growth factor-beta (TGF-β1), vascular endothelial growth factor (VEGF), and insulin-like growth factor (IGF), among others (Yuksel et al. 2016). PDGF serves as a chemoattractant for neutrophils, MSCs, and fibroblasts (Mishra et al. 2009). In addition to attracting fibroblasts, PDGF also contributes to their proliferation by acting as a mitogen. Similarly, IGF and TGF-β1 also contribute to fibroblast proliferation, as well as stimulating the synthesis of collagen (Zabrzynski et al. 2018, Mishra et al. 2009). VEGF in wound healing serves to stimulate the formation of new blood vessels via angiogenesis (Mishra et al. 2009, Zabrzynski et al. 2018, Yuksel et al. 2016). In the wound healing of tendons, these growth factors play key roles in different phases of tendon recovery, with some being utilized through the entire process of healing. IGF and TGF-β1 are important growth factors in the inflammatory phase of healing. They stimulate the production of the extracellular matrix, notably the production of fibronectin and type III collagen, as well as promote cell migration and proliferation (Molloy et al. 2003). The presence of VEGF is required to form the vascular plexus within the poorly vascularized tendon tissue in the inflammatory phase, but its action grows increasingly important in the

proliferative phase (Yuksel et al., 2016; Schneider et al. 2018). PDGF, in addition to its chemotactic function in the inflammatory phase, also serves as a regulator for gene expression, collagen and non-collagen protein production, and growth factor production, showing high activity in the remodeling phase (Molloy et al., 2003).

Multipotent Mesenchymal Stromal Cells

Mesenchymal stromal cells have also been used as an additive to improve wound healing. MSCs are the cells isolated from various connective stromal tissue, such as bone marrow and adipose tissue (Horwitz et al. 2006). Mesenchymal stem cells, also referred to as multipotent mesenchymal stromal cells, are the cells responsible for differentiation into stromal cells. These stem cells are self-renewing and are capable of differentiation into osteocytes, adipocytes, chondrocytes, and other cell lineages. This differentiation, in vitro, is influenced by certain stimuli, such as cell density, spatial organization, mechanical forces, cytokines, and growth factors (Pittenger 1999). They have been known to have an immunosuppressive effect on the immune system, specifically T lymphocytes. Though the exact mechanism for the immunosuppressive properties is not fully understood, several factors secreted by the MSCs are thought to contribute to immunosuppression. These include hepatocyte growth factor, indolamine-2-3-deoxygenase, and transforming growth factor-α (Brinchmann 2008).

For mesenchymal stromal cells to be classified as stem cells, they must meet certain requirements. According to the International Society for Cellular Therapy (ISCT), mesenchymal stem cells should be plastic adherent when grown in standard cell culture medium. They should express CD 105, CD 73, and CD 90 cell surface molecules and lack the expression of CD 45, CD 34, CD 14, CD 11b, CD 79α, CD 19, and HLA-DR cell surface molecules. Differentiation into

osteoblasts, adipocytes, and chondrocytes should be inducible in vitro under standard cell culture conditions (Dominici et al. 2006). The cell surface molecules CD 90 and CD 105 are found on hematopoietic stem cells and stromal cells, respectively, while CD 73 is a cell surface marker that indicates lymphocyte differentiation. By having these surface molecules, though not unique to MSCs, it indicates that they are present. The ISCT also recommends the lack of expression of hematopoietic surface antigens with a maximum acceptable expression of two percent. However, they recognize that the expression of HLA-DR on MSCs is desirable in some applications when the cells are stimulated. In this case, they can be classified as "stimulated MSC" if all other criteria are met, but they cannot be classified as unstimulated MSCs (Dominici et al. 2006).

Experimental Treatment Methods

PRP injections are currently being used by orthopedists, sports surgeons, and maxillofacial surgeons to decrease the recovery time in ligaments and tendons. PRP is easy to prepare, as it can be prepared quickly and provides an autologous source of concentrated growth factors (Yuksel et al., 2016). In addition to its ease of preparation, application of autologous PRP poses little risk to the receiving patient. A previous study examining the effect of Achilles tendon repair in rats showed improved repair and positive results from mechanical testing which showed improved material characteristics in tendon strength, which was then confirmed by histological examination that had shown greater maturation and improved overall repair of the tendon callus, with effects lasting four weeks after administering a single PRP injection (Aspenberg and Virchenko, 2004).

MSCs can be obtained from several adult tissues and are thought to act as an immunomodulator and show paracrine effects in addition to being self-renewing and having the capacity to differentiate into multiple cell lineages (Akino et al., 2005; Brinchmann, 2008; Atoui et al., 2008; Aktas et al., 2016). Bone marrow derived MSCs have been seen to play a role in the healing process of cutaneous wounds by being incorporated into skin, blood vessels, and sebaceous glands (Badivas et al., 2003; Wu et al., 2007). In tendon healing, MSCs have been seen to have positive effects through their post-differentiation production of collagen or through their influence on growth factors, which may improve and accelerate the healing process by influencing the early phases of tendon healing. In these studies, MSCs promoted a greater level of organization to collagen fibers (Chong et al. 2007).

Some studies have used biodegradable scaffolds, such as fibrin or poly(lactide-co-glycolide) scaffolds, to act as a cell carrier or to provide a localized control of an inflammatory response by infusing the scaffolding with cytokines like tumor necrosis factor-α (TNF-α) (Chong et al., 2007; Aktas et al., 2016). Recently, there have been promising studies examining the effects of PRP and MSC, used individually and in combination with each other, to determine if they may have a use in regenerative medicine (Yuksel et al., 2016; Fedato et al., 2019). These studies have seen increased levels of anti-inflammatory cytokines at the site of the injury, in addition to showing overall improved tendon healing. However, the studies on MSC and PRP combinations have only administered their treatments via injection and did not include a scaffold or a cell carrier, nor did they measure the strength and time of maximum healing of the repaired tendons.

In the present study, we will expand upon the previous studies and aid in the search for an improved treatment method for ruptured tendons through the use of biologics in combination. This study will investigate the effect that combining PRP, MSCs, and a collagen

carrier has on the healing rate and quality in Achilles tendon rupture using a rat model. The MSCs will be obtained from the bone marrow of rat long bones (tibia and femur) and cultured until the point of their administration, immediately following a surgical transection and repair of the Achilles tendon. PRP will be prepared from the whole blood of the rats. The collagen carrier will be applied to the damaged Achilles tendon during the surgical transection in the form of a malleable collagen tape (CollaTape).

Specific Aims and Hypothesis

The specific aim of this study is to determine the effect of using a combination of platelet-rich plasma, mesenchymal stromal/stem cells, and a collagen scaffold carrier in a therapeutic manner has on healing of a ruptured calcaneal tendon in our four-phase study design (**Figure 1**). We will be investigating the rate and quality of healing by tensile testing at 1- and 2-week recovery times. Additionally, we will be investigating the quality of the healing by using RT-PCR on the damaged tendons to determine the ratio of collagen type I to collagen type III. We will also determine if the mesenchymal stromal cells extracted from the bone-marrow of rats that will be used in the treatments show stem cell qualities by utilizing cell culture and differential staining techniques on mesenchymal stromal cells that have been maintained in differentiation inducing media.

The hypotheses of this project is that there will be significant improvement in the Achilles tendon healing rate, as well as improvement in the biomechanical performance in the tendons treated with a combination of all three biologics and that improved biomechanical performance will correlate with a higher expression of type I collagen in the treated tendons.

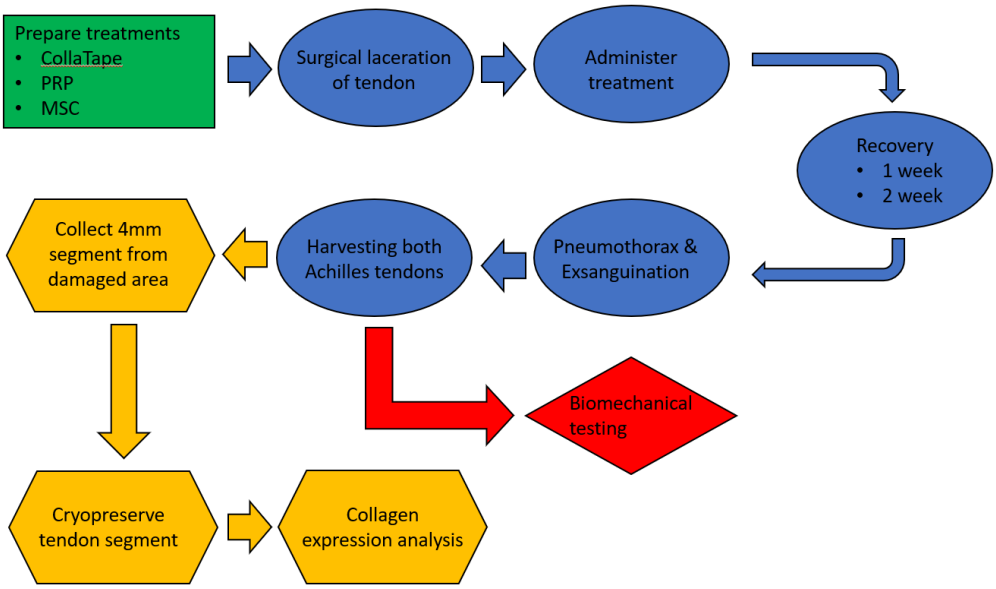

Figure 1: Schematic of the four-phase study design. The green box represents the Phase 1 biologic treatments preparation. The blue circles represent a timeline of creating the simulated Achilles tendon rupture, administering the treatment, and harvesting the tendon samples in Phase 2. Blood collected from exsanguination was used to prepare more PRP. Phases 3 and 4 are represented by the red diamond and orange hexagons for the biomechanical tensile testing and collagen expression analysis, respectively.

Materials:

Male Lewis Rats were purchased from Charles River Laboratories International Inc. (Wilmington, MA). 3-isobutyl-1 methylxanthine, Serum free alpha-minimum essential medium, Alcian Blue, Alizarin Red S, Oil Red O, Ascorbic acid 2-phosphate, β-Glycerophosphate, Dexamethasone, Fetal Calf Serum, GlutaMAX, Penicillin-Streptomycin, and Trypsin/EDTA reagents were purchased from Sigma-Aldrich (Saint Louis, MO). CollaTape was purchased from Zimmer Dental Inc. (Warsaw, IN). Vinyl sutures were purchased from Ethicon (Cornelia, GA). The cell titer 6 AQ Solution, Wizard Genomic DNA Purification kit, and the GoTaq Hot Start Green Master Mix kit was purchased from Promega (Madison, WI). Heparin was purchased from STEMCELL Technologies Inc. (Cambridge, MA). The RNeasy Fibrous tissue mini kit was purchased from Qiagen (Germantown, MA). The Proscript II cDNA FirstStrand synthesis kit, Quick-Load 1 kb Extend DNA ladder, and 100 bp DNA ladder were purchased from New England BioLabs (Ipswich, MA). The NucleasEliminator was obtained from Ameresco (Solon, OH). The forward and reverse primer sets for Col1a1, Col3a1, and GAPDH were obtained from Integrated DNA Technologies (Coralville, IA).

Methods:

Animal Care Protocol

Consent was obtained from the Institutional Animal Care and Use Committee at Youngstown State University before beginning the study. In total, 124 male Lewis rats were used in the experiments. Upon delivery, the rats were housed in groups of three at the Youngstown State University animal care facility in clear acrylic cages with approximately two inches of Aspen wood-shavings bedding over a lining of cob bedding. The animal models were fed *ad-libitum*, their water was changed once daily, and their cages were changed weekly to supply fresh bedding. The animals were put on a 12-hour reverse day-night cycle (10 AM – 10 PM) and allowed two weeks to acclimate to the animal facility prior to their use in any procedures.

Prior to a surgical procedure and during transport, the cages were kept covered to prevent the introduction of unnecessary stress to the animals. The animals were initially administered analgesic immediately after a survival surgical procedure; however, adverse reactions were observed in the rats when the analgesic was administered while the rat was under the effect of the anesthesia, leading to the death of the rat. To avoid the fatal reaction, the rats were monitored until the anesthetic effect had begun to wear off before being given the analgesic. This change in administering the analgesic led to no further adverse reactions in the rats.

After a survival surgery, the rats were placed into new, clean cages to prevent the infection of wounds made during the surgery. The limb from the surgical procedure was not casted or immobilized, allowing load to be applied to the damaged tendon. The animals were monitored daily for signs of infection, biting at the sutures, autophagia, or unnecessary discomfort following a surgical procedure.

For non-survival surgeries, the rats were administered anesthetic, and work was only conducted when a response from the toe pinch reflex was no longer present in the rat. Once under anesthesia, the rats were euthanized via exsanguination (heart puncture) and pneumothorax (severing of the diaphragm muscle) procedures to ensure a humane death of the rat. The blood collected from the exsanguination was used for platelet-rich plasma preparation. The pneumothorax was done as an additional measure to ensure the death of the animal as well as severing the aorta, vena cava, as well as lacerating the right and left ventricles after exsanguination was complete.

Platelet Rich Plasma Preparation

Blood was collected from anesthetized male Lewis rats via a heart puncture using a 21-gauge needle and a 10-mL syringe containing 1/10 volume of heparin (10µL/mL) in saline. The blood was injected into a blood collection tube containing 10% EDTA (pH 8.0) and stored on ice until PRP preparation.

To prepare the PRP for cryopreservation, the blood was first centrifuged at room temperature in a conical tube for 10 minutes at 200 x g. After centrifugation, the plasma layer was removed and centrifuged at 700 x g for 10 minutes. The upper (platelet-poor) plasma layer was removed and stored at –20 ^{O}C for later use in preparing the PRP used in the treatment injection, leaving a 1-mL portion with the platelet pellet. The pellet (platelet rich) was re-suspended following the addition of 5% DMSO. The PRP was frozen slowly by gradually decreasing temperature to –80 ^{O}C. Subsequently, the frozen pellets were stored in liquid nitrogen.

In order to thaw PRP for their use in the tendon repair treatment, the frozen pellet was thawed to release the pellet from the cryovial by rolling the vial around between two hands until the pellet was no longer frozen to the sides of the vial. The rest of the pellet was quickly melted by adding it to 1 mL of 37 °C plasma and mixed by pipetting until the pellet was dispersed. The PRP was then centrifuged at 700 x g for 10 minutes at 4 °C. The plasma was aspirated off and the remaining pellet was re-suspended in 1 mL platelet poor plasma. The platelets were counted using a Hemocytometer to determine that the plasma was enriched with platelets and above physiological levels of platelets. For the PRP injection that was administered, 100 uL of platelet rich plasma was drawn into sterile 1 mL syringes using a 26 G needle. After the tendon laceration and repair procedure, the PRP was injected subcutaneously near the repaired incision immediately following Achilles surgery while the rat was still under the effect of anesthesia.

Due to the inherent variability of the source of blood used to prepare the PRP, to determine the consistency of our PRP preparations, three additional vials of PRP were prepared. The prepared PRP was serial diluted 1:100 and 1:1000, then counted using the same methods to determine the average dosage of PRP used in the treatment injection. A one-way ANOVA was done to determine if a significant difference existed between the three PRP preparations at either the 1:100 or 1:1000 dilutions.

Isolation and Expansion of Mesenchymal Stromal Cells

The rats were anesthetized with isofluorane before performing pneumothorax and exsanguination to euthanize them. The hindlimbs of each rat were removed and the larger sized long bones (femur and tibia) of the hindlimb harvested. The hindlimbs were cleaned of muscle

and connective tissue before extraction of the bone marrow from the femur and tibia. The central canal of the long bones, containing the marrow, were flushed using α-MEM media containing 20% FCS, 2 mM L-glutamine, 100 U/mL penicillin, 100 ug/mL streptomycin and 25 ng/ml amphotericin B. The media containing the marrow was rested for 5 minutes to allow clumps to settle, leaving the mesenchymal stromal cells in the supernatant. The supernatant was removed, and the mesenchymal stromal cells were counted using a hemocytometer. After counting, the mesenchymal stromal cells were centrifuged at 400 x g for 10 minutes at 25 °C. The pellet was resuspended to 1 x 10^5 – 1 x 10^6 cells/ml in complete medium (α-MEM containing 20% FCS, 2 mM L-glutamine, 100 U/ml penicillin, 100 ug/ml streptomycin and 25 ng/ml amphoteracin B) and 10 ml added to a T-75 flask.

The bone marrow derived mesenchymal stromal cells were then incubated for 4 days in α-MEM media. After 4 days, the non-adherent cells were removed, and the adherent cells allowed to grow. The cells were passaged three times at 80% confluence by treatment with trypsin/EDTA. The cells were frozen and stored in complete medium containing 10% DMSO in liquid nitrogen. Before use in injections post-surgery, the cells were thawed and plated one day prior to the surgery. The MSCs were collected by trypsinization and re-suspended in saline or PRP at 1 x 10^5 cells/100 µL.

MSC Differentiation Assays

All differentiation assays were adapted from Chen et al. (2009). All differentiation assays were conducted on 2 x 10^5 mesenchymal stromal cells that were passaged three times. The cell cultures for the differentiation assay were all seeded into a 6 well plates and allowed to become confluent. For each plate, three out of six wells of the plate were cultures that were maintained

with undifferentiating α-MEM complete media and will act as the control cultures in the differentiation assays. All plates were incubated at 37 °C in 5% atmospheric CO_2. All cultures were visualized using an inverted phase contrast microscope.

Osteogenic Differentiation

The cell cultures were differentiated using an osteogenic medium. This medium consisted of 200 µM ascorbic acid 2-phosphate, 100 nM dexamethasone, 10 mM β-glycerophosphate, 10% fetal bovine serum, 2 mM glutaMAX, and 1% penicillin/streptomycin in DMEM high glucose. The cells were grown for three weeks using this media, changing the media every three days. The media was changed 2-3 times a week by aspirating off old media in a sterile cabinet, careful not to disturb the cell lawn on the bottom of the well, and aseptically adding 2 mL of the osteogenic media directly to the wells.

After the three-week period, the cells were washed with PBS then fixed with a 10% formalin solution. The cells were incubated at room temperature for one hour before removing the formalin and washing with distilled water. Alizarin Red S was dissolved in distilled water to obtain a 2% staining solution, and the pH was adjusted to 4.2 with a 0.1% solution of NH_4OH before being filtered. The Alizarin Red S stain was added to the wells such that the stain covered the bottom of the wells and allowed to incubate in the dark for 45 minutes at room temperature. The cells were washed 4 times with distilled water. After the washing, the cells were completely covered with sterile PBS and visualized at 100X and 200X magnification.

Adipogenic Differentiation

The cell cultures were incubated using an adipogenic medium. This medium consisted of 500 µg/mL insulin, 1 µM dexamethasone, 1 µM indomethacin, 500 µM 3-isobutyl-1 methylxanthine, 10% fetal bovine serum, 2 mM glutaMAX, and 1% penicillin/streptomycin in DMEM high glucose. The cells were maintained using for three weeks using this media, changing the media every three days. The media was changed by aspirating off old media in a sterile cabinet, careful not to disturb the cell lawn on the bottom of the well, and aseptically adding 2 mL of the adipogenic media directly to the wells.

A stock solution of Oil Red O stain was prepared by dissolving 300 mg of Oil Red O in 100 mL of 70% isopropanol, making a 0.3% solution of the stock stain. This stock stain was then diluted using 2 parts distilled water to 3 parts of the stock solution. The Oil Red O stain was then syringe filtered

After the three-week period, the cells were washed with PBS then fixed with a 10% formalin solution for 30 minutes before being washed with distilled water. The cells were then allowed to incubate under 60% isopropanol for 5 minutes before the isopropanol was removed. The Oil Red O stain was then applied to the cells so that they were completely covered by the stain and incubated at room temperature for 15 minutes. After incubation, the cells were washed with distilled water until the wash became clear. Once the wash was clear, sterile PBS was added to the wells and visualized at 100X and 200X magnification.

Chondrogenic Differentiation

The cells were differentiated using a chondrogenic medium. This medium consisted of 50 µg/mL ascorbic acid, 100 nM dexamethasone, 1% insulin-transferrin-selenium, 10 ng/mL TGF-β1, 2 mM glutaMAX, and 1% penicillin/streptomycin in DMEM high glucose. The cells were maintained for three weeks using this media, changing the media every three days. The media was changed by aspirating off old media in a sterile cabinet, careful not to disturb the cell lawn on the bottom of the well, and aseptically adding 2 mL of the chondrogenic media directly to the wells.

After the three-week period, the cells were washed with PBS then fixed with a 10% formalin solution dissolved in PBS. The cells were incubated at room temperature for one hour before removing the formalin and washing twice with distilled water. Alcian Blue stain was prepared by dissolving 10 mg of Alcian Blue 8 GX dye in a 60: 40 solution of ethanol and acetic acid. The Alcian blue stain was added to the wells such that it completely covered the bottom of the well. The plate was incubated in the dark overnight at room temperature. A de-staining solution was prepared by adding 80 mL of acetic acid to 100 mL of ethanol. After the overnight incubation, the stain was carefully aspirated, and 1 mL of the de-staining solution was added to the wells and allowed to incubate for 20 minutes. The de-staining solution was carefully aspirated, replaced with PBS to cover the cells, and then visualized at 100X and 200X magnification.

Calcaneal Tendon Laceration, Surgical Repair, and Tissue Harvest

Preparation for Surgical Procedure

The rats that underwent the surgical procedure and provided the tendon samples were anesthetized using Isofluorane (2.5 L/min). Initially, the anesthetic was administered in a gas chamber to sedate the subjects, which was then immediately followed by administration through a nose cone to fully anesthetize the rat. The toe-pinch reflex was done while the rat was in the nose cone to determine if the anesthetic had taken affect. If there was no visible reaction to the toe-pinch reflex, the rat was considered anesthetized, and the surgical laceration of the calcaneal tendon procedure would begin. All tools (i.e., scalpel handles, hemostats, scissors, and forceps) were sterilized prior to the surgical procedure via autoclaving. During the procedure, the tools were sterilized between rats using a dry bead sanitization unit between rat subjects.

Laceration of the Calcaneal Tendon, Repair, and Experimental Treatment

The surgical area on the rats were prepared by first shaving the hair from the hindlimb when the animal was sedated. Once fully anesthetized, the hindlimb was cleaned with 7.5% povidone-iodine and alcohol pads prior to any incisions. A midline skin incision was made directly over the Achilles tendon in anesthetized rats. The Achilles tendon was cut 6 mm proximal to the insertion into the calcaneus bone to create the simulated complete tendon rupture. Following the creation of the defect, a modified Kessler suture using coated Vicryl (Polygalactin 910) undyed Braided 5-0 suture (Ethicon) was used to approximate the transected tendon ends. The plantaris tendon was left intact to act as a splint during the healing of the tendon. CollaTape (8mm x 10 mm) was wrapped around the tendon for all rat subjects, except for the surgical control group which received no additional treatment other than the

approximation of the tendon ends and post-surgical analgesic. The skin was approximated with an individual coated Vicryl braided 5-0 subcuticular suture and the skin incision was closed with monofilament nylon sutures (Ethicon). The rats received a subcutaneous injection of PRP, MSCs, or a combination of both (for the appropriate study animals) adjacent to the incision site. The rats dedicated to the surgical control group received no additional post-operation injection. After the effects of anesthesia dissipated, the rats received buprenorphine (0.01-0.05 mg/kg, s.c.), and again at 12 and 24 hours after surgery.

Harvesting of the Tendon Tissue

After the designated time periods for healing (1 or 2 weeks), the rats were anesthetized following the same procedure as described previously using isofluorane prior to performing a pneumothorax and exsanguination via heart puncture. Working quickly to minimize drying of the tissues and rewetting with phosphate-buffered saline (PBS) as necessary, the hindlimbs of both the control and treated tendons were carefully skinned down to the midfoot while avoiding disturbance of scar tissue formed after surgery. The gastrocnemius and soleus muscles were separated from the deep posterior leg muscles and were cut transversely in the middle of the muscle body. The Achilles tendon was carefully freed from the posterior tibia and fibula by cutting the retinacula, ligaments, and undesired tendons (such as the flexor digitorum longus, the anterior tibial, and posterior tibial tendons among others) which surround the ankle joint. The foot was separated from the tibia and fibula and the distal half of the foot was removed, keeping the calcaneal bone intact, and excess muscle tissue surrounding the calcaneus was removed. The harvested tendons that would be used for the biomechanical testing were wrapped in gauze soaked in PBS, placed in bags, and stored at -20 °C until needed for testing.

The tendon samples that were used for collagen expression analysis required further processing. The tendons that were used for collagen mRNA analysis were harvested following the same method described above, but only the segment that was transected was needed. Therefore, the calcaneal tendon was cut 2 mm superiorly and inferiorly of the initial defect made during the surgical laceration of the tendons. A section of the control, unoperated tendon from the same region was also collected. Using the defect from the surgical procedure that was made 6 mm from the insertion of the calcaneal tendon to the calcaneus bone as a reference, the control tendons will be cut at 8 mm and 4 mm, mirroring the cuts made from the tendons with the surgical defect. Once these sections of tendons were excised, they were weighed, their mass recorded, and then immediately flash frozen in an RNase treated mortar filled with liquid nitrogen. Once frozen to liquid nitrogen temperatures, the tendon segments were placed in sterile microfuge tubes and transferred to a – 80 °C freezer where they were stored until needed for total RNA extraction.

Biomechanical Testing of Tendon Tissues

Blinding Procedures

The experimenter's conducting the biomechanical testing for this study were blinded during the testing to ensure that they did not know which sample, recovery time sub-group, or treatment group was being tested and avoid potential bias. However, because all samples from the surgical control group were done after all samples that received treatment have been tested and analyzed, a new blinding protocol was devised for tensile testing the surgical control group. The experimenters testing the surgical control group were blinded such that the experimenters

conducting the biomechanical testing on the tendons did not know which sample had a 1-week or 2-week recovery time.

Sample Preparation

On the morning of tensile testing, while still in individually labeled Ziploc bags wrapped in PBS-soaked gauze, the tendon samples were thawed and allowed to warm to room temperature. Though a study by Jung et al. (2011) concluded multiple freeze-thaw cycles of tendon tissue shows minimal effect on the tissue's structural or mechanical properties, effort was made to minimize the number of freeze-thaw cycles, only thawing samples that would be tested that day. Prior to the biomechanical testing of the harvested tendon samples, each sample was thoroughly inspected to ensure that all additional tissues, such as excess muscle tissue attached near the calcaneus bone/tendon and any remaining skin near the incision site, were removed. If additional tissues were found, they were carefully removed prior to testing. Any damaged tendon samples were removed from testing entirely. For the surgically repaired tendons, intact or non-absorbed suture material was carefully removed for mechanical testing purposes. After inspection, measurements of the tendon length and width at the top (near the musculotendinous junction), middle (near or approximately near the site of damage), and bottom (near the insertion to the calcaneus) were taken. During the pre-testing inspection and measurements, the tendon samples were continuously hydrated using PBS to prevent desiccation during preparation and were hydrated again just prior to testing.

Tendon Vise Method of Tensile Testing

The upper grip was custom designed clamping grip with course sandpaper glued to the grip. The muscle portion of the tendon was also glued to sandpaper, giving a tight grip with no slip. This avoided the common procedure of freezing the tendon to the grip. The clamping grip did not prevent the tendon on the bottom having no muscle from slipping, so a custom designed tendon vise was produced, and the Achilles and plantar tendons were left attached to the calcaneus (heel) bone. The bone was slipped under the vise before it was closed forming a firm stop to prevent the tendon from slipping.

The biomechanical testing was performed using an Instron Tensiometer, Model 5500R equipped with a 100 N load cell capable of 0.25% accuracy over the entire range. The tendons were pre-loaded with 1 N to eliminate slack in the tendon before being pulled at a constant extension rate of 1 mm/sec until failure where the tendon was half torn, and the experimenters noted where the tear had occurred for each sample. The stress and strain data were collected and recorded using Bluehill3 software (Instron Corp) on a computer connected to the tensiometer, then analyzed.

All tendons that had received CollaTape only, Collatape + PRP, CollaTape + MSC, or CollaTape + MSC + PRP treatment, for both 1- and 2-week recovery time sub-groups, were tested using this method. A 2-way ANOVA statistical analysis was conducted for these samples as both unnormalized data and normalized data expressed as a percentage of the control, unoperated tendon from the same animal. For the surgical control group that received no additional treatment, five tendon pairs (one tendon pair being the operated and unoperated tendon from the same animal) from both 1- and 2-week recovery time subgroups were tested using this method. A one-way ANOVA statistical analysis was conducted to determine if a

statistically significant difference exists between the surgical control group and the treatment groups when expressed as normalized data.

Determining Collagen Expression via RT-PCR

Reagent and Material Preparation

Prior to starting the RNA extraction from the tendon tissue samples, all of the included reagents in the RNeasy Fibrous Tissue Mini Kit (Qiagen) were prepared according to the manufacturer's instructions. The RLT buffer working solution was replaced every month with a new solution according to the manufacturer's recommendation. This was done by adding 10 µL of β-mercaptoethanol to 1 mL of the included RLT stock buffer solution in an RNase-free microfuge tube. The DNase I provided in the RNase-free DNase set included in the Qiagen Fibrous tissue mini kit was divided into 10 µL aliquots and frozen at -20 °C until needed in the total RNA extraction and purification.

For each sample undergoing an RNA extraction, the mortar and pestle was cleaned to prevent contamination between samples and treated with NucleasEliminator (Ameresco) to eliminate any RNase that may be present. This was done by adding 1 mL of 7x cleaning solution to the mortar with a small amount of tap water, then scrubbing the mortar and pestle with a brush until they were as clean as possible. The mortar and pestle were then rinsed twice with tap water, and twice again with deionized water to remove any remaining cleaning solution. After the final rinse with deionized water, the mortar and pestle were moved into a sterile cabinet and 1 mL of NucleasEliminator was added to the mortar. The NucleasEliminator was spread around the inside surface of the mortar and the surface of the pestle using a paper towel. The treated mortar and pestle were then allowed to incubate at room temperature in the

sterile cabinet for 5 minutes before being rinsed twice with sterile millique water twice, and the mortar and pestle were allowed to dry in the sterile hood. This process was repeated for a total of two washings of the mortar and pestle. After the second washing, the mortar and pestle were covered with aluminum foil until needed in the RNA extraction of the tendon tissues. Any additional metal tools (i.e., spatulas and forceps) were autoclaved in a sterilization pouch before their use in the extraction.

Tendon RNA Extraction and Purification

RNA extraction from the tendon tissue samples and subsequent cDNA synthesis methods were adapted from methods previously used by De Oliveira et al. (2019) and Eliasson et al. (2012). Disruption of tendon tissue using a mortar and pestle and homogenization of the tissue using a syringe and needle were adapted from the Qiagen RNeasy mini handbook (2019). Total RNA preparation and DNase digestion followed the purification of total RNA protocol from the Qiagen RNeasy Fibrous Tissue Mini Handbook (2020).

The RNase treated mortar and pestle was precooled to close to liquid nitrogen temperatures. When the boiling of the nitrogen was less vigorous, the pre-weighed tendon tissue sample was added and crushed to a fine powder before being transferred to a sterile microfuge tube in a frozen state. RLT lysis buffer (100 µL) was added to the tube and homogenized by drawing the lysate into a sterile 1 mL syringe and 21-gauge needle until a homogenous lysate was achieved. To the lysate, 520 µL of RNase-free water and 10 µL of Proteinase K was added, mixed via gentle pipetting, and incubated in a hot water bath set at 55°C for 10 minutes. After incubation, the lysate was centrifuged at 10,000 x g for 3 minutes at 15°C - 25°C and the supernatant was transferred to a new, sterile microfuge tube. A volume of

anhydrous ethanol that was approximately half of the volume of the transferred supernatant was added and mixed via pipette. The mixture was centrifuged at 8000 x g for 15 seconds at 15°C - 25°C through a RNeasy mini spin column placed in a 2 mL collection tube provided in the Qiagen Fibrous Tissue Mini Kit in 700 µL aliquots. The spin column, which contained the extracted RNA, was washed by adding 350 µL of the included RW1 wash buffer and centrifuging 8000 x g for 15 seconds at 15°C - 25°C and the flow-through was discarded.

The DNase I incubation mix was prepared just prior to its use in the RNA extraction and purification. The 10 µL aliquot of DNase I provided in the RNase-free DNase set included in the Qiagen Fibrous tissue mini kit was thawed and 70 µL of the included RDD buffer was added to the DNase I tube. The DNase incubation mixture was gently inverted to mix to avoid physical denaturation of the DNase enzyme. The entire 80 µL of the DNase incubation mix was applied to the spin column membrane, ensuring complete coverage of the membrane to avoid incomplete DNA digestion, and incubated at room temperature for 15 minutes.

After incubation, 350 µL of RW1 buffer was added to the spin column to wash the column and centrifuged as in the previous washing step. Two washing steps were performed using 500 µL of the prepared RPE buffer. The first RPE wash was added to the spin column and centrifuged at 8000 x g for 15 seconds at 15°C - 25°C and the flow-through was discarded. The second RPE wash was done similarly to the first wash but was spun for 2 minutes to dry the spin column. The spin column was then transferred to a new collection tube and centrifuged at 10,000 x g for 1 minute at 15°C - 25°C to ensure that no ethanol is carried over in the RNA elution.

The spin column was placed in a new sterile 1.5 mL collection tube and 30 µL of RNase-free water was added directly to the spin column membrane and centrifuged at 8000 x g for 1

minute at 15°C - 25°C to elute the RNA. A 2 µL sample was taken from this first elution and used to determine the concentration and purity of the extracted RNA using NanoDrop spectrophotometry (NanoDrop One). A second elution using 30 µL of RNase-free water was done using a new second sterile 1.5 mL collection tube. This was done in order to avoid potentially diluting or contaminating the first elution and was analyzed in the same way as the first elution. An RNA concentration from elutions that were equal to or above 16.67 $\frac{ng}{\mu L}$ was considered viable to proceed to cDNA synthesis as any less than this would be insufficient to obtain the 100 ng of RNA needed for the synthesis method. This was repeated until the NanoDrop determined that an elution contained less than the minimum viable RNA concentration to proceed to cDNA synthesis. Afterwards, cDNA synthesis was conducted immediately afterwards on samples with a concentration between 16.67 – 100 $\frac{ng}{\mu L}$. Though, if necessary, the extracted RNA from the tendon samples were frozen at -20 °C until cDNA synthesis could be performed.

cDNA Synthesis from RNA Extracted from Tendons

The protocol for cDNA synthesis from the total purified RNA extracted from the tendon samples was followed according to the Protoscript II cDNA FirstStrand synthesis kit (New England BioLabs) using their Standard Protocol (2020). The components of the Protoscript II cDNA FirstStrand synthesis kit were thawed on ice and inverted to mix as recommended by the manufacturer. All reagents of this kit were kept on ice until needed.

The concentration of extracted RNA from the tendon samples was used to calculate the volume of eluted RNA needed to obtain approximately 100 ng of RNA using the formula:

$$\frac{100\ ng\ RNA\ needed}{conc.\ RNA\ extracted\ from\ sample} = X\ \mu L\ sample\ needed$$

Once the necessary volume of extracted RNA was determined, it was added to a sterile 200 µL PCR tube along with 2 µL of the included Oligo-d(T) mix. If necessary, nuclease-free water was added to the PCR tube to achieve a final volume of 8 µL. A second tube was prepared following the same method and act as a control. The RNA/primer mix was then denatured in a thermocycler set to 65 °C for 5 minutes. Immediately after denaturing, the tubes were placed on ice. To both the experimental and the control tube, 10 µL of the included Protoscript II reaction mix was added to the denatured RNA/Primer mixture. Protoscript II enzyme mix (2 µL) was added to the experimental tube and the control received 2 µL on nuclease-free water instead of the enzyme mixture. The PCR tubes were placed in a thermocycler which was programed for one cycle of 42 °C for 60 minutes, then 80 °C for 5 minutes, and finally to hold at a temperature of 4 °C. After cDNA synthesis, the samples were stored at -20 °C until use in the PCR reaction.

Amplification of cDNA by PCR

PCR Reagent Preparation

The procedure for amplification was followed according to the manufacturer's recommended standard application method, following a 25 µL reaction volume, in the GoTaq Hot Start Green Master Mix usage information (Promega, 2018) with a slight modification for efficiency testing multiple samples (discussed below). The primers that will be used are based on previous work from Heinemeier et al. (2007) and were sourced from Integrated DNA Technologies (IDT). Forward and reverse primers were obtained for Col1a1 (collagen type I alpha

chain), Col3a1 (collagen type III alpha chain), and GADPH which will act as a housekeeping gene and allow us to determine the relative expression of the collagen types being tested.

The GoTaq Hot Start Green Master mix was thawed at room temperature and centrifuged before use, as recommended by the manufacturer. 100 µM primer stock solutions were prepared according to the instruction provided by the IDT product information; However, TE buffer was used instead of Nuclease-free water (NF-H_2O) to allow higher stability of the primer stock solutions and prevent primer degradation. After preparing the 100 µM primer stock solutions, they were stored at -80°C until needed and thawed at room temperature. A 1:10 dilution was done by adding 10 µL of the 100 µM primer stock solution to 90 µL of NF-H2O to obtain the 10 µM forward and reverse primer working solutions. The working primer solutions were briefly vortexed and centrifuged to mix and collect the material in the bottom of the tubes. Synthesized cDNA was thawed at room temperature and mixed before use. PCR tubes were labeled with, "X" designating control cDNA synthesis reactions that received no reverse transcriptase enzyme. All reaction mixes were prepared over ice to prevent degradation of the primers.

Preparing the PCR Master Reaction Mix

A single 25 µL reaction volume was prepared by adding 12.5 µL of the GoTaq Hot Start Green Master Mix 2X, 2 µL of each the 10 µM upstream primer and the 10 µM downstream primer, and between 1 to 5 µL of the synthesized cDNA, such that the final volume of cDNA added is below 250 ng. The reaction volume was brought up to 25 µL with nuclease-free water (Promega, 2018). However, since multiple samples will be tested, for efficiency, a master reaction mixture that excludes addition of synthesized cDNA was prepared on the day of the

PCR reaction based on the number of samples being tested. The volumes required to prepare the master reaction mixture was calculated using the following equation:

$$(X\mu\text{L}) \times (Y + 2) = Z\mu\text{L needed for Y samples}$$

Where *X* = volume of material (i.e. 2X GoTaq, 10µM forward/reverse primer, or NF-H_2O) needed to prepare a single reaction, *Y* = the number of samples being tested, and *Z* = volume of reagent "X" needed to prepare the master reaction mix. Enough master reaction mix was prepared to allow for two additional tubes; one for a control tube testing for DNA contamination in the provided NF-H_2O, and another to account for potential losses during pipetting and ensuring enough master reaction mix is prepared for all samples.

Once the reaction mixture was prepared, 24 µL of the mix was added to chilled 200 µL PCR tubes. For test reactions (i.e. from the cDNA synthesis samples regardless of if enzyme was added), 1 µL of synthesized cDNA was added to its corresponding tube. For the control reaction testing for NF-H2O contamination, 1 µL of NF-H2O was added. Each tube was kept closed during the entire process, only being opened during an addition and immediately re-closed to avoid possible contamination. After every reaction mixture was complete, the tubes were flicked to mix then briefly centrifuged to bring the material to the bottom of the tube.

Thermocycling Program

The tubes were placed in a thermocycler at room temperature. The thermocycler was programmed with an initial denaturation at 95 °C was done to inactivate the antibody in the GoTaq Hot Start Green Master Mix and initiate the hot-start PCR. Any denaturation steps after

this initial denaturation were 60 seconds long. The annealing temperature was set at 55 °C. The annealing step took place 60 seconds.

The extension portion of the reaction took place at optimal temperatures for Taq DNA polymerase (72 – 74 °C) and lasted approximately 1 minute per every 1 kbp of DNA to be amplified according to the manufacturers protocol. This was done for an initial, pilot PCR reaction. Because the mRNA transcripts for Col1a1 (5,843 bp), Col3a1 (4,792 bp), and GAPDH (1,306 bp) are different lengths, all samples were programmed to go through a 6-minute extension cycle based off of the largest transcript being tested, allowing equal treatment of the samples. This was later changed to 30 seconds for all samples after the pilot reaction because the predicted PCR product from the mRNA transcripts for Col1a1 (129 bp product), Col3a1 (143 bp product), and GAPDH (98 bp product) were all under 1 kb without promiscuous binding of the primers to the undesired product (determined using Primer-BLAST search through NCBI). There were 25 cycles of amplification performed. The final extension was 10 minutes long. After the final extension, a soak cycle set to hold the PCR reaction at 25 °C was done. After the program completed, the samples were removed from the thermocycler and either stored or electrophoresed immediately. For storage, the amplified cDNA was stored at -20°C until needed for electrophoresis.

Electrophoresis of PCR Product on 1% Agarose Gel

A precast 1% agarose gel containing a fluorescent green dye was placed an Embi Tec RunOne electrophoresis unit with the wells oriented toward the cathode. 1X TBE buffer was added to the fill line and completely covered the gel. Air bubbles in the wells were removed by flushing them with the 1X TBE buffer using a pipettor. One well was loaded with 10 µL of Quick-

Load 1kb Extend DNA Ladder and a second well was loaded with 10 µL of a 100 bp ladder (New England BioLabs). Because the GoTaq HotStart Green Master Mix contains the dye and glycerol to increase the density, no additional loading dye was mixed with the samples. Instead, 5 µL of the amplified cDNA from the PCR was added to each well directly. The electrophoresis unit was run at 100V for approximately 30 minutes. Once complete, the gel was removed from the electrophoresis unit and as much excess TBE buffer as possible was allowed to drip off of the gel before moving to the PrepOne Illuminator for imaging and viewing. Images of the gel were taking using a camera and the picture files were transferred to a computer and saved. Once the gel was imaged and saved, the gel was discarded.

Testing Primers Against Tendon Genomic DNA of Subject A85[a] (Sample #96c[a])

Harvesting of the 4mm Tendon Segment from #96c[a]

All metal instruments (such as surgical scissors, forceps, scalpel handle with metric length graduations) were washed and autoclaved as described previously prior to 4mm segment genomic DNA extraction. Additionally, a mortar and pestle were washed and treated using NucleasEliminator prior to extraction as described previously.

Harvesting the 4mm tendon segment from sample 96c[a] was conducted following the same procedure as described previously for the samples destined for RNA extraction with some exception due to the nature of the sample and the intended use. Primarily, this 4mm segment was not cryopreserved under liquid nitrogen after original harvest following sacrifice of subject A85[a], but was stored at -20°C, nor was the 4mm segment cryopreserved after excision. Instead, after harvesting the segment and obtaining the mass of the segment, this sample was immediately used for extracting genomic DNA. The remainder sample 96c[a] (i.e., the foot, tricep

surae muscles, and the rest of the tendon without the 4mm segment) was re-wrapped in PBS-soaked gauze and stored at -20°C to serve as a source of genomic DNA if needed for future extraction. With the exception of these changes to the original tendon segment harvesting for collagen analysis method, the remainder of the previously described methods were followed identically.

Genomic DNA Extraction and Purification from Tendon Segment

The genomic DNA extraction and purification of the 4mm tendon segment of sample #96c[a] was performed using the Wizard Genomic DNA Purification Kit following the Animal Tissue (Mouse Tail) protocol outlined by the manufacturer in the "Isolating Genomic DNA from Tissue Culture Cells and Animal Tissue" section. Briefly, 120 µL of 0.5M EDTA (pH 8.0) and 500 µL of the provided Nuclei lysis solution were mixed in a 1.5 mL microfuge tube and chilled over ice. The NucleasEliminator treated mortar and pestle were prechilled to liquid nitrogen temperature prior to adding the 4 mm tendon segment. The tendon segment was allowed to cool to liquid nitrogen temperature through three liquid nitrogen addition and evaporation cycles before grinding the tissue to a powder. Once powderized, the sample was added to a clean 1.5 mL microfuge tube along with 600 µL of the prepared EDTA/Nuclei lysis solution and 17.5 µL of Proteinase K (from the Qiagen RNeasy Fibrous Tissue Mini Kit), then incubated at 55°C in a water bath for 3 hours with vigorous vortexing once per every half hour. Once the sample has been completely digested, 3 µL of RNase A solution was added, mixed by inverting the tube, and incubated at 35°C for 15 minutes. After incubation, the solution was allowed to cool to room temperature before adding 200 µL of the provided protein precipitation solution, followed by vortexing at high speed for 40 seconds. After thoroughly vortexing the mixture, the tube was

chilled over ice for 5 minutes to precipitate the proteins. The mixture was centrifuged for 4 minutes at 15,000 x g to pellet the precipitated protein. After pelleting, the supernatant containing the DNA was transferred to a microfuge tube containing 600 µL of room temperature 100% isopropanol, capped, and inverted several times to mix and precipitate the DNA. The DNA was collected by centrifuging the tube at 15,000 x g for 1 minute to pellet the DNA. The supernatant was discarded, and the DNA was washed using 600 µL of room temperature 70% EtOH, capping, and inverting the tube several times. The tube was again centrifuged at 15,000 x g for 1 minute to pellet the DNA and the majority of the EtOH was removed via pipette with care taken to not disturb the pelleted DNA. The DNA was air-dried by opening the tube and inverting the open tube over paper towel for 30 minutes. After drying, 100 µL of the provided DNA rehydrating solution was added to the DNA and allowed to rehydrate for 3 days at 4°C. After rehydrating, the concentration of the DNA was determined via NanoDrop. To confirm that the extracted DNA was present as intact DNA from the extraction, the DNA was electrophoresed on 1% agarose gel at 3 different DNA concentrations (3 µL, 5 µL, and 10 µL) mixed with 2 µL of tracking dye each, then visualized.

DNA PCR of Tendon Genomic DNA using RT-PCR Primer Sets

The PCR reagents used to amplify the genomic DNA samples were prepared identically to the reagent preparation described above for amplifying the synthesized cDNA with the exception of preparing the master mix for multiple PCR reactions. Instead, a single reaction mixture was prepared individually for each primer set. For each primer set, two tubes were prepared, with one that will act as the experimental sample and the other that would act as an internal control to ensure contamination of the reagents did not occur. To prepare the

individual PCR reaction mixes, 12.5 µL of 2X GoTaq HotStart Green Master mix, 7.5 µL of the provided nuclease-free water, and 2 µL of each prepared 10 µM forward and reverse primers were added to 200 µL PCR tubes. To the experimental sample tube, 1 µL of the extracted genomic DNA was added while the control tube received an additional 1 µL of nuclease-free water. Reaction mixes were prepared for all three primer sets before mixing by flicking the tubes, then briefly centrifuging to bring the reaction mixtures to the bottom of the tubes before loading into the thermocycler. The thermocycler was programmed to use the same cycles as described previously with exception to the extension time. The extension cycle was set for 6 minutes to allow the possibility for full extension of the largest mRNA transcript (Col1a1 = 5,843 bp). The remainder of the temperatures, times, and number of cycles in the program remained the same. Once the program had finished, the 5 µL from each tube were loaded into wells of a 1% agarose gel, with the first well being loaded with 10 µL of Quick-Load 1kb Extend DNA Ladder (New England BioLabs), then electrophoresed at 100V for 30 minutes. The finished gels were visualized and imaged as described previously.

Results:

Quantifying Platelet Concentration Range in PRP Injection

The Platelet-rich plasma (PRP) was prepared from the blood collected from the Lewis rat subjects used in this study. The blood was obtained via exsanguination at the time of sacrifice from non-survival surgeries, such as harvesting the fibula and tibia bones for preparing the Mesenchymal stromal cells (MSCs) and the repaired tendon tissues. Fibrin clot formation was prevented during collection using anti-coagulant agents. Complete preparation and cryopreservation for storing the PRP was done on the day that the blood was collected which was thawed and prepared as needed. A platelet count using 10 µL of diluted PRP was visualized under 400X magnification on a hemacytometer. Each platelet count was conducted in triplicate on three separate PRP sample preparations. We diluted the sample 1:100 and 1:1000 prior to each count. The platelets were counted from the four edge corners of the central grid of a hemacytometer (**Figure 2**). Because only 4 of the 25 total grid squares were counted, we calculated the average number of platelets per large square (i.e., the whole grid) by adding the platelets counted in the four counted grid squares, then dividing by 4 to obtain the average number of platelets in the grid square. This number was multiplied by 25 to obtain the average number of platelets per large square. A sample calculation for sample 1 diluted 1:100 is shown below in **Sample calculation 1**. From this, we calculated our platelet count in $\frac{platelets}{mL}$ by using the equation shown in **Equation 1**.

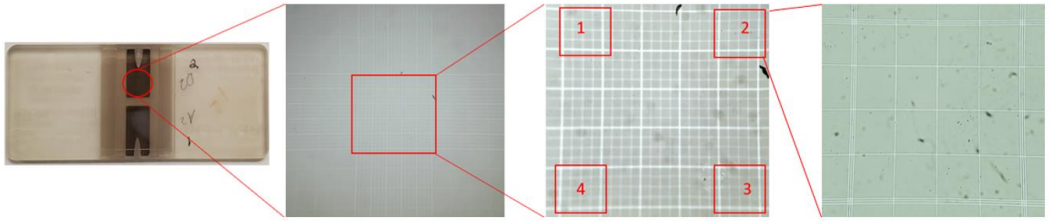

Figure 2: Platelet count method using a hemacytometer. The pictures above show the hemacytometer grids (without applying a PRP sample) visualized through a light microscope at the corresponding magnifications. The second image after the hemacytometer depicts the grid magnified at 40X magnification under light microscopy. The central grid was used for the platelet count and is magnified in in the following image. The boxed and numbered sections of the grid visualized at 100X magnification represents one “small square”. Due to the size of the platelets, the platelets were identified and counted under 400X magnification depicted in the final image.

$$31 + 25 + 59 + 47 = 162\ total\ platelets\ counted\ in\ four\ small\ grid\ squares$$

$$\frac{162\ total\ platelets\ counted}{4} = 40.5\left(\frac{platelet\ average}{small\ grid\ square}\right)$$

$$\left(40.5\left(\frac{platelet\ average}{small\ grid\ square}\right)\right) x\ 25\ total\ grid\ squares = 1.0x10^3\ \frac{platelets}{large\ square}$$

Sample Calculation 1: Average number of platelets per large grid square for PRP sample 1 diluted 1:100 in 1X PBS.

$$Platelets\ per\ mL = count\ per\ large\ square\ x\ 10^4\ x\ \left(\frac{1}{dilution}\right)$$

Equation 1: Calculating $\frac{platelets}{mL}$ from average number of platelets per large grid square counted using the hemacytometer, where 10^4 is the constant factor used to correct for the volume under the cover slip in one large square and convert it to a count for 1 ml of solution.

The mean and standard deviations were calculated for each platelet count at a 1:100 and a 1:1000 dilution. A one-way ANOVA was performed on both dilutions to determine if there was a significant difference between the three samples. All samples tested had a higher platelet count than the 2.0 x 10^5 $\frac{platelets}{mL}$ physiological platelet concentration. The mean platelet concentration ranged from 0.75 x 10^9 $\frac{platelets}{mL}$ to 2.35 x 10^9 $\frac{platelets}{mL}$ with a standard deviation ranging from 0.16 x 10^9 $\frac{platelets}{mL}$ to 1.31 x 10^9 $\frac{platelets}{mL}$. The result of the one-way ANOVA determined that no significant differences exist ($p > 0.05$) between the PRP preparations in either the 1:100 ($p = 0.37$) or the 1:1000 ($p = 0.84$) dilutions (**Table 1**). The mean platelet concentration from our count was found to be within or exceed our targeted platelet concentration range of 6.0x10^7 – 1.5x10^9 $\frac{platelets}{mL}$ for platelet enriched plasma.

<u>Table 1:</u> Platelet injection concentrations of three PRP samples prepared separately.

PRP Sample [a]	1		2		3	
Dilution [b]	**1:100**	**1:1000**	**1:100**	**1:1000**	**1:100**	**1:1000**
	1.00 x10^9	1.60 x10^9	1.13 x10^9	1.70 x10^9	0.78 x10^9	2.75 x10^9
	0.66 x10^9	2.90 x10^9	1.00 x10^9	3.80 x10^9	0.92 x10^9	1.60 x10^9
	0.58 x10^9	1.25 x10^9	0.77 x10^9	1.40 x10^9	1.10 x10^9	2.70 x10^9
Mean [c]	***0.75* x10^9**	***1.92* x10^9**	***0.97* x10^9**	***2.30* x10^9**	***0.93* x10^9**	***2.35* x10^9**
SD	*0.23 x10^9*	*0.87 x10^9*	*0.18 x10^9*	*1.31 x10^9*	*0.16 x10^9*	*0.65 x10^9*
p-value [d]					**0.37**	**0.84**

[a] Platelet concentrations were determined by counting platelets from 10µL of the diluted samples using a hemocytometer and the average platelet concentration was calculated. Each PRP count was performed in triplicate.

[b] 1:100 and 1:1000 dilutions were chosen for a more accurate count as a 1:10 dilution showed too many platelets in the test sample to accurately count.

[c] Mean platelet concentrations ranged from 7.45 x 10^8 - 2.35 x 10^9 $\frac{platelets}{mL}$. All samples tested had a higher platelet count than the 2.0 x 10^5 $\frac{platelets}{mL}$ physiological platelet concentration.

[d] A one way ANOVA was conducted to determine if significant differences were seen between three separate PRP preparations at a 1:100 and 1:1000 dilutions. The samples showed no statistically significant differences ($p > 0.05$) between the PRP preparations in either the 1:100 ($p = 0.37$) or the 1:1000 ($p=0.84$) dilutions.

MSC Preparation

Mesenchymal stromal cells were harvested from the femurs and tibias from Lewis Rats. The bones were cleaned of any extraneous muscle or connective tissue prior to removal of the proximal and distal epiphysis regions of the bones. The bones were flushed using α-MEM media, serving to extract the bone marrow containing the mesenchymal stromal cells, suspend them in the media, and remove the large pieces of extra tissues and bone fragments. The suspended cells were counted using a hemacytometer, as previously described, and resuspended in complete α-MEM to achieve a concentration of $5x10^5 \frac{cells}{mL}$. The cells were placed in a T-75 flask and cultured for 4 days before removing the non-adherent cells from the flask. The adherent cells were cultured and passaged 3 times by treatment with Trypsin and EDTA and dilution into twice as much media in two flasks. After three passages, the cells were slowly frozen and stored in 10% DMSO in liquid nitrogen until needed.

Differentiation Assays

To determine if the isolated mesenchymal stromal cells could be classified as mesenchymal stem cells (MSCs), differentiation assays were performed. For the Differentiation assays, $2x10^5 \frac{cells}{mL}$ of our third passage Mesenchymal stromal cells were plated in three 6-well plates, with each well being maintained using complete α-MEM media for the first day. On the second day, three of the six wells were switched to differentiation media, while the remaining three wells continued to be maintained using α-MEM complete media. The cells were cultured for three-weeks then stained using Alizarin red S, Oil red O, and Alcean blue stains to determine osteogenic, adipogenic, and chondrogenic differentiation, respectively. Each 6-well plate provided results in triplicate, with each triplicate assay being done twice.

For all differentiation assays, the control cultures that were maintained using α-MEM media were all seen to be plastic adherent, showing a spindle-shaped morphology. The control cultures showed no staining when each stain was applied to the cultures, indicating that differentiation did not occur in the cultures maintained using the non-differentiation inducing α-MEM media (**Figure 3**, **Figure 4**, **Figure 5**).

Osteogenic Differentiation Assay

The cultures maintained using the osteogenic media (**Fig. 3**, A and C) were seen to have altered morphology in comparison to the controls after three weeks (**Fig. 3**, B and D). Rather than the spindle-shaped cells seen in the control cultures, clusters of aggregated, cuboidal shaped cells were visible. (**Fig. 3**, A and C). Additionally, reddish-brown staining was observed in the osteogenic cultures when the Alizarin red S stain was applied to the culture (**Fig. 3A**). The Alizarin red S stain was used to assess used to evaluate Calcium rich deposits by cells in culture (Gregory et al., 2004). The morphological change of the cells and the positive staining of calcium deposition indicates the development of osteoblasts or osteocytes within these cultures.

Adipogenic Differentiation Assay

The cultures maintained for 3 weeks using the adipogenic media (**Fig. 4**, A and C) were visualized after staining using Oil red O stain. Oil red O is a stain that is soluble in lipids and stains triglycerides (Vader et al. 2011). When used in cell cultures, Oil red O stains the intracellular lipid droplets found in adipocytes and serves as an indicator of the occurrence of lipogenesis. The cell cultures maintained using this differentiation media had morphological

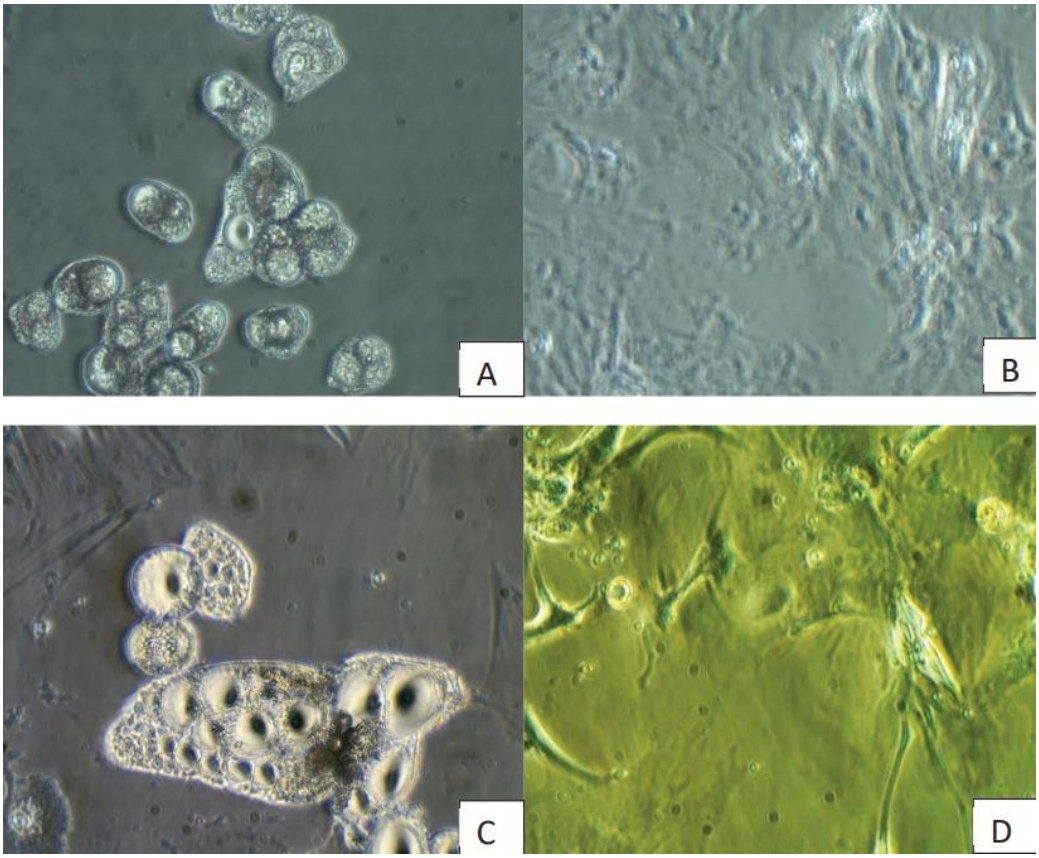

Figure 3: Osteogenic Differentiation Assay. MSCs cultured 3 weeks with (A and C) and without (B and D) osteogenic differentiation media and stained with Alizarin red S stain. *A)* MSCs cultured in osteogenic media stained using Alizarin red S stain imaged at 100X magnification. *B)* MSCs cultured in α-MEM media and stained using Alizarin red S stain imaged at 100X magnification. *C)* MSCs cultured in osteogenic media stained using Alizarin red S stain imaged at 200X magnification. *D)* MSCs cultured in α-MEM media and stained using Alizarin red S stain imaged at 200X magnification. Reddish-brown staining indicates calcification of the extracellular matrix. Morphological changes from fibroblast-like cells to aggregated nodules of cells with a cuboidal appearance also indicate successful differentiation of the MSCs.

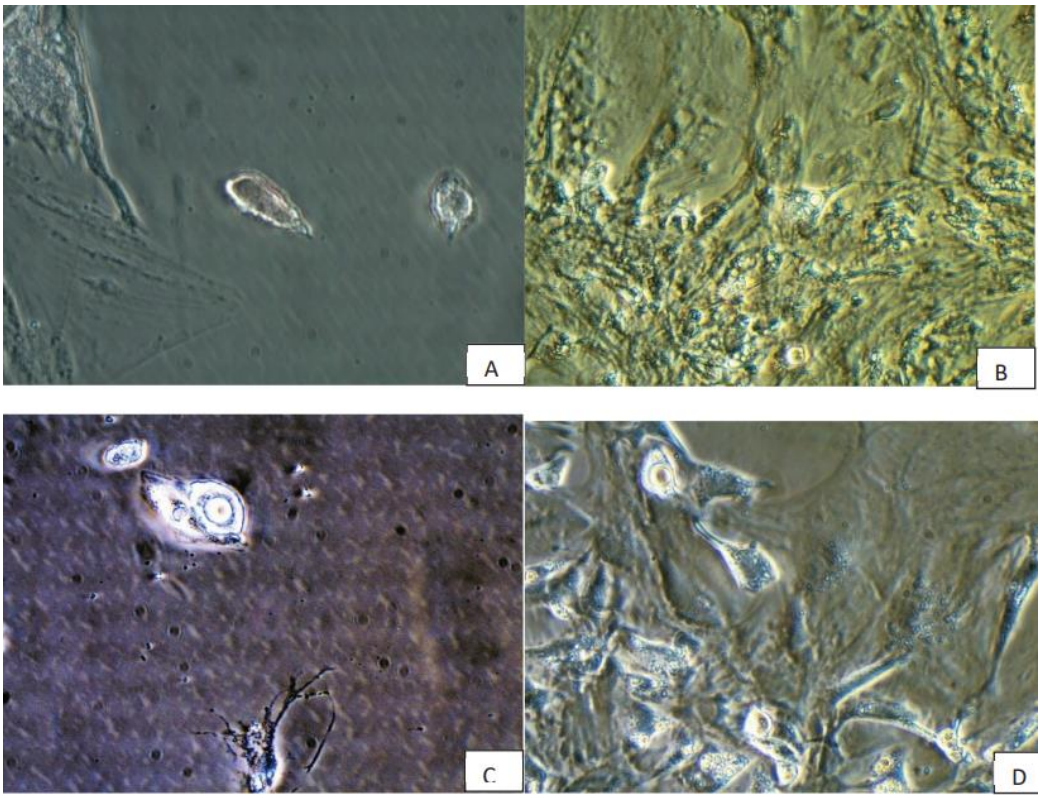

Figure 4: Adipogenic Differentiation Assay. MSCs cultured 3 weeks with (A and C) and without (B and D) adipogenic differentiation media and stained with Oil red O stain. *A)* MSCs cultured in adipogenic media stained using Oil red O stain imaged at 100X magnification. *B)* MSCs cultured in α-MEM media and stained using Oil red O stain imaged at 100X magnification. *C)* MSCs cultured in adipogenic media stained using Oil red O stain imaged at 200X magnification. *D)* MSCs cultured in α-MEM media and stained using Oil red O stain imaged at 200X magnification. Red staining and intracellular lipid droplet inclusion indicates occurrence of lipogenesis. Morphological changes, such as intracellular lipid droplets, indicates successful MSC differentiation.

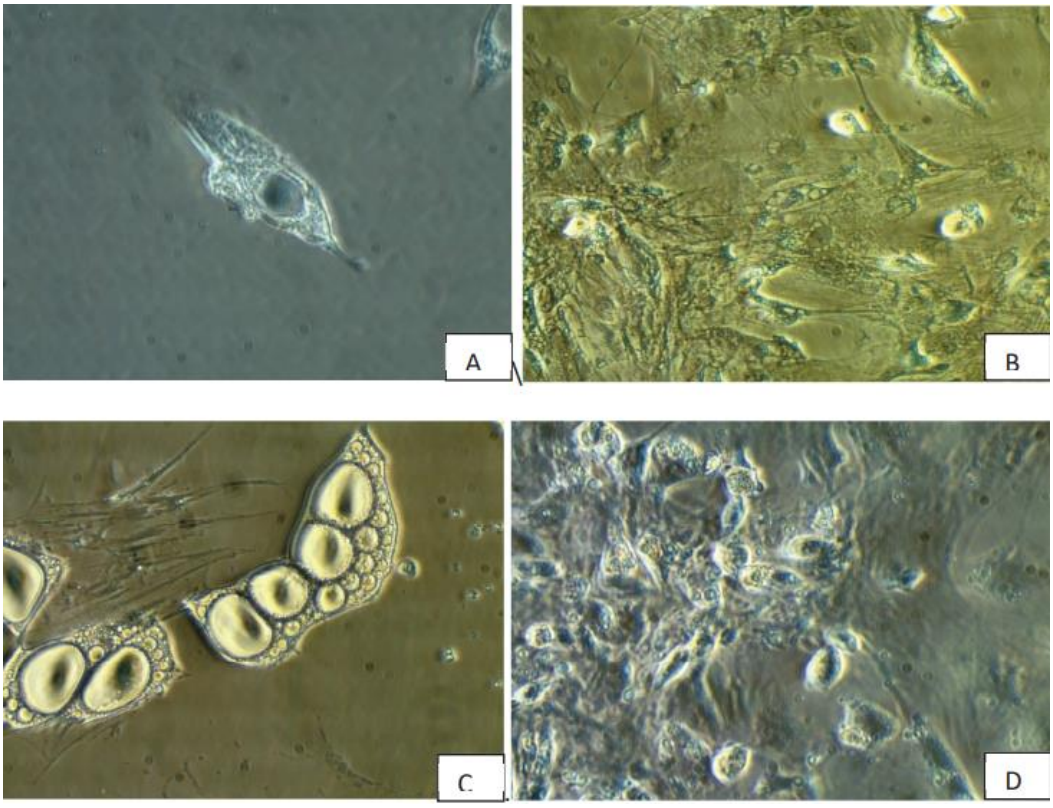

Figure 5: **Chondrogenic Differentiation Assay.** MSCs cultured 3 weeks with (A and C) and without (B and D) chondrogenic differentiation media and stained with 0.01% Alcean blue stain. *A)* MSCs cultured in chondrogenic media stained using Alcean blue stain imaged at 100X magnification. *B)* MSCs cultured in α-MEM media and stained using Alcean blue stain imaged at 100X magnification. *C)* MSCs cultured in chondrogenic media stained using Alcean blue stain imaged at 200X magnification. *D)* MSCs cultured in α-MEM media and stained using Alcean blue stain imaged at 200X magnification. Blue staining indicates deposition of collagen. Morphological changes such as the loss of the fibroblast-like shape and the formation of large, rounded cells surrounded by a collagen rich ECM, indicates successful differentiation of the MSCs.

changes (**Fig. 4C**) indicating the formation of an intracellular lipid droplets. These lipid droplets are a distinguishing characteristic of adipogenic cells. Positive red staining from the Oil red O was observed in these cells. The positive staining was easiest to see when visualized at a lower magnification such as depicted in **Figure 4A**. At a higher magnification (**Fig. 4C**), this staining as also present. The control cultures were also treated using the same Oil red O staining procedure which resulted in a negative staining result (**Fig. 4**, B and D). These results suggest successful differentiation of the MSCs down the adipogenic cell lineage.

Chondrogenic Differentiation Assay

The cell cultures maintained using the chondrogenic differentiation media (**Fig. 5**, A and C) also had morphological changes when compared to the control cultures maintained using the non-differentiation inducing media (**Fig. 5**, B and D). Similar to the morphological changes seen in the osteogenic differentiation, we observed changes from a fibroblast-like morphology to a more rounded shape with a large ECM, arranged in a way that visually appears similar to isogenous groups found in cartilage tissue sections (**Fig. 5C**). The rich blue staining observed when Alcean Blue was applied (**Fig. 5A**) indicates collagen deposition to the extracellular matrix. These results indicate successful differentiation of the MSCs down the chondrogenic cell lineage.

Surgical Manipulations and Subject Use

In total, 124 male Lewis rats were used in this study, including the 2 rats used to obtain the initial MSC stock and 3 rats used to obtain the blood used to prepare the initial PRP stock. Of those, 119 underwent the surgical laceration and repair of the calcaneal tendon. There was a

total of 104 that were used for tensile tests (**Table 2** and **Table 3**). Three rats expired after administration of the post-operational analgesic. The death of these subjects may have been due to severe respiratory depression initially caused by the anesthetic effect of isofluorane but became fatal when the buprenorphine was administered while the animal was still anesthetized. This resulted in a minor change in procedure where buprenorphine was administered only after the anesthesia effect from the isofluorane began to wear off and the animal became ambulatory. No additional fatalities occurred after this procedural change. Four samples from treatment receiving subjects sustained damage prior to tensile testing, which may have affected the final results and required replacement. As these losses occurred early in the sample collection phase, these four lost samples from the treatment receiving groups were able to be replaced. However, one operated sample (sample #96[a] from subject A85[a]) from the surgical control group was damaged during harvesting, making it so both samples could not be used for tensile testing. Due to this occurring late in the sample collection phase, Dr. Drew's availability, and low subject availability coupled with the necessary acclimation time required in obtaining more Lewis rat subjects, this sample could not be replaced. This was the only sample that could not be replaced. However, the companion unoperated tendon (sample #96c[a] of subject A85[a]) was intact after harvest and was used to supplement data in the Collagen analysis. Our total for animals designated for tensile testing was 99. Of the surgical control group, 5 animals were designated to use the tendon vise lower fixturing method which we used for our analysis as it is consistent with the method used to test the treated tendons. The remaining 5 were designated for tensile testing using a separate epoxy box lower fixturing method (results not shown). The weight of the rats used in the 1-week recovery sub-groups for tensile testing ranged from 238g – 363g and those in the 2-week recovery group ranged from 267g – 361g. Three subjects from each group were designated for use in collagen analysis, totaling 15 subjects with no losses

Table 2: Study Design

Experimental group	Sub-group	Treatment	Time of sacrifice (weeks)
1	A	CollaTape[a] only	1
	B	CollaTape only	2[e]
2	A	CollaTape + PRP[b]	1
	B	CollaTape + PRP	2[e]
3	A	CollaTape + MSC[c]	1
	B	CollaTape + MSC	2[e]
4	A	CollaTape + MSC + PRP	1
	B	CollaTape + MSC + PRP	2[e]
5	A	Surgical control[d]	1
	B	Surgical control	2[e]

[a] An 8mm by 13mm strip of CollaTape (Col) was wrapped around the site of repaired Achilles tendon.

[b] After approximating the skin post-repair, 0.1 mL of PRP was injected subcutaneously adjacent to the site of surgical laceration of the Achilles tendon.

[c] After approximating the skin post-repair, 1 x 10^5 $\frac{cells}{mL}$ of rat MSCs was injected subcutaneously adjacent to the site of surgical laceration of the Achilles tendon.

[d] The damaged tendon received no additional treatment following the surgical repair.

[e] A subset of 2-week recovery from each group were used for collagen expression analysis (n=3)

Table 3: Achilles tendon surgery and harvest schedule.

Sample #	Treatment	Healing Time	Surgery Date	Harvest Date	Use	n
A1 - A5	col [e]	1 wk a	2/6/2019	2/13/2019	tensile testing	6 [b]
A6 - A8	col	1 wk c	3/1/2019	3/8/2019	tensile testing	3
A9 - A10	col	1 wk c	4/9/2019	4/16/2019	tensile testing	2
A11 - A15	col+PRP [f]	1 wk a	2/6/2019	2/13/2019	tensile testing	6 [b]
A16 - A19	col+PRP	1 wk c	3/1/2019	3/8/2019	tensile testing	4
A20	col+PRP	1 wk c	4/9/2019	4/16/2019	tensile testing	1
A21 - A24	col+MSC [g]	1 wk b	2/27/2019	3/6/2019	tensile testing	5 [b c]
A25 - A26	col+MSC	1 wk b	4/9/2019	4/16/2019	tensile testing	2
A27 - A31	col+MSC	1 wk d	4/4/2019	4/11/2019	tensile testing	5
A32 - A36	col + both [h]	1 wk b	2/27/2019	3/6/2019	tensile testing	5
A37 - A41	col + both	1 wk d	4/4/2019	4/11/2019	tensile testing	5
A42 - A46	col	2 wk a	2/13/2019	2/27/2019	tensile testing	5
A47 - A51	col	2 wk c	3/22/2019	4/5/2019	tensile testing	5
A52 - A56	col+PRP	2 wk a	2/13/2019	2/27/2019	tensile testing	5
A57 - A61	col+PRP	2 wk c	3/22/2019	4/5/2019	tensile testing	5
A62 - A66	col +MSC	2 wk b	3/8/2019	3/22/2019	tensile testing	5
A67 - A71	col+MSC	2 wk d	3/29/2019	4/12/2019	tensile testing	5
A72 - A76	col+both	2 wk b	3/8/2019	3/22/2019	tensile testing	5
A77 - A81	col + both	2 wk d	3/29/2019	4/12/2019	tensile testing	5
A81[a] - A90[a]	none[a i]	2 wk e	10/22/2019	11/5/2019	tensile testing	10 [d]
A91[a] - A100[a]	none[a]	1 wk f	10/29/2019	11/6/2019	tensile testing	10
Total						104
A101 - A103	none	2 wk	11/6/2019	11/20/2019	collagen analysis	3
A104 - A106	col	2 wk	11/6/2019	11/20/2019	collagen analysis	3
A107 - A109	col+PRP	2 wk	11/8/2019	11/22/2019	collagen analysis	3
A110 - A112	col+MSC	2 wk	11/8/2019	11/22/2019	collagen analysis	3
A113 - A115	col+both	2 wk	11/8/2019	11/22/2019	collagen analysis	3
Total						15

[a] The surgical controls designated for tensile testing (A81[a] – A100[a]) were conducted after all samples that had received treatment using the biologics (A1 – A81) had undergone biomechanical testing. The sample and blinding numbers for the surgical controls represent a separate version of subject labeling.

[b] After surgical repair of the lacerated tendon and administration of treatment, one subject from the CollaTape only (conducted on 2/6/19), CollaTape with PRP injection (conducted on 2/6/19), and CollaTape with MSC injection (conducted on 2/27/19) had died after administration of 0.1 mL 0.03$\frac{mg}{mL}$ buprenorphine analgesic. To account for the lost subjects, and additional surgery date was scheduled to obtain the samples (conducted 4/9/19).

[c] Prior to tensile testing, structural damage was observed in a tendon harvested from this group (conducted 2/27/19) that would affect the final results and was therefore removed from the study. An additional MSC was done to replace a damaged one for tensile testing (conducted 4/9/19).

[d] The operated sample from subject A85[a] (sample #96[a]) was damaged during harvest and both samples could not be used in tensile testing. Due to time, subject availability, and scheduling complications, this sample could not be replaced.

[e] The subjects that received the CollaTape only treatment (col) had a 8 x 13 mm piece of CollaTape wrapped around the surgically repaired calcaneal tendon (right hindlimb) before approximating the skin to close the surgical incision. These subjects received no injection of the other biologics (i.e, PRP or MSC) used in this study.

[f] The subjects that received the CollaTape with a 0.1 mL injection of Platelet-Rich Plasma treatment (col+PRP) followed the treatment for Collatape only but after closing the surgical incision received one subcutaneous injection of 0.1 mL Platelet-Rich Plasma adjacent to the incision site.

[g] The subjects that received the CollaTape with a 0.1 mL injection of $5 \times 10^5 \frac{cells}{mL}$ Mesenchymal Stem Cells in physiological saline treatment (col+MSC) followed the treatment for Collatape only but after closing the surgical incision received one subcutaneous injection of 0.1 mL of $5 \times 10^5 \frac{cells}{mL}$ Mesenchymal Stem Cells in physiological saline adjacent to the incision site.

[h] The subjects that received the CollaTape with both a 0.1 mL injection of $5 \times 10^5 \frac{cells}{mL}$ Mesenchymal Stem Cells in physiological saline and a 0.1 mL injection of Platelet-Rich Plasma treatment (col+both) followed the treatment for Collatape only but after closing the surgical incision received two subcutaneous injections adjacent to the incision site after closure of the surgical wound. The first injection was of 0.1 mL of $5 \times 10^5 \frac{cells}{mL}$ Mesenchymal Stem Cells in physiological saline and the second injection was a 0.1 mL of Platelet-Rich Plasma.

[i] The subjects in the surgical control group (none) received no additional treatment outside of the surgical repair of the lacerated right calcaneal tendon and the post-operational analgesic received by all subjects that underwent surgery. After the repair, the skin was approximated and closed.

experienced during collection (**Table 3**). The total number of subjects intended for use in either tensile testing or collagen analysis in this study are summarized in **Table 3**.

Biomechanical Tensile Testing

Blinding Procedures

The tendons that received treatment (i.e., Col only, Col + PRP, Col + MSC, and Col + PRP + MSC experimental groups) were tensile tested by Brittany Austin (2019). To ensure equal treatment of the samples and avoid potential for bias, the tendon samples were coded to blind the experimenters conducting the tensile tests by assigning a randomized number (ranging from 1 to 81) to the samples. This randomized blinding number was assigned to both the operated tendon and the control tendon, with the unoperated control tendon being designated with the letter "c". This designation to the unoperated control was primarily for ease of tracking which sample came from which subject. Additionally, due to the formation of scar tissues which allowed for a characteristic increase in the operated tendon cross-sectional areas (CSA) and other obvious differences in appearance between the operated and unoperated tendons, attempting to blind the experimenters to operated verses unoperated samples would be unsuccessful. Yet, blinding through the treatment group tested and the post-operation recovery period ensured that the experimenters would not be able to anticipate the outcome based on our hypotheses made for the treatments used, allowing for unbiased testing of samples.

After all of the tendons from subjects that received treatment were tested and the data analyzed, an additional, purely surgical control group was performed that received no CollaTape or other additive after the surgical repair of the tendon. A new blinding system was devised such that the experimenters knew that they were working with surgical controls but did not know the

healing period of the subjects prior to harvest. Additionally, a new numbering system was devised which started at 81^{a}, but unlike subject A81 that received additional biologics treatment, the surgical controls were denoted with a superscript "a" (i.e., subject A81 received Col + PRP + MSC, but subject $A81^{a}$ was a surgical control). The blinding protocol used for this study for both the tendons that received treatment and the surgical controls are summarized in **Table 4**.

Tensile Testing of the Tendons

To determine the effect that the treatments used in each study group had on wound healing, the mechanical properties of the treated tendons were tested. Treatment using only CollaTape was compared to treatments using a combination of CollaTape with an injection of PRP only, MSC only, and both PRP and MSC. This study was conducted in collaboration with the Department of Mechanical Engineering at Youngstown State University and the Department of Orthopedic Surgery at Mercy Health, Youngstown.

A complete rupture of the calcaneal/Achilles tendon was simulated by a transverse surgical laceration and repair conducted by Dr. Stewart Drew (Department of Orthopedic Surgery at Mercy Health Youngstown). Before approximating the skin and closure of the surgical site, CollaTape was wrapped around the repaired tendons of all treatment groups (experimental groups 1 – 4 from **Table 2**). A representation of this procedure is depicted in **Figure 6**. Subjects in experimental groups 2, 3, and 4 (**Table 2**) received an additional treatment injection of PRP only, MSC only, or injections of both PRP and MSC, respectively. These experimental groups were subdivided to have either a 1-week recovery period (Sub-Group A, **Table 2**) or 2-week recovery period (Sub-Group B, **Table 2**) prior to sacrifice. Following recovery, animals were

Table 4: Blinding protocol used for biomechanical testing of the tendons.

Treat.	Col		Col+PRP		Col+MSC		Col+Both		None[a]	
	Sample #	Blinding # [b]	Sample #	Blinding # [b]	Sample #	Blinding # [b]	Sample #	Blinding # [b]	Sample #	Blinding # [b]
1 wk heal time	A1	74	A11	29	A21	20	A32	66	A91[a]	82[a]
	A2	45	A12	13	A22	70	A33	80	A92[a]	83[a]
	A3	36	A13	72	A23	4	A34	39	A93[a]	87[a]
	A4	76	A14	31	A24	49	A35	11	A94[a]	88[a]
	A5	21	A15	75	A25	68	A36	15	A95[a]	92[a]
	A6	47	A16	67	A26	81	A37	34	A96[a]	81[a]
	A7	26	A17	63	A27	53	A38	60	A97[a]	91[a]
	A8	61	A18	79	A28	77	A39	69	A98[a]	85[a]
	A9	25	A19	8	A29	78	A40	64	A99[a]	84[a]
	A10	65	A20	37	A30	56	A41	2	A100[a]	86[a]
					A31	7				
2 wk heal time	A42	30	A52	51	A62	42	A72	3	A81[a]	97[a]
	A43	50	A53	55	A63	59	A73	43	A82[a]	94[a]
	A44	6	A54	1	A64	28	A74	16	A83[a]	100[a]
	A45	71	A55	5	A65	41	A75	17	A84[a]	90[a]
	A46	24	A56	52	A66	57	A76	62	A85[a b]	96[a c]
	A47	48	A57	73	A67	18	A77	22	A86[a]	93[a]
	A48	23	A58	46	A68	27	A78	14	A87[a]	89[a]
	A49	35	A59	10	A69	54	A79	44	A88[a]	95[a]
	A50	12	A60	33	A70	38	A80	58	A89[a]	99[a]
	A51	40	A61	32	A71	9	A81	19	A90[a]	98[a]

[a] The surgical controls (none) were conducted after all animals that received treatment using the biologics (A1 – A81) had undergone biomechanical testing. The sample and blinding numbers for the surgical controls represent a separate version of subject labeling. Instead of blinding the experimenters conducting the tensile tests based on the treatment received, the experimenters were blinded based on the healing time before harvest.

[b] Each sample number corresponds to one animal. Both the left (intact) and right (repaired) were labeled using the blinding number. The intact tendon was signified as a sample control and signified by the letter "c" with the blinding number (i.e., sample #57c is an example of an intact tendon for subject A66, but sample #57 is the repaired tendon from the same subject).

[c] During harvesting of the tendon tissue from subject A85[a], the surgically repaired tendon (sample #96[a]) was damaged, such that it could not be used for tensile testing. Instead, the undamaged control unoperated companion tendon (sample #96c[a]) was used as a source of genomic DNA to compare PCR primer products to those achieved via RT-PCR.

<u>Figure 6:</u> Surgical laceration and repair of Achilles tendon. Depicted is a generalized order of the surgical procedure. The subjects were anesthetized using the anesthesia delivery system depicted in the far-left picture. Once anesthetized, the surgical laceration and repair of the right Achilles tendon was performed (middle picture). For all groups except the surgical control, an 8x10 mm piece of CollaTape was wrapped around the repaired tendon before closing the incision site. After closure of the wound, the subjects were moved to clean recovery cages (right picture) where, if required by their study grouping, they would receive additional treatment injections of PRP, MSC, or both. The first dose of post-operational analgesic was administered in the recovery cage after the anesthetic effects from the isofluorane began to diminish to avoid lethal respiratory depression.

sacrificed via exsanguination and pneumothorax procedures, the animals were weighed and the (right) operated tendon and the (left) unoperated tendon were harvested via sharp dissection.

Brittany Austin (Department of Mechanical Engineering at Youngstown State University) conducted the tensile testing of all samples from treatment receiving subjects. All tensile testing in this study were conducted using the Tendon Vise method depicted in **Figure 7**. A tensile force was applied at a constant rate to the tendon and data was collected until complete tendon failure was observed. Additionally, the locations and modes of failure were also noted (such as the commonly seen failures depicted in **Figure 8**). Results were obtained from each sample for the maximum stress (deformation) and strain (force or load) applied to the tendons, the strain at failure and ultimate tensile strength (UTS), average Young's Modulus (modulus of elasticity), and the elastic and total strain energy. A pictorial representation of the analysis of stress-strain curves can be seen in **Figure 9**.

The initial analysis as raw, unnormalized data can be seen in **Figure 10**. The Col + PRP, Col + MSC, and the combination of Col + PRP + MSC treatments were compared to the Col only group, which was viewed to act as a vehicle for the other biologics. An increase was observed in the maximum stress and average modulus of elasticity between the 1- and 2-week recovery periods in all treatment groups. For the maximum endured stress that the tendons after 1 week of recovery, there was no difference between the treatment groups. Though after a 2-week recovery period, the largest observed increases resulted from the Collagen + PRP and Collagen + MSC treatment groups (**Fig. 10 A**). No significant differences were observed in the strain at failure between the 1- and 2-week recovery sub-groups or between the treatment groups when analyzed as non-normalized data (**Fig. 10 B**). The Col + MSC treatment and the combination of Col + PRP + MSC treatments achieved the highest strain at UTS after 1-week of recovery and the Col + PRP treatment group had shown the largest increase between the 1- and 2-week recovery

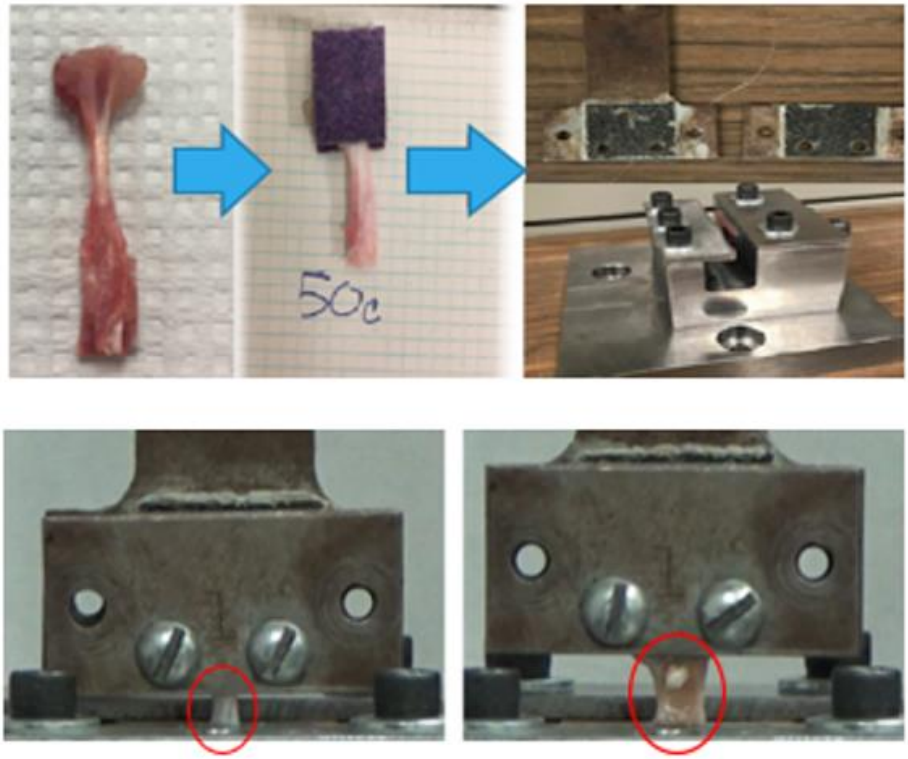

<u>Figure 7:</u> Tensile testing using tendon vise method. (*Top row*) The tendon samples were cleaned of any extra tissues left over from the harvesting procedure and kept hydrated using 1X PBS (far left picture). The muscle portion of the tendon was adhered to the non-gritted side of course sandpaper using a cyanoacrylate glue (middle picture). The calcaneus bone was slipped under the jaws of the tendon vise to be positioned and clamped at 30° of dorsiflexion (far right, bottom picture) and the muscle portion clamped in the upper grips (top picture). (*Bottom row*) the tendon was subjected to a constant tensile force (left) until failure (right). All samples treated with biologics were tested with this method. For the surgical controls, tendon samples from 5 subjects were used for both 1- and 2-week recovery times.

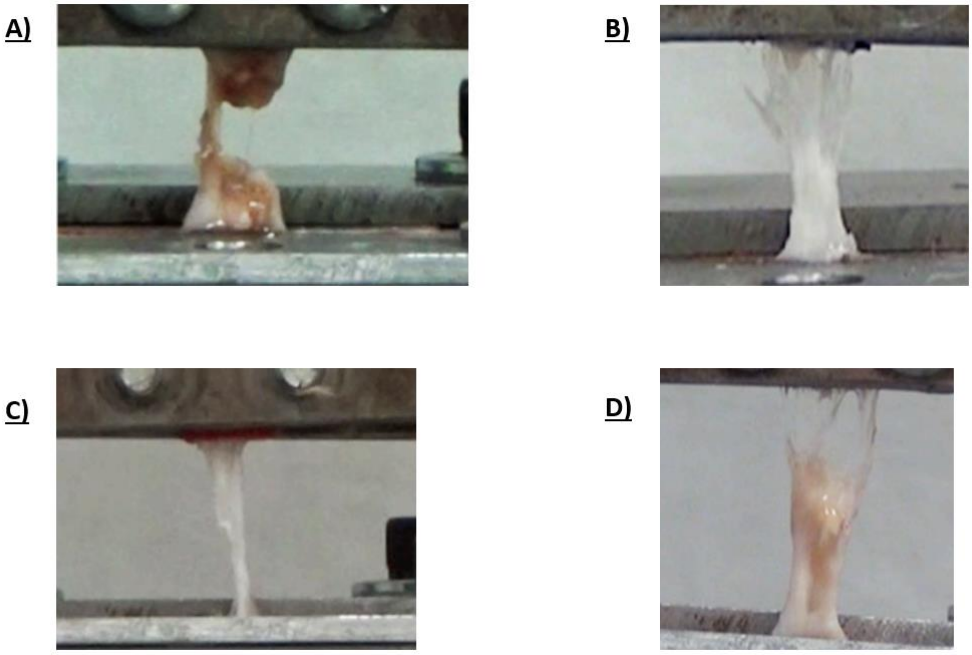

Figure 8: Common locations of failure observed. *A*) Tendons recovering for 1-week often showed failure at the site of repair. *B*) Control, unoperated tendons commonly shown failure near the upper musculotendinous region or *C*) Failure near the Achilles tendon insertion into the calcaneus. *D*) Failure of the repaired Achilles tendon (2-week recovery) above the surgical site. (Austin, 2019)

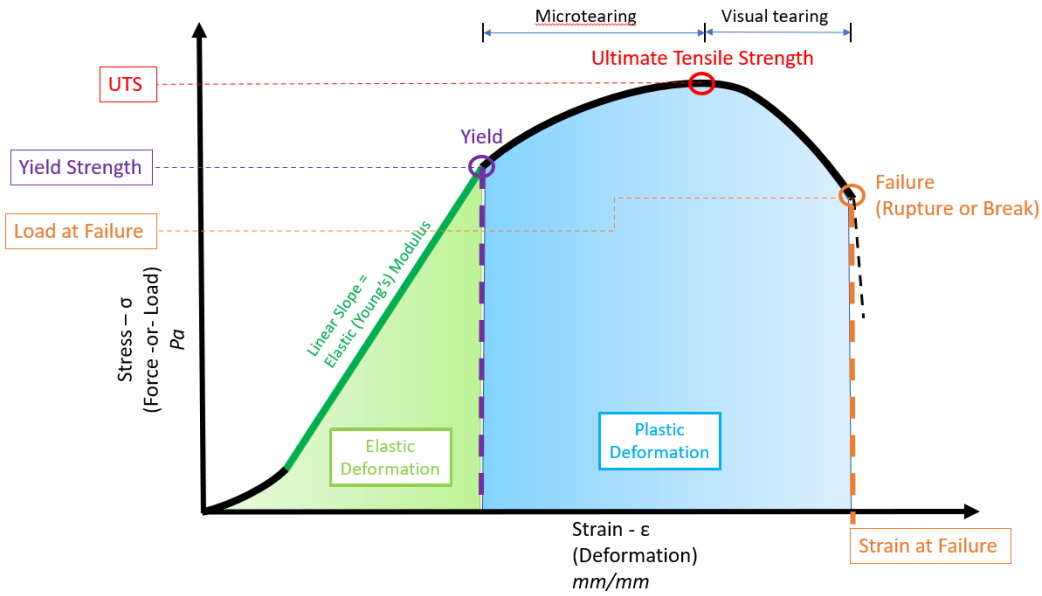

Figure 9: Example of Stress-Strain curve. The image depicted above is a representative example of a Stress-Strain curve, indicating regions of interest for our biomechanical tensile tests. As force/load is applied to the material (stress), the original shape of the material (i.e., cross-sectional area) begins to deform as more load is applied (Strain). The elastic portion of the curve represents the material's ability to resist deformation and return to its original shape (elastically deform) without being permanently deformed (plastically deformed). The yield point indicates the transition from elastic to plastic deformation. A steeper linear slope in the elastic portion of the curve (i.e., a higher Young's Modulus) indicates a more elastic material. The ultimate tensile strength is the maximum stress tolerated by the material. The failure point is where the material is completely bisected, and no portion of the material can transmit the applied load. The areas under the curve represent the amount of energy absorbed by the material as either elastic strain energy (area under the elastic deformation portion of the curve) or total strain energy (combined area under both elastic and plastic deformation portions of the curve).

period (**Fig. 10 C**). In addition to the observed increase in the average modulus of elasticity between the 1- and 2-week recovery periods for all treatment groups, an apparent increase was observed in the Col + MSC treatment group after 1-week of recovery in comparison to those seen in the Col only group (**Fig. 10 D**). However, none of these increases were determined to be statistically significant when calculated as unnormalized data through 2-way ANOVA statistical analysis. Possibly be due to the large variation in the masses of the subjects, large standard deviations were observed.

Due to the large deviations observed in the unnormalized data, the data was normalized as a percentage of the control tendon. By normalizing the treated tendons as a percentage of the control tendon, this considers the size of the animal subjects, possible strength of the tendons, as well as accounting for differences in the maturity of the tendons within the group. The results of the tensile testing of the treated groups are summarized in **Figure 11**.

The group that received only CollaTape (Collagen) as treatment was able to achieve 45.5% of the max stress and 47.2% of the max force experienced by the unoperated control at 1 week. At week 2 there was an 82% recovery in max stress and an 81.8% in max force in comparison to the unoperated controls. The strain at failure in this treatment group recovered 76.7% of what was observed in the control tendons at 1 week and 57.8% at 2 weeks. The strain at UTS was achieved by the treated tendons were determined to be 74.5% of the unoperated tensons at 1 week and 65.6% at 2 weeks. The Youngs Modulus, which is a measure of the elasticity of a material, showed that the treated tendons recovered 63.5% of the elasticity compared to the unoperated tendons at 1 week and 82.9% at 2 weeks. The elastic and total strain energy of the treated tendons at 1 week had a 33.3% recovery in elastic strain energy and a 35.8% recovery of the total strain energy stored in the unoperated tendons, respectively. At 2

A)

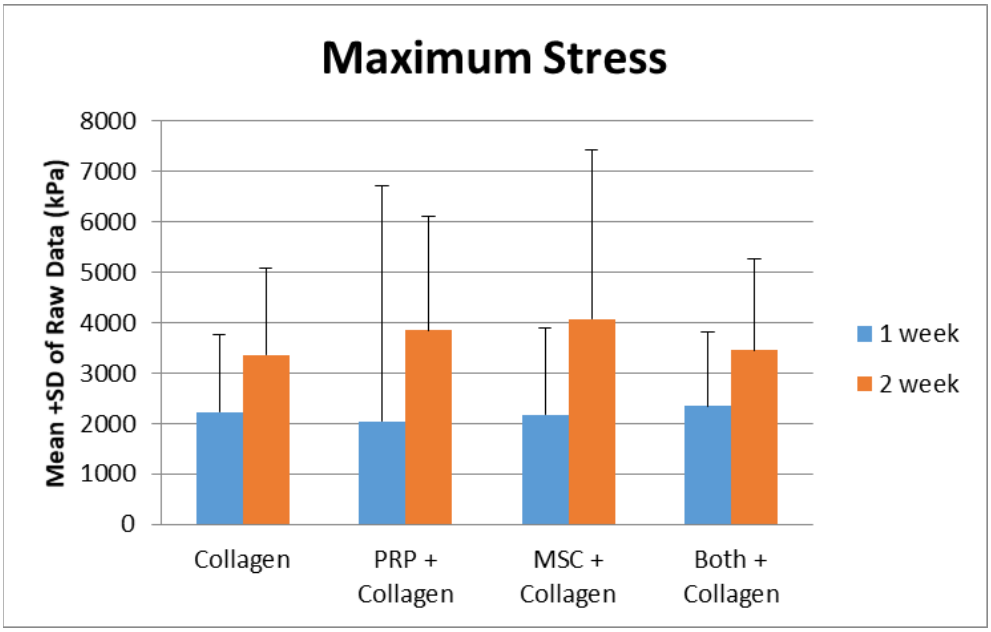
Maximum Stress
Mean +SD of Raw Data (kPa)
8000
7000
6000
5000
4000
3000
2000
1000
0
Collagen
PRP + Collagen
MSC + Collagen
Both + Collagen
1 week
2 week

B)

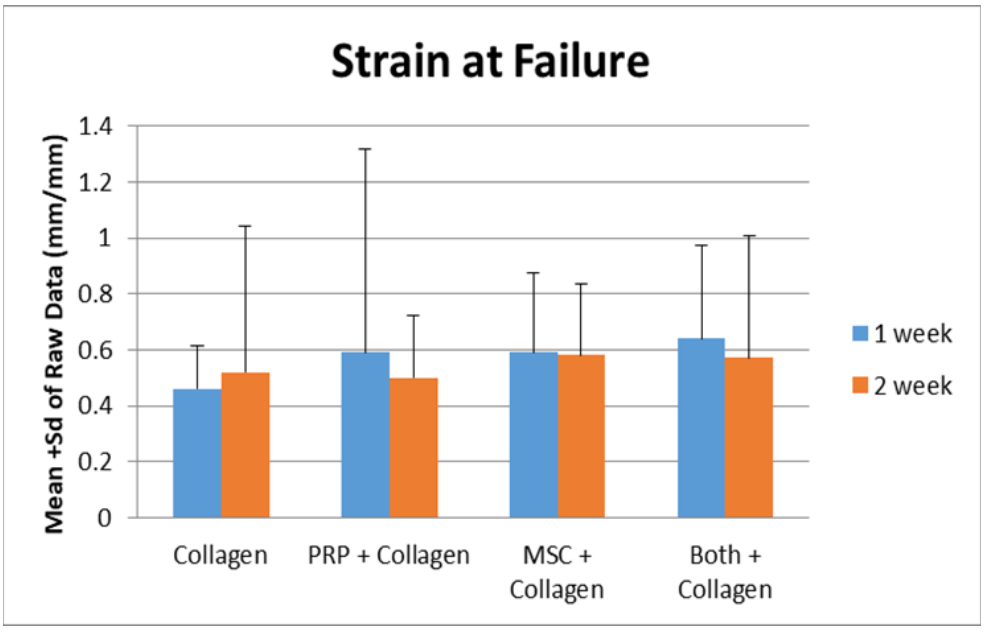
Strain at Failure
Mean +Sd of Raw Data (mm/mm)
1.4
1.2
1
0.8
0.6
0.4
0.2
0
Collagen
PRP + Collagen
MSC + Collagen
Both + Collagen
1 week
2 week

C)

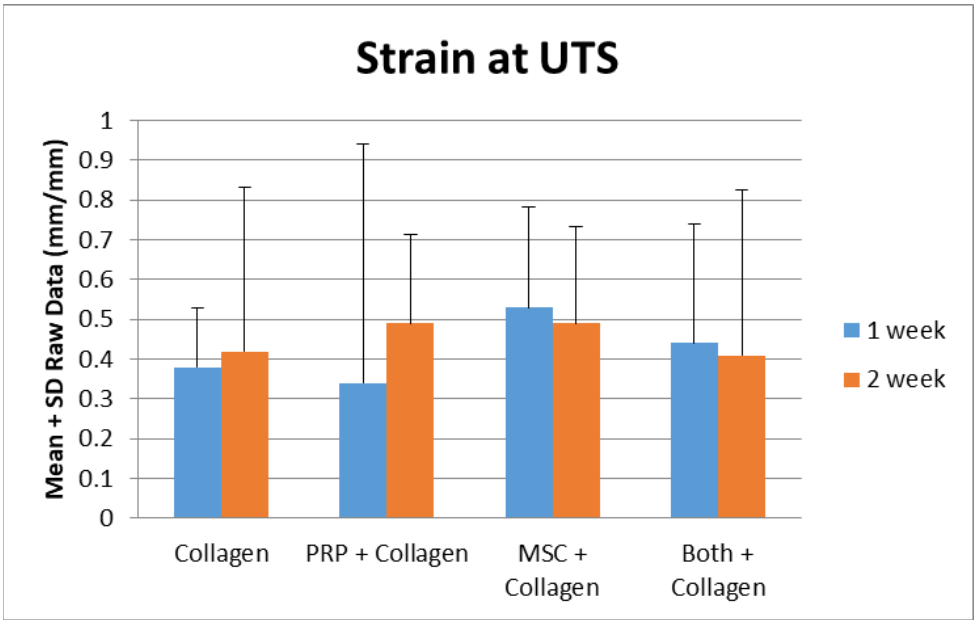

D)

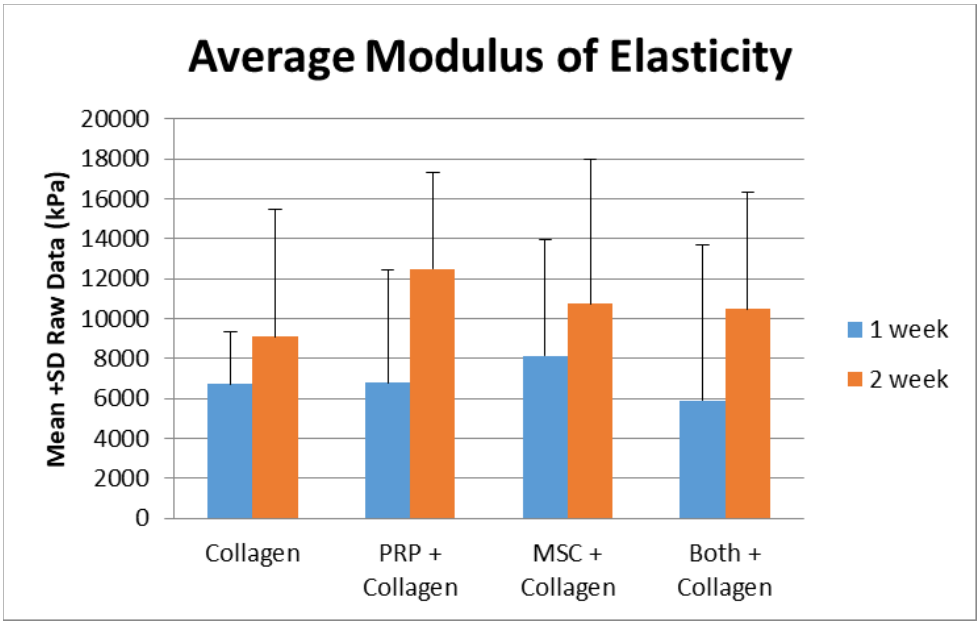

Figure 10: Raw, non-normalized comparison of results obtained from biomechanical testing of the groups that received treatments. The blue bars represent the data obtained from the 1-

week recovery sub-group and the orange represent the 2-week recovery sub-group. The experimental treatment groups given on the x-axis of each graph. All samples that received treatment were tested using the tendon vise method. These graphs represent *A)* Maximum stress, *B)* Strain at failure, *C)* Strain at the ultimate tensile strength (UTS), and the *D)* Average modulus of elasticity data acquired from the treated tendons. No significant differences ($p < 0.05$) were observed among the groups.

A)

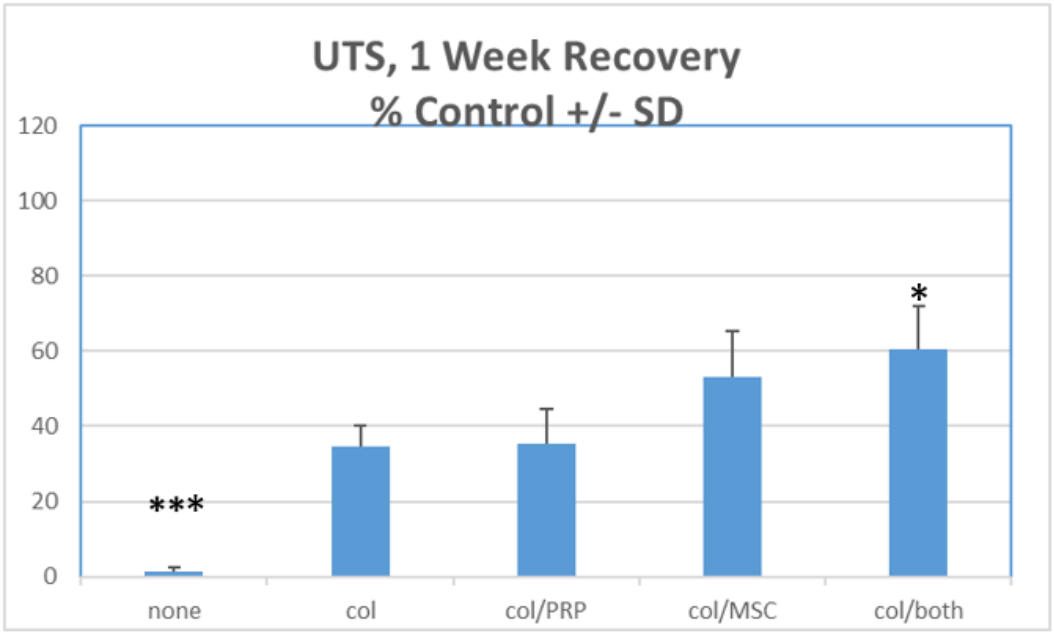

B)

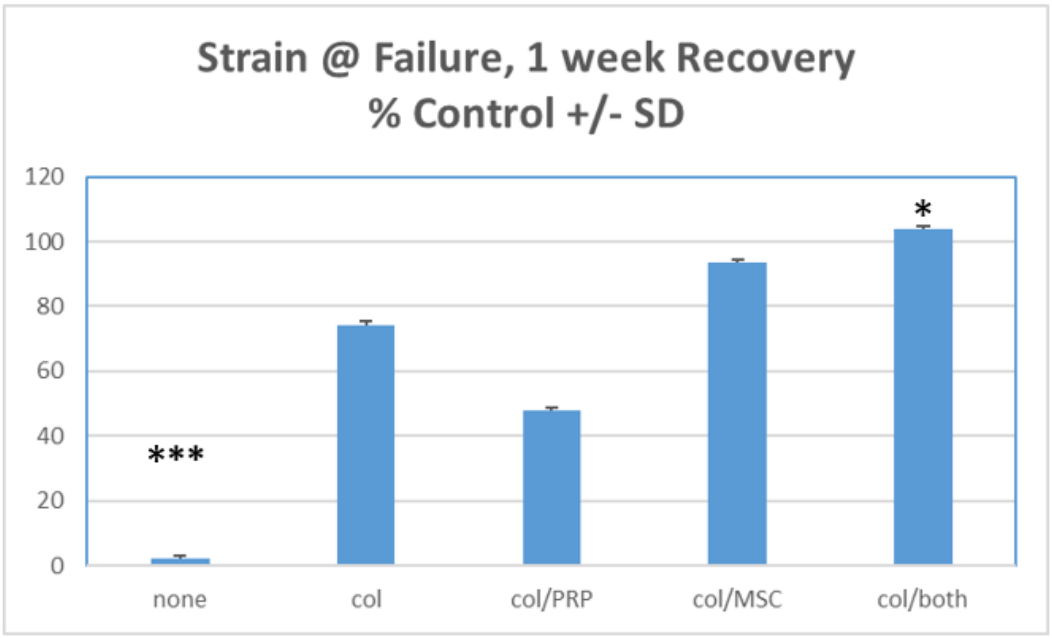

Figure 11: Comparison of results obtained from normalized biomechanical testing data, including no treatment control. When expressed as a percentage of the control, unoperated

tendons, the most notable results were seen after 1-week recovery. The normalized data considers the size, strength, and possible maturity of the tendons between the animals of each group. The Col only, Col/PRP, Col/MSC, Col/Both treatment groups were compared. A statistically significant difference ($p < 0.05$) was observed in the strain at ultimate tensile strength (UTS) ($p = 0.029$) and the strain at failure ($p = 0.024$) after 1 week of recovery in the group that received the col/both treatments and is signified by a single asterisk (*). All treatment groups showed significant improvement in the UTS ($p = <0.001$) and strain at failure ($p = < 0.001$) when compared to the surgical control group (none) which received no additional treatment after repair ($p < 0.001$ = ***) over the surgical control group. All samples were tested using the tendon vise method.

weeks, the treated tendons had shown a 78.8% recovery of the elastic strain energy compared to the unoperated tendons and a 37.2% recovery in total strain energy.

The group that received CollaTape with an injection of PRP only, was able to tolerate 39.0% of the max stress and 38.4% of the max force in comparison to the unoperated controls with 1 week of recovery. At 2 weeks, the treated tendons were capable of tolerating 71.2% max stress and 68.9% of the max force experienced by the unoperated tendons. The strain at failure in this group achieved 61.4% of what was observed in the control tendons at 1 week and 78.1% at 2 weeks. The strain at UTS achieved by the treated tendons was determined to be 37.8% of the unoperated tensons at 1 week and 87.5% at 2 weeks. The Youngs Modulus of the treated tendons recovered 82.3% of the elasticity seen in the unoperated tendons at 1 week and recovered 106.9% at 2 weeks. The elastic and total strain energy of the treated tendons at 1 week had a 19.5% recovery in elastic strain energy and a 29.1% recovery of the total strain energy stored in the unoperated tendons. At 2 weeks, the treated tendons showed a 47.5% recovery of the elastic strain energy when compared to the unoperated tendons and a 45.3% recovery in total strain energy.

The group receiving CollaTape with an injection of MSC only, was able to tolerate 56.9% of the max stress and 51.6% of the max force in comparison to the unoperated controls with 1 week of recovery. At 2 weeks, the treated tendons were capable of tolerating 89.7% max stress and 80.8% of the max force experienced by the unoperated tendons. The strain at failure in this group achieved 109.3% of what was observed in the control tendons at 1 week and 107.4% at 2 weeks. At 1 week recovery, the strain at UTS achieved by the treated tendons showed no difference from the unoperated tendons (i.e., the treated tendon achieved 100% of the Strain at UTS that the unoperated tendon achieved). However, at 2 weeks, the treated tendons had experienced strain at UTS to be 116.7% of the unoperated tendons. The Youngs Modulus

showed the treated tendons to have recovered 70.8% of the elasticity seen in the unoperated tendons at 1 week and recovered 101.8% at 2 weeks. The elastic and total strain energy of the treated tendons at 1 week was 28.5% recovery in elastic strain energy and a 46.2% recovery of the total strain energy stored in the unoperated tendons. At 2 weeks, the treated tendons had a 115.7% recovery of the elastic strain energy when compared to the unoperated tendons and an 84.8% recovery in total strain energy.

The tendons from the treatment group that received CollaTape with both PRP and MSC injections were able to tolerate 62.7% of the max stress and 63.7% of the max force in comparison to the unoperated controls with 1 week of recovery. At 2 weeks, the treated tendons were capable of tolerating 71.6% max stress and 72.3% of the max force experienced by the unoperated tendons. The strain at failure in this group achieved 98.5% of what was observed in the control tendons at 1 week and 69.5% at 2 weeks. The strain at UTS achieved by the treated tendons was determined to be 81.5% of the unoperated tensons at 1 week and 70.7% at 2 weeks. The Youngs Modulus of the treated tendons recovered 56.5% of the elasticity seen in the unoperated tendons at 1 week and recovered 115.4% at 2 weeks. The elastic and total strain energy of the treated tendons at 1 week had an 82.9% recovery in elastic strain energy and a 55.6% recovery of the total strain energy in the unoperated tendons. At 2 weeks, the treated tendons had a 62.0% recovery of the elastic strain energy compared to the unoperated tendons and a 45.9% recovery in total strain energy.

The results after normalization were significantly improved for strength and strain measurements (i.e., strain at ultimate tensile strength and strain at failure) after 1-week of recovery. These results can be seen in the graphs displayed in **Figure 11**. The Col + PRP treatment group showed little difference from the Col only group for strain at UTS, and an observed decrease was also seen in this treatment group for the strain at failure when

compared to the Col only treatment group. However, in both cases, the normalization of the data resulted in an observed increase in these measurements in both the Col + MSC and Col + PRP + MSC treatment groups. Additionally, statistically significant differences were observed for the strain at UTS ($p = 0.029$) and the strain at failure ($p = 0.024$) for the treatment group receiving the treatment with all three biologics in combination after 1-week of recovery when compared to using CollaTape alone as a treatment. This result gives an indication that the tendons treated using the combination of PRP and MSCs on a Collagen scaffold in the form of CollaTape may have improved resistance to strain in the tendon tissue during the healing process. In addition, the data for surgical group receiving no treatment is included in **Figure 11**. The data for the strain at UTS and strain at failure for the surgical control group was significantly different from all treatment receiving groups ($p < 0.001$).

Collagen Expression Analysis

Total RNA was extracted from cryopreserved 4 mm tendon segments that were excised from the subjects that recovered for two weeks prior to harvest. The RNA extracted from these samples were reverse transcribed into cDNA for GAPDH, Col1a1, and Col3a1. PCR amplified cDNA was electrophoresed to determine if these mRNA transcripts were expressed. By comparing all three primer sets from one subject in each treatment group, we can determine the relative expression of Collagen type 1 and Collagen type 3 using the constitutively expressed GAPDH transcript for comparison.

RNA Extraction of Tendon Segments

Total RNA was extracted from the 4 mm preserved tendon segment samples using a RNeasy Fibrous Tissue Mini Kit following the protocol outlined by the manufacturer with the exception of the disruption and homogenization of the tendon tissue. We adapted the protocol to use mortar and pestle tissue disruption and a syringe homogenization step described in a related RNA extraction product from Qiagen. As RNase contamination or contamination from a previous RNA extraction would affect the final RNA product, all tools were sterilized prior to use and the mortar and pestle were washed and NucleasEliminator treated twice prior to use. The mortar was kept covered with a clean aluminum foil covering during tissue disruption to avoid introduction of outside sources of contamination. Attempts were made to keep the disruption step as short as possible to minimize potential exposure to contaminants. This was also minimized the chance of tendon fragments coming out of the mortar due to the crushing process ("popping").

Despite these precautions, some common issues arose during the extraction procedure. First, it is worth noting that surgically repaired tendon samples #106 and #112 were dropped during the cryopreservation procedure and may have been subject to possible environmental RNase contamination. During the first extraction conducted on sample #112c, as recommended by the manufacturer, the RNA was eluted using 80 µL of nuclease free water. However, this resulted in the final RNA concentration being too diluted to be considered viable for cDNA synthesis. This prompted us to change our elution volume to be 30 µL which allowed for elution of RNA at a higher concentration. The crushing process used during RNA extraction was able to achieve a fine powder for most of the samples. Some of the tendon samples would form a flattened but semi-intact "sheet" that would conform to the bottom of the mortar (a result I will refer to as "sheeting"). The "sheeting" behavior of these tissue samples typically resulted in

longer times spent disrupting the tissues and a courser final result, more akin to small granules than a fine powder.

Another common issue experienced was having remnants of unabsorbed suture material remaining in the sample in the samples that had undergone the surgical repair. Large remnants of suture material were often easy to detect and remove cleanly with sterilized forceps after the initial crushing of the sample or syringe homogenization. However, smaller pieces of suture material were more difficult to detect and caused more concern, sometimes resulting in small portions of the tendon sample being held together during the crushing. When undetected suture material went undetected after disruption and homogenization, fine fibrous remains of the material would often cause a failure to pellet the lipids and digested protein. This would result in a slight loss of RNA containing supernatant that could be transferred cleanly without contamination. The typical loss of supernatant volume was approximately 60 +/- 15 µL (estimated visually) of the total 630 µL volume added, which was considered acceptable to preserve the purity of the final RNA product.

One sample had a loss of supernatant due to suture contamination that was considered unacceptable. A loss of approximately 200 µL was experienced in sample #114. As a result, the extraction process was first performed on the initial fraction of supernatant that was cleanly transferred (we will refer to this clean fraction as the “first attempt”). The other fraction containing the remaining supernatant, fibrous suture remnants, and loosely pelleted material (which we will refer to as the “second attempt”) was saved by chilling over ice. Once the extraction of the first, clean fraction was complete, the RNA was prepared for cDNA synthesis and placed in a thermocycler. While in the thermocycler, a “second attempt” was made to recover the RNA from the remaining 200 µL of supernatant. A second centrifugation of the material was done, this time at 15,000 x g, in an attempt to form a solid pellet of undesired

material and allow for a cleaner transfer of the RNA containing supernatant. Though the pellet was still loose, approximately 150 µL of supernatant was able to be salvaged and a second extraction was done. Interestingly, this "second attempt" to salvage the RNA from the supernatant yielded comparable RNA concentrations to the "first attempt" (102.8 $\frac{ng}{\mu L}$ from the first elution and 23.9 $\frac{ng}{\mu L}$ from the second) , but the $\frac{A_{260}}{A_{280}}$ and the $\frac{A_{260}}{A_{230}}$ ratios values (ranging between 1.93 – 2.03 and 1.63 – 2.28, respectively) from the "second attempt" indicated a more pure nucleic acid product was achieved. However, because the "second attempt" supernatant was exposed to Proteinase K for a longer duration than in other extraction samples used were from the "first attempt". The "first attempt" elutions produced 3 viable samples above the minimum RNA concentration of 16.67 $\frac{ng}{\mu L}$ threshold, when compared to the "second attempt" which only produced 2 viable elutions, indicating that most of the RNA was recovered in the "first attempt." No other tendon samples experienced a loss of supernatant above acceptable amounts.

The results obtained from the NanoDrop measurements of the RNA extracted from the tendon samples which proceeded to cDNA synthesis are outlined in **Table A1**. All samples eluted with RNA concentrations greater than 16.67 $\frac{ng}{\mu L}$, but less than 100 $\frac{ng}{\mu L}$, were used for cDNA synthesis. If multiple eluates from one sample were within this range, the elution with the $\frac{A_{260}}{A_{280}}$ and $\frac{A_{260}}{A_{230}}$ ratio values closest to the range of 1.80 – 2.00 were selected for cDNA synthesis, as this indicates high purity. However, most of the samples were shown to be below the minimum ratio of 1.8 to be considered a high purity nucleic acid product.

Control tendon samples #112c, #114c, or #115c did not have a high enough RNA concentration to continue to cDNA synthesis. As a result, there was no viable sample to perform

the RT-PCR reaction for the unoperated tendons of subjects receiving the combination of all three biologics. We were able to obtain RNA from tendon segments for both tendons, unoperated control and surgically repaired, for the surgical control, Collatape only treatment, Collatape with PRP treatment, and Collatape with MSC treatment groups.

The total amount of RNA extracted from the tendon samples were then calculated. This was done for each sample by multiplying the RNA concentrations that were determined through NanoDrop by the volume of nuclease-free water used to elute the RNA from the spin column (**Table A3**). This data was normalized to express the total amount of RNA (in ng) extracted per milligram of starting tendon tissue. The total amount of RNA extracted for each sample was divided by the mass of the starting 4 mm tendon sample segment. The average and standard deviations of the starting mass of the tissue samples (**Table A2**), total amount of RNA extracted (**Table A3**), and the normalized amount of RNA extracted from the tissue samples were calculated for each group and are expressed in **Table A4**. The values for the averaged raw, non-normalized total amount of RNA extracted from each group and the normalized average amount of RNA extracted per mass of starting tissue for each group were then plotted and displayed as a bar graph which are depicted in **Figure 12**.

For the samples in the surgical control group, the average mass of the excised operated tendon tissues was 51.5 +/- 19.1 mg of tissue (**Table A2**), from which 8167.5 ng of RNA was able to be extracted (**Table A3**). The unoperated tendon sample masses were both 20 mg (**Table A2**), but the RNA extracted from the samples differed slightly, averaging 1287 ng of total RNA extracted from the sample (**Table A3**). When normalized, the operated surgical control tendons produced 160.3 +/- 9.13 $\frac{ng\ RNA}{mg\ Tissue}$ while the unoperated samples produced 64.5 +/- 4.45 $\frac{ng\ RNA}{mg\ Tissue}$ (n = 2) (**Table A4** and **Figure 13**).

A)

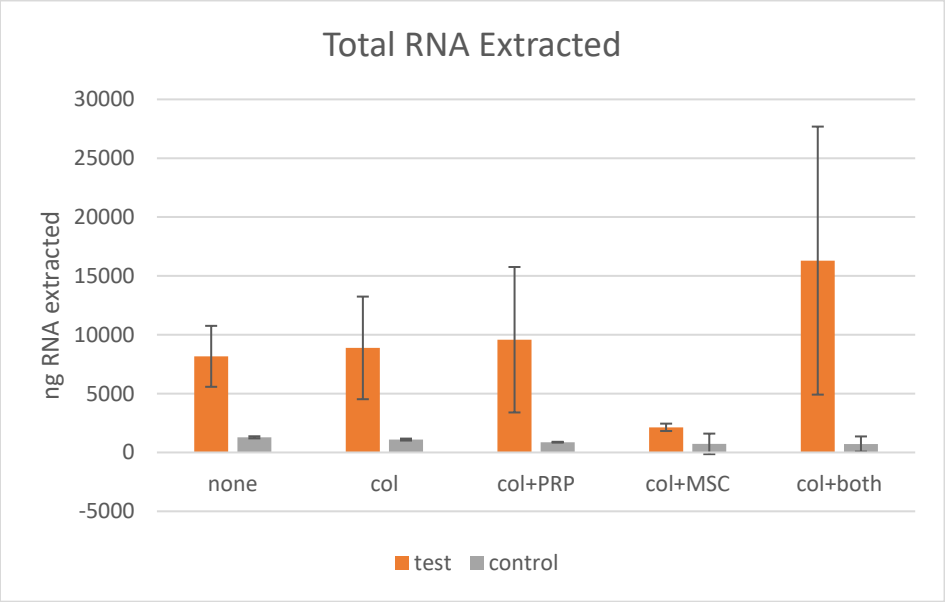

B)

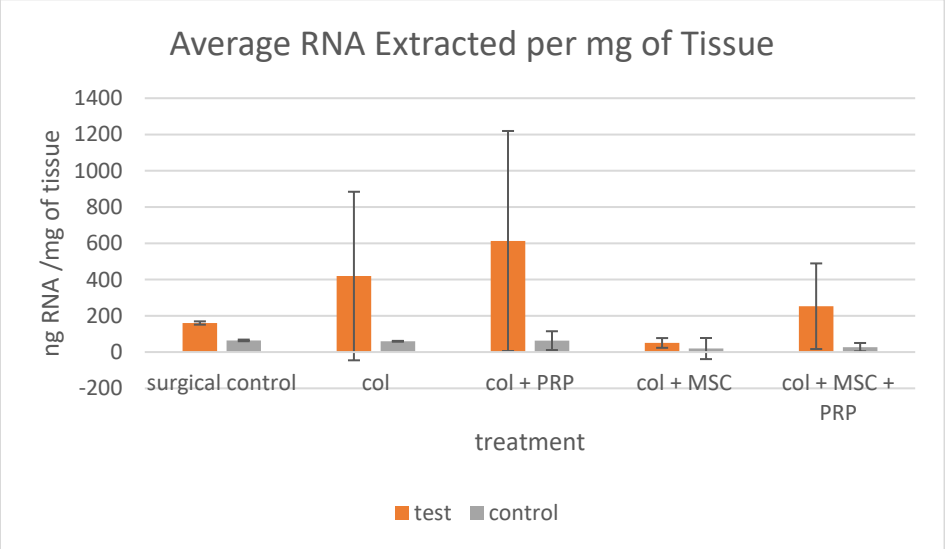

Figure 12: RNA extraction results. The results obtained from the operated tendons (test = orange) and the control, unoperated tendons (gray) results for each experimental group. The experimental groups are labeled in the order of the surgical control (no additive/none),

CollaTape only (col), CollaTape + PRP, CollaTape + MSC, and finally the combination of all three biologics treatments (col+both/Col+MSC+PRP) in both graphs. *A)* Average amount of total RNA extracted from each group represented in ng amounts. *B)* Average amount of RNA expressed as percent of unoperated tendon that was extracted per mg of starting tendon tissue.

A)

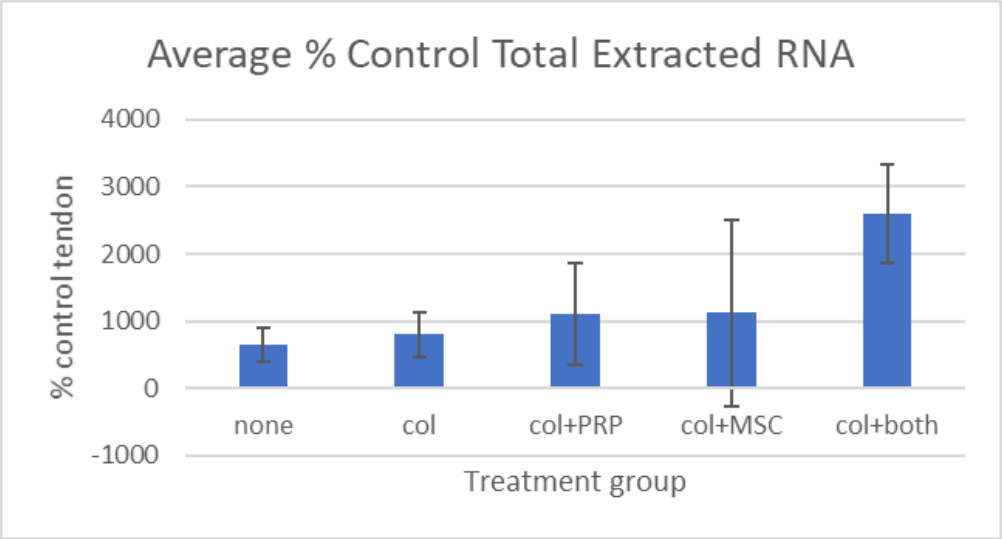

B)

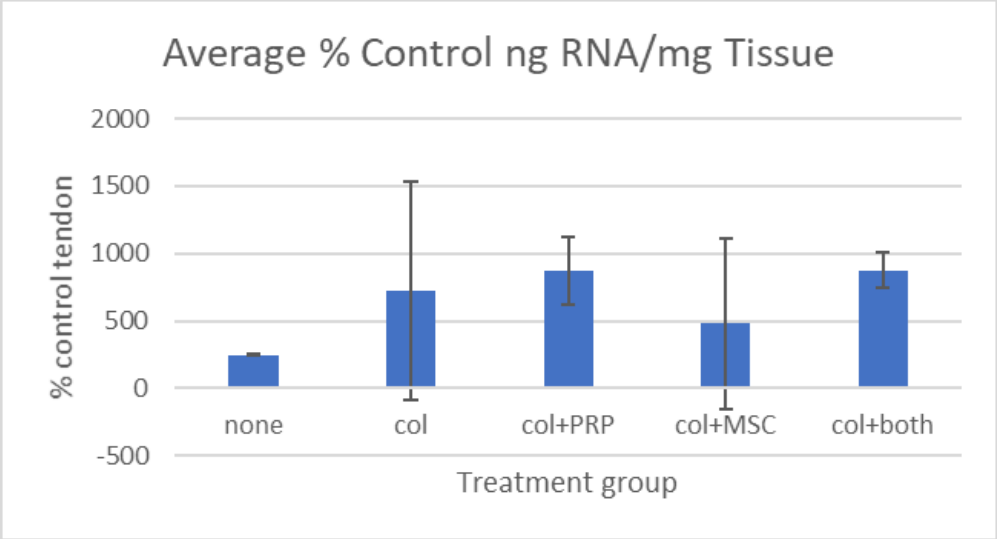

<u>Figure 13:</u> Average total extracted RNA (A) obtained from 4 mm tendon segments and average amount of RNA extracted per mg of starting tissue (B) expressed as a percent of the unoperated tendon [(operated tendon/unoperated tendon) x 100].

The group that received only CollaTape as treatment after surgical repair had an average mass of 40 +/- 33.9 mg for the operated tendons and 18.5 +/- 2.1 mg for the unoperated tendons. A notable difference was seen in the amount of RNA extracted when comparing the operated tendon to the unoperated tendon. We were able to extract an average of 8884.5 ng of RNA from the operated tendons. However, there was also a large deviation of the mean of +/- 4359.3 ng of extracted RNA (n = 2). The unoperated tendon samples produced an average of 1096.5 +/- 82.7 ng of RNA (n = 2). The normalized average for the operated tendon samples produced 419.3 +/- 464.8 $\frac{ng\ RNA}{mg\ Tissue}$ and the unoperated samples produced 59.4 +/- 2.3 $\frac{ng\ RNA}{mg\ Tissue}$ (n = 2).

The tendon samples from animals receiving CollaTape and a PRP injection had an average sample mass of 40 +/- 50.2 mg for the operated tendon samples and 20.5 +/- 16.2 mg for the unoperated tendon (n = 2). From this group, we were able to extract an average of 9557.5 +/- 6179.4 ng of total RNA from the operated samples and 871.5 +/- 36.1 ng of total RNA from the unoperated samples (n = 2). When normalized, the operated tendon samples produced an average of 612.6 +/- 606.8 $\frac{ng\ RNA}{mg\ Tissue}$ and the unoperated tendon samples produced an average of 63.1 +/- 51.8 $\frac{ng\ RNA}{mg\ Tissue}$ (n = 2).

The tendon samples in the group treated with CollaTape and an injection of MSCs had an average sample mass of 47.5 +/- 19.1 mg for the operated tendon samples (n = 2). Both of the unoperated tendon sample masses were 15 mg without deviation (n = 2). From this group, we were able to extract an average of 2136.0 +/- 314.0 ng of total RNA from the operated samples and 729.5 +/- 873.3 ng of total RNA from the unoperated samples (n = 2). When normalized, the

operated tendon samples produced an average of 50.4 +/- 26.9 $\frac{ng\ RNA}{mg\ Tissue}$ and the unoperated tendon samples produced an average of 48.6 +/- 58.2 $\frac{ng\ RNA}{mg\ Tissue}$ (n = 2).

The tendon samples in the group treated with CollaTape and an injection with both PRP and MSCs had an average sample mass of 77.0 +/- 26.9 mg for the operated tendon samples and 25.5 +/- 2.1 mg for the average unoperated tendon (n = 2). From this group, we were able to extract an average of 16,300.5 +/- 11,385.1 ng of total RNA from the operated samples and 718.5 +/- 642.8 ng of total RNA from the unoperated samples (n = 2). When normalized, the operated tendon samples produced an average of 252.9 +/- 236.1 $\frac{ng\ RNA}{mg\ Tissue}$ and the unoperated tendon samples produced an average of 27.2 +/- 22.9 $\frac{ng\ RNA}{mg\ Tissue}$ (n = 2).

RT-PCR Amplification of Extracted RNA with 6-minute Extension Time

The primer sets used in this study were selected to amplify the synthesized cDNA that reverse transcribed from the mRNA transcripts for Col1a1, Col3a1, and GAPDH targets. The sequence used for the primer sets were from a previous study conducted by Heinemeier et al. (2007). The sense (forward primer) and antisense (reverse primer) sequences are shown in **Table 5**.

An initial pilot RT-PCR reaction was conducted using the primer sets for GAPDH with a thermocycling program which originally called for a 55°C annealing temperature and a 6-minute extension time prior to electrophoresis on a 1% agarose gel. Specifics on how the gels were loaded and in what order will be discussed later when we report the results using the collagen primer sets, however the results of this initial RT-PCR are summarized in **Figure 14**. The original decision to use a 6-minute extension assumed that the primer sets would amplify nearly the

Table 5: Primer sets for RT-PCR

Primer	Sequence (5' - 3')
rat collagen 1 sense	ATCAGCCCAAACCCCAAGGAGA
rat collagen 1 antisense	CGCAGGAAGGTCAGCTGGATAG
rat collagen 3 sense	TGATGGGATCCAATGAGGGAGA
rat collagen 3 antisense	GAGTCTCATGGCCTTGCGTGTTT
GAPDH sense	CCATTCTTCCACCTTTGATGCT
GAPDH antisense	TGTTGCTGTAGCCATATTCATTGT

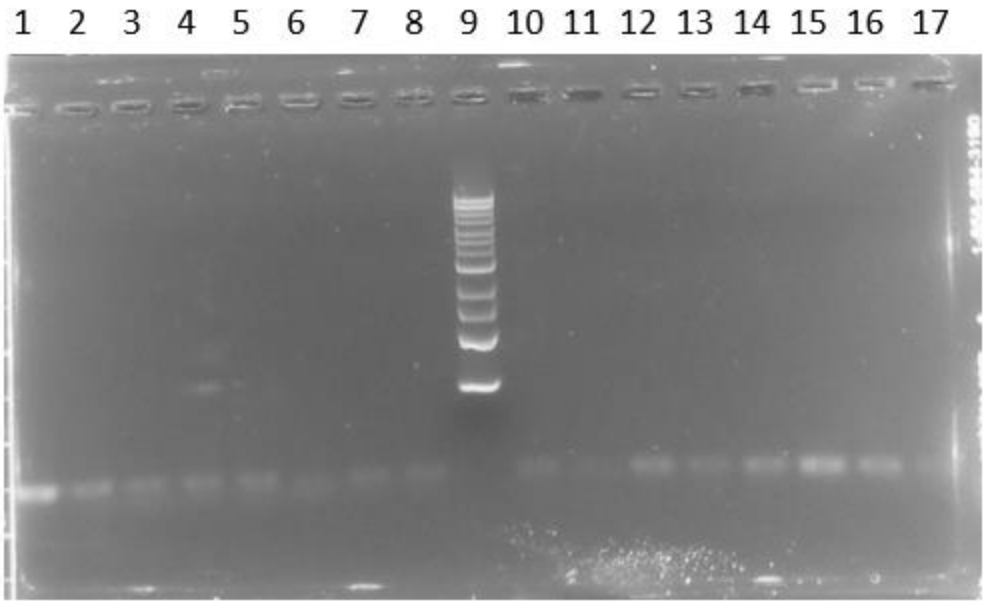

Lane	1	2	3	4	5	6	7	8
Sample	**101** (none)	**X101** (none)	**101c** (none)	**X101c** (none)	**103** (none)	**X103** (none)	**103c** (none)	**X103c** (none)

Lane	9	10	11	12	13	14	15	16	17
Sample	**1 kb ladder**	**104** (Col)	**X104** (Col)	**104c** (Col)	**X104c** (Col)	**106** (Col)	**X106** (Col)	**106c** (Col)	**X106c** (Col)

Figure 14: Initial RT-PCR results on 1% agarose gel using GAPDH Primer set with 6-minute extension time. The figure above depicts the results from electrophoresis set-up one in a 17-well 1% agarose gel. All samples were tested using RT-PCR, where RNA was extracted using the RNeasy Fibrous Tissue Mini kit, cDNA synthesis done using the Proscript II cDNA FirstStrand synthesis kit, and amplification using the GoTaq Hot Start Green Master Mix kit that includes a green tracking dye as part of the mix. 5 µL of sample was used in the electrophoresis, 1x TBE buffer as the electrolyte, and electrophoresed for 30 minutes. The gels were imaged in a PrepOne Illuminator under UV light. The lanes were loaded according to the accompanying table below the imaged gel. The "X" nomenclature indicates an RT-PCR control where no reverse transcriptase enzyme was added during cDNA synthesis and a "c" indicates that the sample

originates from the unoperated control tendon of the indicated subject. The imaged gels from electrophoresis set-up two and three can be seen in the Appendix section.

entire synthesized cDNA sequence and the time was therefore selected to amplify the largest mRNA sequence (Col1a1 = 5,843 bp). However, the result of this RT-PCR reaction determined that this was not the case. Briefly, the amplified samples were separated on a 1% agarose gel and used a 1 kb ladder which we intended to compare to the RT-PCR product. However, these samples did not show bands at the expected size (GAPDH mRNA sequence = 1,306 bp). Instead, bands of varying visual intensity were observed further in the gels. For most of the gels, these bands were observed at approximately the same length. We could not determine with certainty if the varying intensity of the bands were due to amplification of the RT-PCR product but having poor band separation or if the bands resulted from the formation of primer dimers. However, the gel that included a RT-PCR water control (**Figure A1** - right gel), fortunately did show band separation in some samples, as well as revealing where a band should be if primer dimers were present. These bands were visible above the region where primer dimers were seen to be present (as determined by the water control).

Random samples were later selected from this RT-PCR reaction and electrophoresed on a 2% agarose gel, again using a 1kb ladder for comparison. However, unlike the previous electrophoresis, 10 µL was loaded into the wells as opposed to 5 µL as done previously. This was due to suspicion that the RT-PCR product may have been in too small a quantity to be visually observed. However, the main purpose of this electrophoresis was to obtain better band separation and determine if the previously seen bands may have been the result of overlapping bands. All synthesized cDNA samples that were able to be obtained (i.e., the cDNA samples from the operated and unoperated tendons, if obtained, and their cDNA synthesis controls) were tested from subjects A101, A106, A109, A112, and A115 (**Table 3**). The result from this electrophoresis can be seen in **Figure 15**. This resulted in the formation of two distinct bands

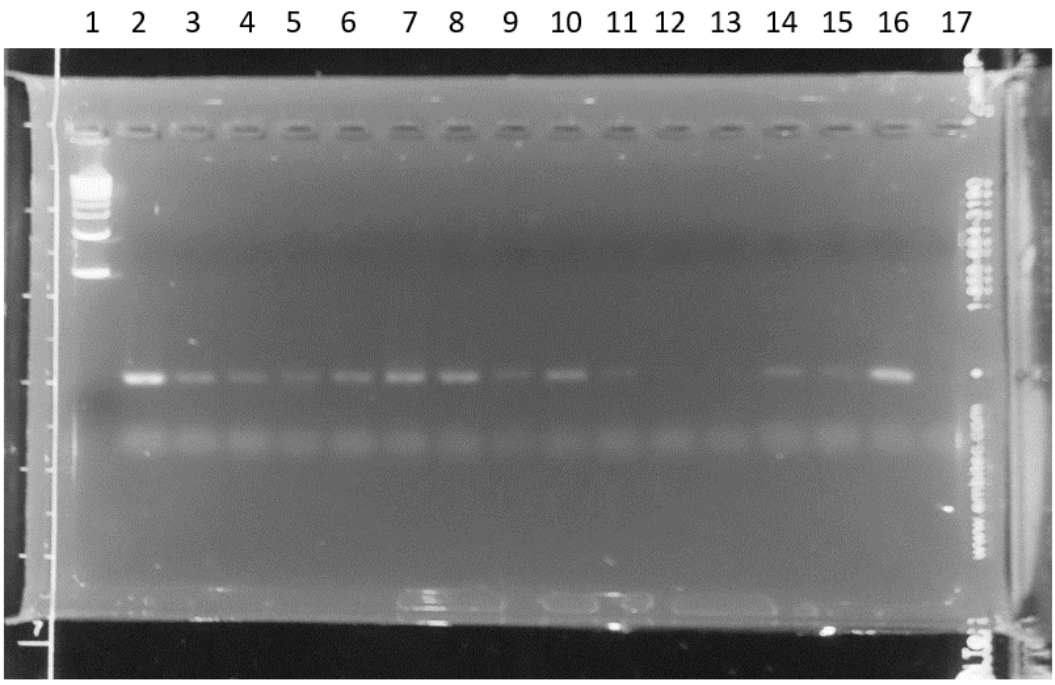

Lane	1	2	3	4	5	6	7	8	9
Sample	**1 kb ladder**	**101** (none)	**X101** (none)	**101c** (none)	**X101c** (none)	**106** (Col)	**X106** (Col)	**106c** (Col)	**X106c** (Col)
Lane	**10**	**11**	**12**	**13**	**14**	**15**	**16**	**17**	
Sample	**109** (Col + PRP)	**X109** (Col + PRP)	**109c** (Col + PRP)	**X109c** (Col + PRP)	**112** (Col + MSC)	**X112** (Col + MSC)	**115** (Col + PRP + MSC)	**X115** (Col + PRP + MSC)	

<u>Figure 15:</u> Electrophoresis of Initial RT-PCR product using GAPDH primer set on a 2% agarose gel. All samples obtained from subjects A101, A106, A109, A112, and A115 were selected at random to be tested. Method and RT-PCR products used are identical to that seen in Figure 13 with the exceptions that 10 µL of the RT-PCR product was used in leu of 5 µL and the samples were electrophoresed on a 2% agarose gel instead of a 1% agarose gel as seen in Figure 13. The loading of the lanes is described according to the accompanying table below the gel image.

being observed in nearly all lanes that contained the samples with the exception of both samples tested from 109c, X109c, and X115.

From these results, under these conditions, an indication that a RT-PCR product may have been produced. The size could not be determined accurately as the shortest band present in the 1 kb ladder has a length of 500 bp. However, through visual examination of the gel, the product size obtained through this initial RT-PCR reaction, was estimated to be approximately between 100 - 200 bp in length. The visual bands seen in synthesized cDNA control samples (i.e., those samples denoted with the letter "X") electrophoresed in the 2% agarose gel suggests the possibility for a source of contamination present from the total RNA extraction of the tendon samples. To determine if DNA was source for contamination, we decided test our primer sets against genomic DNA. However, the rationale behind this decision and results obtained from using the primer sets for standard DNA PCR will be presented later. Regardless, from these initial RT-PCR results, we determined that it was clear adjustments to the thermocycling program needed to be made for future RT-PCR reactions based on the size of the GAPDH RT-PCR product obtained here. We suspected that unnecessarily long extension time at 72°C may be adversely affecting the enzymatic activity of the polymerase, further contributing to the decision to alter the thermocycling program.

Evaluating Predicted Size of RT-PCR Product

To determine the predicted size of the amplified RT-PCR product using these primer sets, a search using the GenBank tool from the NCBI database was done to obtain the cDNA converted mRNA transcripts for GAPDH (RefSeq: NM_017008.4), Col1a1 (RefSeq: NM_053304.1), and Col3a1 (RefSeq: NM_032085.1) for *Rattus Norvegicus* species, from which

the strain of rat subjects used in this study (Lewis Rat) are derived. These sequences were used as the template that we would match our primer sets to determine the RT-PCR product size. This was done through a query using the Primer-BLAST tool from the NCBI database to match the template sequences to their respective primer sets. Additionally, queries were also conducted for each primer set that were intentionally mismatched to the other transcripts that the primer set were not intended to amplify (i.e., a query where the primer set for Col1a1 would search for product matches in the Col3a1 transcript). This was done to ensure that promiscuous binding of the Col1a1 and Col3a1 primer sets would not occur and cause confusion of the final results.

The outputs from the Primer-BLAST queries mismatching the primer sets to the wrong transcripts could not identify any RT-PCR products when the incorrect primer set was paired with a template the set was not intended to amplify. However, when the primer set was matched to the correct template, this resulted in one RT-PCR product for each template-primer pair and a prediction of the RT-PCR product size to be expected. The graphical outputs from the Primer-BLAST queries are depicted in **Figure 16**. The predicted size of the RT-PCR product using the primer set for GAPDH was determined to be 98 bp (**Fig. 16A**). For the Collagen transcripts, the primer set and transcript for Col1a1 was predicted to yield a RT-PCR product of 128 bp (**Fig. 16B**) and the Col3a1 pairing was predicted to yield a 143 bp RT-PCR product (**Fig. 16C**). It is also worth noting that, from the graphical output of the Primer-BLAST, we can see that each mRNA RT-PCR product amplified by the primer sets cross a predicted site where a splicing event occurred (**Fig. 16**). This would allow us to test the primer sets against genomic DNA to determine if DNA contamination were present in the RNA Extracted from the tendon segment samples. However, the results obtained from testing the primer sets against genomic DNA will be discussed later.

<u>Figure 16:</u> Graphical output determining the estimated RT-PCR product size for each primer set from the search queries using the Primer-BLAST tool from the NCBI database. *A)* Primer-BLAST search query result matching the GAPDH mRNA sequence (RefSeq: NM_017008.4) to the GAPDH sense and antisense primer set. The predicted RT-PCR product is estimated to be 98 bp in length. *B)* Primer-BLAST search query result matching the Col1a1 mRNA sequence (RefSeq: NM_053304.1) to the Col1a1 sense and antisense primer set. The predicted RT-PCR product is estimated to be 128 bp in length *C)* Primer-BLAST search query result matching the Col3a1 mRNA sequence (RefSeq: NM_032085.1) to the Col3a1 sense and antisense primer set. The predicted RT-PCR result is estimated to be 143 bp in length.

With these predicted RT-PCR product size results, we were able to determine the appropriate extension time and annealing temperature to use in the thermocycling program to amplify the synthesized cDNA obtained from the total RNA extraction of the sample tissues. As the GoTaq HotStart Green calls for a 1-minute extension time for every 1 kbp of template to be amplified, we decided to program the thermocycler to allow extension to occur for 30 seconds. Assuming the activity of the GoTaq HotStart polymerase scales linearly with the extension time, this would allow for a maximum PCR product of approximately 500 bp. Though all of our predicted products are under 200 bp, this allowed for the possibility to determine if the predicted products were shorter than in reality, but also avoid staying at the extension temperature too long and possibly affecting enzyme function.

RT-PCR Amplification of Extracted RNA using 30-second Extension Time

For the annealing temperature, we chose to set the temperature to 55°C. This based off of the melting point of the primers and a previous study from our lab conducted by Mike Kelly (2017) who had previously used and evaluated the same primer sets for RT-PCR to measure the genetic activity of Collagen 1 and 3 in MSC and fibroblast co-cultures at various annealing temperatures. We decided to follow the recommended number of amplification cycles recommended by the manufacturer's outlined protocol (25 cycles), giving us the option to adjust the number of cycles if necessary (i.e., if all bands appeared faint and difficult to clearly identify after electrophoresing on 1% agarose gels). However, we were able to detect distinct bands from most electrophoresed samples in the gels using 25 cycles of amplification, ultimately leading to the decision to use these parameters as the standard thermocycling program used on our samples.

For sake of time and efficiency, all available samples of synthesized cDNA were amplified using one primer set and electrophoresed on the same day or electrophoresed the following day after short storage at -20°C before testing another primer set. For electrophoresing the samples, three electrophoresis set-ups were used. However, due to the availability of prepared 1% agarose gels to test the initial samples accounting for two subjects per group, the gels used in each electrophoresis set-up varied as follows: Set-up 1) one 17-well gel, set-up 2) two 8-well gels, and set-up 3) one 8-well gel. However, this had no apparent affect that would impact the final results. Each sample was run next to its accompanying cDNA synthesis control (designated with the letter "X"), which lacked the addition of reverse transcriptase enzyme, to test if DNA contamination was present the original extracted RNA sample.

As previously mentioned, distinct bands of the amplified cDNA product were visible after electrophoresing 5 µL of sample loaded in the wells of a 1% agarose gel from most of the samples. Specifically, these bands were seen in the amplified Collagen samples (i.e., Col1a1 and Col3a1) from the cDNA synthesized from the extracted total RNA (**Figure 17** and **Figure 18**, respectively). These samples utilized the information obtained through the NCBI database, and therefore followed the 30 second extension time during amplification. The bands, when compared to the 100 bp ladder, appeared to be larger than 100 bp but smaller than 200 bp. With exception to the lanes containing ladders, additional bands were present in every lane that were smaller than 100 bp. These additional bands were determined to be primer dimers, as evident by the water controls (**Fig. A3*b*** and **Fig. A4*b***). Additionally, on two of the 8-well gels, a 1 kb ladder was also run such that we could compare results with the PCR products from genomic DNA (discussed later). The RT-PCR products for both Col1a1 and Col3a1 were seen to be well below the shortest 500 bp band of the ladder. Examples of these gels are seen in **Figure 17** for

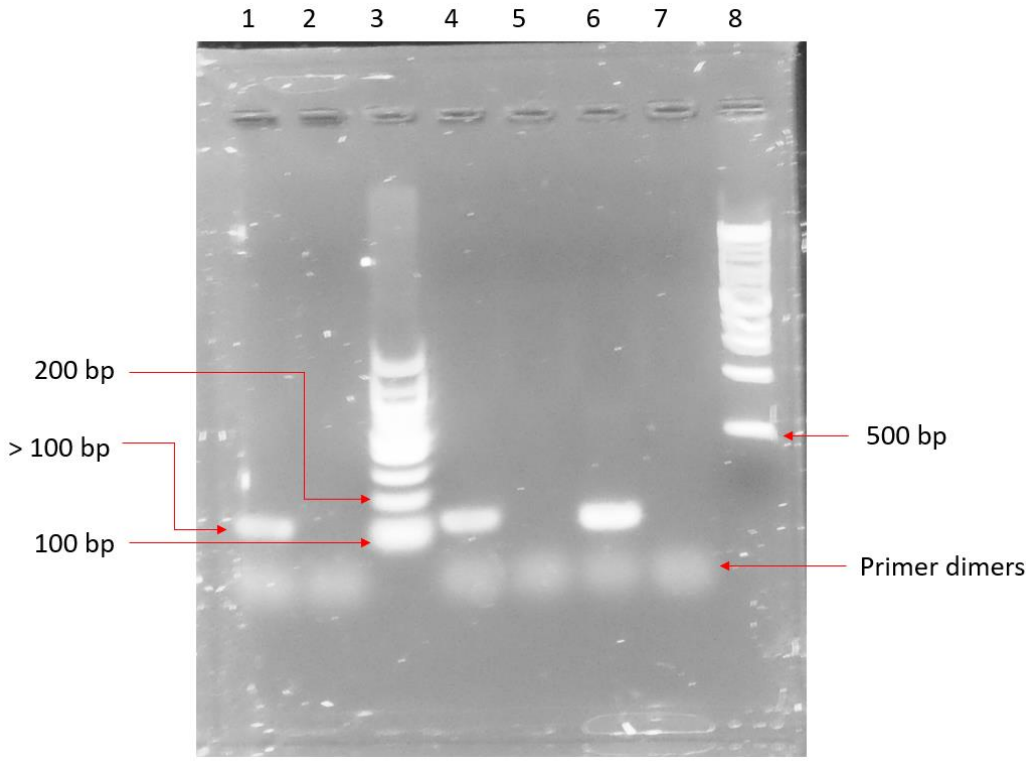

Lane	1	2	3	4	5	6	7	8
Sample	**111** (Col + MSC)	**X111** (Col + MSC)	**100 bp ladder**	**111c** (Col + MSC)	**X111c** (Col + MSC)	**115** (Col + PRP + MSC)	**X115** (Col + PRP + MSC)	**1 kb ladder**

Figure 17: Representative results of PCR amplification of synthesized cDNA using Col1a1 primer set with 30-second extension time run on 1% agarose gel. The result shown here depicts electrophoresis set-up three using a 30 second extension time. The loading of the lanes is described in the accompanying table. The predicted PCR product of the PCR reaction using the Col1a1 primer set was determined by a Primer-BLAST search to be 128 bp. Results for the remainder of the samples can be found in the Appendix section.

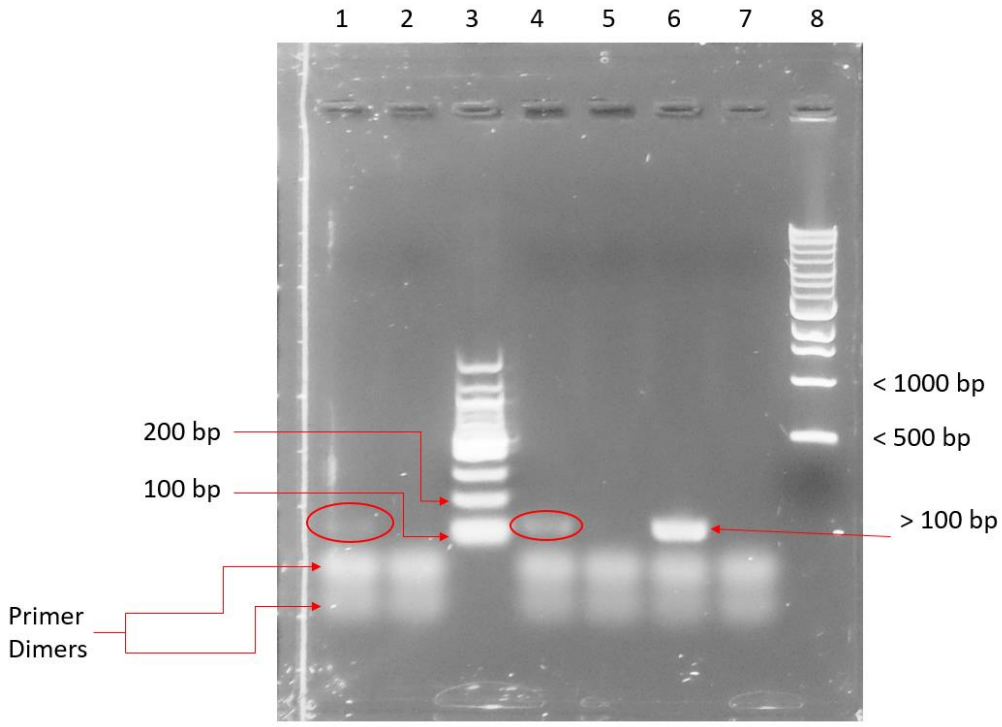

Lane	1	2	3	4	5	6	7	8
Sample	**111** (Col + MSC)	**X111** (Col + MSC)	**100 bp ladder**	**111c** (Col + MSC)	**X111c** (Col + MSC)	**115** (Col + PRP + MSC)	**X115** (Col + PRP + MSC)	**1 kb ladder**

Figure 18: Representative result of PCR amplification of synthesized cDNA using Col3a1 primer set with 30-second extension time run on 1% agarose gel. The result shown here depicts electrophoresis set-up three using a 30 second extension time. The loading of the lanes is described in the accompanying table. The predicted PCR product of the PCR reaction using the Col3a1 primer set was determined by a Primer-BLAST search to be 143 bp. Results for the remainder of the samples can be found in the Appendix section.

the RT-PCR product using the Col1a1 primer set and **Figure 18** RT-PCR product using the Col3a1 primer set. The remaining gels could be viewed in the Appendix in **Figure A3** and **Figure A4**, respectively.

For the initial RT-PCR using the primer set to amplify Col1a1 (using a 30 second extension time) and electrophoresis run accounted for two of three subjects for each experimental group designated for collagen analysis. None of the cDNA synthesis control samples displayed visible bands on any gel when the gels were visualized. This gives an initial indication that there was no DNA contamination present in the original extracted RNA samples.

In the first electrophoresis set-up (**Fig.A3*a***), which ran a 17-well 1% agarose gel, samples 101 (lane 1), 101c (lane 3), 103 (lane 5), 103c (lane 7), 104 (lane 10), 104c (lane 12), 106 (lane 14), and 106c (lane 16) were run through the gel along with their accompanying cDNA synthesis controls in the next sequential lane (i.e., lane 1 contained sample 101 followed by X101 in lane 2). A 100 bp ladder was run in lane 9 which we compared the approximate band sizes to. Bright, clearly visible bands were able to be identified in lane 1 (#101), lane 10 (#104), and lane 12 (#104c). Less bright, but distinct bands were visible in lanes 5 (#103) and 16 (#106c). One band from lane 3 (#101c) was present, but the least vibrant band to appear on the gel. Samples in lanes 7 (#103c) and 14 (#106) did not show bands that were able to be identified visually. However, the detection of bands gave the indication that a 30 second extension period for the thermocycling program was an appropriate change to the original method and would be used for amplifying Col3a1 synthesized cDNA.

The second electrophoresis set-up (**Fig. A3*b***), which ran two 8-well gels, ran samples 108 (lane 2), 108c (lane 4), and 112 (lane 6) along with a 100 bp ladder in lane 1 and a 1 kb ladder in lane 8 in the first gel. In the second gel, samples 109 (lane 1), 109c (lane 4), and 114

(lane 6) were run along with a 100 bp ladder (lane 2), and a PCR nuclease-free water control to test for contamination of the PCR reagents (lane 8). Similar to the first set-up, each sample was run next to its accompanying cDNA synthesis control with exception to control sample X109 (lane 3) and the PCR water control. From the first gel, clearly visible bands were seen in lane 2 (#108) and lane 6 (#112). However, from visual inspection, a band could not be seen in lane 4 (#108c). From the second gel in this set-up, Clear bands were seen in lanes 1 (#109) and 6 (#114) but not in lane 4 (#109c). The PCR water control only showed banding in the area where primer dimers had formed, indicating that the PCR reagents were not contaminated.

The third electrophoresis set-up (**Figure 17**) contained one 8-well gel loaded with samples 111 (lane 1), 111c (lane 4), and 115 (lane 6) with the synthesized cDNA controls sequentially following its respective test sample. A 100 bp and 1 kb ladder were run on lanes 3 and 8, respectively. For this gel, all samples formed clear bands in lanes 1 (#111), 4 (#111c) and 6 (#115).

For the RT-PCR using the primer set to amplify Col3a1 and electrophoresis run, again, accounted for two of three subjects for each experimental group. None of the cDNA synthesis control samples on any of the gels run displayed visible bands when the gels were visualized. Again, this gives an indication that there was no DNA contamination present in the original extracted RNA samples. Similar to the gels using the Col1a1 primer set, three electrophoresis set-ups were used, and the wells were loaded identical to those previously described. Though the bands were not as clean for the Col3a1 primer set samples in comparison to those seen with the Col1a1 set due to less-than-ideal band separation, however bands were able to be identified.

In the first electrophoresis set-up (**Fig. A4*a***), visible bands were able to be identified in lanes 1 (#101), 5 (#103), 10 (#104), and faintly in lane 12 (#104c). The sample run on lane 16 (#106c) could not be determined with certainty in this initial run as we could not determine the presence of a faint or if what we thought may have been a band was due to smearing of the higher primer dimer band from poor separation. Samples in lanes 3 (#101c), 7 (#103c), and 14 (#106) did not show bands that were able to be visually identified.

The gels in the second electrophoresis set-up (**Fig. A4*b***) behaved similarly to those using the Col1a1 primers. Visible bands were seen in lane 2 (#108) and lane 6 (#112) but could not be seen in lane 4 (#108c) from visual inspection in the first gel. From the second gel in this set-up, bands were seen in lanes 1 (#109) and 6 (#114) but not in lane 4 (#109c). However, what differs from the Col1a1 gels were the results from the PCR water control where the lane had shown two blurry, but distinct bands in similar location on the gel as all lanes that received samples (i.e., lanes not containing a ladder). This result from the PCR water control indicates that these bands showed in the area where primer dimers had formed while also further indicating that the PCR reagents were not contaminated for these reactions.

The third electrophoresis set-up (**Figure 18**) once again performed similarly to those using the Col1a1 primer set. For this gel, all samples formed clear bands in lanes 4 (#111c) and 6 (#115). A band was able to be identified in lane 1 (#111) but was much fainter in comparison to the other bands present on this gel.

With the successful identification of RT-PCR product bands observed using the primer sets to amplify the collagen transcripts using a 30 second extension time in the thermocycling program, we re-attempted the RT-PCR reaction using the GAPDH primer sets under these same conditions used for the collagen samples. After amplification, the gels were electrophoresed on

1% agarose gels and imaged as done previously (**Figure 19**). However, since we have previously found that the resulting PCR product result will be shorter than 500 bp, even under conditions in which larger products could be produced, the 1 kb ladder was not added. Instead, a PCR water control reaction was added to lane 7 and a 100 bp ladder was added to lane 8 (**Fig. 19B**). To lanes 1 – 4, the amplified cDNA originating from subject A111 was added in the order starting with sample 111 added to lane 1, then X111 being added to lane 2, followed by 111c to lane 3, and X111 to lane 4. Lanes 5 and 6 contained the available samples from subject A115 with amplified cDNA sample 115 being added to lane 5 and X115 added to lane 6.

The images depicted in **Figure 19** shows the results of the pilot RT-PCR reaction which used had a 6-minute extension time (A) and the RT-PCR reaction using a 30 second extension time (B) after imaging of the gel. Though band separation still proved to be less than ideal as some samples continued to show little separation, there was a slight improvement over the pilot reaction in band separation between the RT-PCR product bands and the bands that resulted from the formation of primer dimers. This allowed us to make this distinguishment between some of the bands more confidently. This was most clearly demonstrated when comparing the results of sample 115 from this reaction (**Fig. 19B**, lane 5) to the pilot reaction (**Fig. 19A**, lane 6). Additionally, with the inclusion of the water control and the 100 bp ladder, we were able to more accurately estimate both the size of the PCR product which appeared slightly lower than, if not exactly at the 100 bp band of the ladder, and of the primer dimers which appeared even lower, approximately between 80 – 90 bp. Though better separation using a higher percentage gel would allow for more definitive identification of additional bands as well as a more accurate estimation of size, this result aligns with the predicted size of our product, indicating successful amplification of the GAPDH mRNA transcript through RT-PCR.

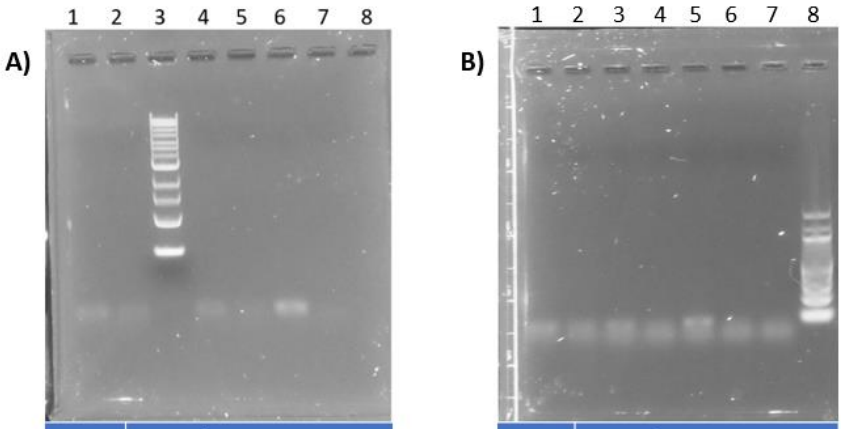

Lane	Sample
1	**111** (Col + MSC)
2	**X111** (Col + MSC)
3	**1 kb ladder**
4	**111c** (Col + MSC)
5	**X111c** (Col + MSC)
6	**115** (Col + PRP + MSC)
7	**X115** (Col + PRP + MSC)
8	**Blank**

Lane	Sample
1	**111** (Col + MSC)
2	**X111** (Col + MSC)
3	**111c** (Col + MSC)
4	**X111c** (Col + MSC)
5	**115** (Col + PRP + MSC)
6	**X115** (Col + PRP + MSC)
7	**Water control**
8	**100 bp ladder**

Figure 19: Comparison of the 6-minute and 30 second extension time RT-PCR amplification products of synthesized cDNA using the GAPDH primer set on 1% agarose gel using the same samples. *A)* Result obtained from using a 6-minute extension time in the thermocycling program. A 1 kb ladder was run in lane 3 and lane 8 was left blank. The sample in each lane corresponds to the table below the image. *B)* Result obtained from using a 30 second extension time in the thermocycling program. A PCR nuclease-free water control was run in lane 7 and a 100 bp ladder was run in lane 8. The sample in each lane corresponds to the table below the image. The predicted RT-PCR product of the PCR reaction using the GAPDH primer set was determined by a Primer-BLAST search to be 98 bp.

Comparison of RT-PCR Product to Standard DNA PCR Product

Genomic DNA Extraction of Sample Tendon #96c^{a} (Subject A85^{a})

During the harvesting of the tendon samples that would be used for biomechanical tensile testing the surgical control group, the surgically repaired tendon of subject A85^{a} (sample #96^{a}) was structurally damaged. This resulted in the decision to not use the tendon samples provided by subject A85^{a} for tensile testing. However, the control, unoperated companion tendon of subject A85^{a} (sample #96c^{a}) was not damaged during harvesting after sacrifice and was stored at -20°C in PBS-soaked gauze like the other samples destined for tensile testing. This intact unoperated control tendon sample provided an unintended, but fortunate opportunity for other areas of analysis. Though the mRNA from sample #96c^{a} would have been well-degraded due to the unstable nature of RNA when stored under those conditions at those temperatures, the genomic DNA is stable when stored at -20°C and could potentially be extracted from the unoperated tendon sample.

Because of this, we saw an opportunity to test and compare the PCR products obtained from the RT-PCR results to the PCR products achieved by using the primer sets to amplify genomic DNA. After obtaining the results from the initial pilot RT-PCR reaction using the GAPDH primer sets, which had the thermocycler programed for a 6-minute extension time, we wanted to determine the size of the PCR product obtained if the primers were used to amplify genomic DNA through a standard PCR reaction. This comparison would be useful in the context of all three primer sets as it would allow us to determine if the products obtained from the RT-PCR reactions differed from those of standard PCR. If so, then it would indicate the reverse transcribed mRNA transcript was present and amplified in the RT-PCR reaction. However, if the products did not differ, then it implies that there was DNA contamination present in the original

total RNA extraction. This unoperated control tendon from a surgical control rat subject provided the most ideal source which was readily available for obtaining a genomic DNA sample for use in a standard PCR reaction.

The tendon sample was thawed from -20°C to aseptically excise the 4 mm segment from the same location as those taken for RNA extraction and the mass was recorded to be 13.4 mg of tendon tissue. Additionally, the tissues were disrupted using the same mortar and pestle method as before to allow for equal treatment of the samples wherever possible. A Wizard Genomic DNA Purification Kit (Promega) was used to homogenize the disrupted tissue, destroy any remnants of RNA present in the sample, digest and precipitate the proteins from the sample, and to precipitate out the DNA from the sample which was washed, dried, and rehydrated in the provided DNA rehydrating solution. The concentration of the rehydrated DNA was determined using a NanoDrop spectrophotometer in triplicate. The Extracted DNA concentration determined via NanoDrop are outlined in **Table A7**. The average DNA concentration extracted from tendon sample #96c[a] was determined to be 39.2 $\frac{ng}{\mu L}$.

The extracted genomic DNA was prepared for electrophoresis on a 1% agarose gel. Three separate volumes of the DNA sample were prepared to be run on the gel such that three different amounts of DNA would be present on the gel. This was done not only to determine the rough size of the genomic DNA, but also to determine the minimum amount of DNA necessary to form visible bands. If multiple bands form in the lane with a higher amount of DNA added, this may indicate that the DNA had become fragmented during storage or the extraction process.

Each sample was mixed with 2 µL of loading dye in separate tubes, and the DNA concentration from the NanoDrop was used to determine the amount of DNA that was loaded

into the wells of the gel (Fig. 23). A 1kb ladder was added to well 1, 117.6 ng of the DNA sample was loaded in well 3, 196 ng of DNA was loaded in well 5, and 392 ng of DNA was loaded in well 8. After electrophoresing the gel at 100V for 30 minutes, the results were visualized and imaged (**Fig. 20**). The resulting image had shown a bright single band present slightly higher on the gel than the largest size band on the 1 kb ladder (largest ladder band = 48.5 kbp) for all samples tested and are shown in **Figure 20**. This result indicates that genomic DNA was successfully extracted from Sample #96c^{a} and that the extracted genomic DNA sample is viable for testing the PCR primer sets against genomic DNA to determine the size of the genomic DNA PCR products.

PCR Amplification of Genomic DNA from Sample #96c^{a}

Once successful extraction of genomic DNA had been shown, A PCR reaction was performed on the extracted genomic DNA sample using the primer sets used in the RT-PCR. We used the same protocol used to amplify the synthesized cDNA in the RT-PCR method with the major exception being a longer, 6-minute extension time in leu of a 30 second extension time. This exception was made for amplifying the DNA sample to allow for the possibility of full extension of the longest transcript (Col1a1 = 5,843 bp) that we assumed our primer sets were initially designed for. This allows us to determine if the primer sets were specific to cDNA transcripts that had been reverse transcribed from mRNA, or if the primers can also amplify genomic DNA. This would also allow us to determine if the if the RT-PCR products differ from a PCR product obtained from genomic DNA if bands were present, implying that different sequences were amplified in the PCR reaction and the possibility of the occurrence of splicing events. Finally, by comparing these PCR products to those obtained through RT-PCR, it allows us

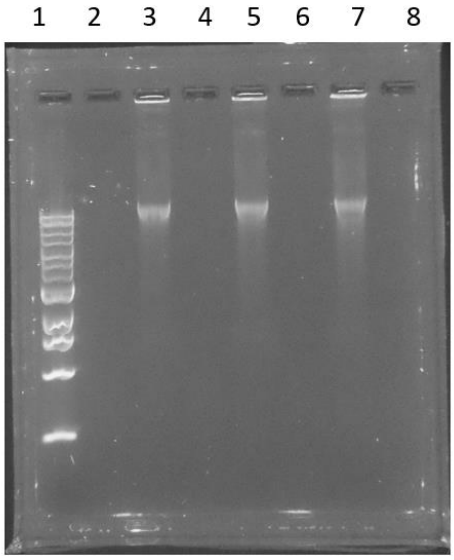

Lane	1	2	3	4	5	6	7	8
Sample # 96c	1 kb ladder	Blank	117.6 ng DNA	Blank	196 ng DNA	Blank	392 ng DNA	Blank

Figure 20: Extracted genomic DNA immediately after extraction. Genomic DNA was extracted from a 4mm tendon segment of Sample #96c[a] using a Wizard Genomic DNA Purification kit. Three different quantities of DNA were electrophoresed on a 1% agarose gel. This electrophoresis was done to confirm that DNA had been extracted and to determine the amount of DNA needed to be visualized. Lane 3 contained 117.6 ng of extracted genomic DNA, Lane 5 contained 196 ng of DNA, and lane 7 contained 392 ng of DNA. A 1 kb ladder was run in the first lane. The loading of the lanes is described in the accompanying table.

to determine if genomic DNA contamination was present from the total mRNA extraction procedure.

After imaging of the gel (**Figure 21**), bands were visible for all experimental reactions using the primer sets and none of the internal controls showed bands. These results were first inspected to determine if any of the primer sets were able to obtain a PCR product of similar length to the mRNA transcript. Despite the longer extension time which would have allowed for extension up to 6 kbp, none of the reactions achieved PCR products larger than 2 kbp. The largest PCR product obtained was from the reaction using the primer sets to amplify the Col3a1 transcript. This reaction showed a band slightly larger than 1000 bp, but far smaller than the 4,792 bp mRNA transcript. This was followed by the second largest band which used the Primer sets for Col1a1, which would have shown a band at approximately 6000 bp if the primers amplified the entire gene, but instead showed a much shorter band of approximately 450 bp. The shortest PCR product was the DNA amplified using the GAPDH primer set, showing a single band with a size ranging between approximately 200 - 250 bp.

These results from the DNA PCR were then compared to the RT-PCR results for each primer set to determine if the primer sets produced a product different to the RT-PCR product. From the RT-PCR results that were electrophoresed with both a 100 bp ladder and a 1 kb ladder for comparison, the products of both Col1a1 and Col3a1 were seen to be larger than 100 bp. However, when compared to the results of the genomic DNA PCR reaction, larger bands were observed we estimate to be at approximately 450 bp and 1,000 bp for the sample amplified using the primer sets for Col1a1 and Col3a1, respectively. This shows that a different PCR product was amplified when the genomic DNA extracted from sample #96c[a] was used as the template strand. For the GAPDH primer set, a PCR product band was observed at approximately 250 bp when visually evaluated. However, though all of these estimations are speculative

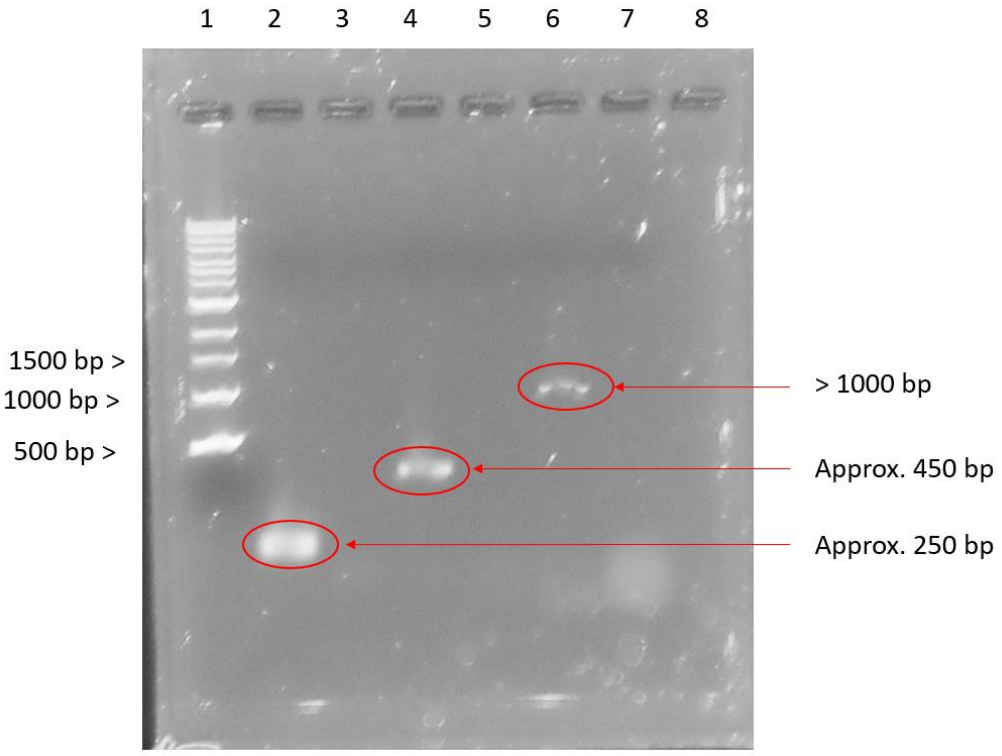

Lane	1	2	3	4	5	6	7	8
Sample # 96c	1 kb ladder	GAPDH	GAPDH control	Col1a1	Col1a1 control	Col3a1	Col3a1 control	Blank

Figure 21: Result of PCR amplification of all three primer sets on genomic DNA of Sample #96c[a] on 1% agarose gel. A 1 kb ladder was run in lane 1. Lanes 2, 4, and 6 contained the amplified genomic DNA products for GAPDH, Col1a1, and Col3a1, respectively. Control reactions received nuclease-free water in replacement of genomic DNA were run in lanes 3, 5, and 7 next to the test lane of their respective primer sets. The loading of the lanes is described in the accompanying table. A 5 µL volume of the PCR products were loaded in each well and electrophoresed at 100V for 30 minutes.

regarding the PCR product size, the estimation of the GAPDH product size may be less accurate than the estimations used for the collagen primer sets. Unlike the result observed from the Col1a1 product, which appeared on the gel below but relatively close to the shortest 500 bp band of the 1 kb ladder, the product for GAPDH appears lower in the gel and further from the 500 bp reference band of the ladder. The validity of these estimations would need to be evaluated.

Evaluating the Predicted DNA PCR Product Size

To determine if our estimations were at the very least plausible, we conducted search queries using the NCBI database similar to what we previously described to determine the predicted RT-PCR product. Briefly, the GenBank tool from the NCBI database was used to conduct a search query for the genomic DNA sequences coding for GAPDH (RefSeq: NC_051339.1), Col1a1 (RefSeq: NC_051345.1), and Col3a1 (RefSeq: NC_051344.1) of *Rattus Norvegicus*. These sequences were then matched to their respective primer sets by again utilizing the Primer-BLAST tool from the NCBI database to conduct a search query which would determine the predicted PCR product size. From the output of these Primer-BLAST search queries, we were able to obtain a predicted PCR product size. The graphical output from the Primer-BLAST search is shown in **Figure 22**.

The results of these searches determined the predicted PCR product size of the GAPDH primer set to be 208 bp in length when used to amplify the genomic DNA (**Fig. 22A**). For the Col1a1 primer set, the predicted genomic DNA PCR product was determined to be 333 bp in length (**Fig. 22B**). Finally, for the Col3a1 primer set, the genomic DNA PCR product was determined to be 854 bp long (**Fig 22C**). Though our estimations for the approximate size of the

A) 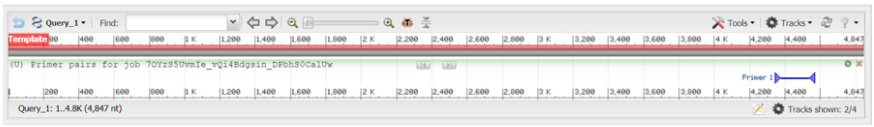

GAPDH

B) 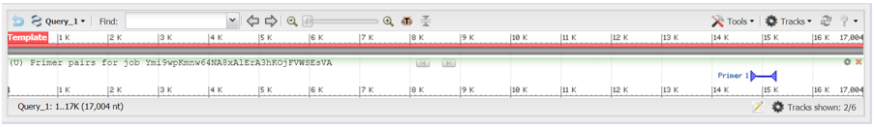

Col1a1

C) 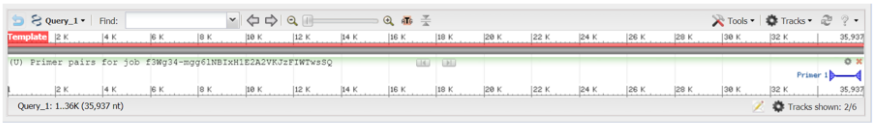

Col3a1

<u>Figure 22:</u> Graphical output determining the estimated PCR product size for each primer set against genomic DNA. these results were obtained from the search queries using the Primer-BLAST tool from the NCBI database. *A)* Primer-BLAST search query result matching the GAPDH genomic DNA sequence (RefSeq: NC_051339.1) to the GAPDH sense and antisense primer set. The predicted standard DNA PCR product is estimated to be 208 bp in length. *B)* Primer-BLAST search query result matching the Col1a1 genomic DNA sequence (RefSeq: NC_051345.1) to the Col1a1 sense and antisense primer set. The predicted standard DNA PCR product is estimated to be 333 bp in length *C)* Primer-BLAST search query result matching the Col3a1 genomic DNA sequence (RefSeq: NC_051344.1) to the Col3a1 sense and antisense primer set. The predicted standard DNA PCR result is estimated to be 854 bp in length.

DNA PCR product bands obtained from the genomic DNA did not match these predicted PCR product sizes, they do, however, follow the trend from the results obtained from these search queries with the PCR product for GAPDH being the smallest in size, the product using the Col3a1 primer set being the largest observed, and that of the Col1a1 set in between. These results give the indication that we were able to amplify portions of the genomic DNA using our primer sets. Additionally, when taken together with the results from the RT-PCR products, these results indicate that the genomic DNA PCR products differ from the products obtained from amplifying the synthesized cDNA obtained from reverse transcription of the RNA of the tendon samples.

Discussion:

Though the calcaneal tendon is the largest and strongest tendon in the human body, it derives its most common nickname from an ancient Greek tale regarding Achilles' debilitating injury. Even today, rupture of the calcaneal (Achilles) tendon remains a debilitating and prevalent injury, accounting for 35% of all tendon injuries, with the rate of occurrence on the rise in recent years (Chiodo at al. 2006, Yuksel et al. 2016, Aktas et al. 2016, Shamrock and Varacallo 2020). The disadvantages of the current treatment methods include long healing times, decreased range of motion after recovery, and a heightened chance of re-rupture. In addition, treating these injuries can often be a burdensome and expensive process to healthcare services as well as posing the risk of negatively impacting a patient's quality of life during and long after recovery. As such, there exists a need to research and investigate treatment methods aimed to improve and accelerate the healing rate of ruptured calcaneal tendons.

One promising method to address this issue has been through the use of biologics, such as collagen scaffolds, platelet-rich plasma (PRP), or mesenchymal stromal cell (MSCs) injections, as an additive to surgical repair. Collagen is the main structural and functional protein in tendon tissues and is deposited late in the inflammatory stage of tendon wound healing, acting as a scaffold for migrating cells, growth factors, and cytokines at the site of injury during the healing process (Schneider et al, 2018; Zabrynski et al. 2018; Gelse et al., 2003). Studies previously conducted by our lab examined the use of a collagen scaffold with the addition of injected platelet-rich plasma (PRP) and mesenchymal stromal cells (MSCs) in fascial healing following the repair of abdominal hernias (Marie et al., 2010; Heffner et al., 2012). These studies revealed that collagen scaffold, in the form of CollaTape, was able to absorb PRP and MSCs (Marie et al., 2010). The addition of CollaTape plus PRP and CollaTape plus PRP and MSCs significantly

increased the tensile strength of repaired fascia and caused a significant acceleration of the healing rate (Heffner et al., 2012). Yuksel et al. (2016) compared the effects of MSCs and PRP treatments in the early healing phases of a calcaneal tendon rupture when used individually (i.e., only PRP or only MSCs). They analyzed the effects of the biologics on the strength and elasticity of the tissue using biomechanical analysis and compared them with results from a semi-quantitative histopathologic evaluation. The histologic studies assessed factors such as tissue vascularity, tissue cellularity, tenocyte morphology and proliferation, as well as the structure, organization, and components (such as glycosaminoglycan and hyaluronic acid content) of the collagen fibers of the recovered tendons. They found that both biologics, when used individually, promoted accelerated healing, improved mechanical properties, such as elasticity and structural strength, when compared to their control group (Yuksel et al. 2016).

There are no studies prior to work from this lab (Ettey, 2019; Austin, 2019) which examine the effect of combining all three of these biologics, platelet-rich plasma, bone marrow derived mesenchymal stromal/stem cells, and a collagen carrier/scaffold (in the form of CollaTape), as additive treatments in the repair of a complete calcaneal tendon rupture. Our previous study (Austin, 2019) did not report the mechanical properties of the treated tendons when normalized as a percentage of the unoperated tendon. The effects of these treatments on calcaneal tendon repair were also not compared to a surgical control group, nor did we study how the treatment combinations affected the relative expression of the collagen genes during the wound healing process in tendon tissues. In these studies, we expand upon our previous study by introducing a surgical control group and determine the relative gene expression collagen types 1 and 3 using RT-PCR. We hypothesized that there would be significant improvements in the biomechanical properties of the repaired tendons that received treatment when compared to the surgical control group, with the treatment group receiving a combination of all three biologics showing

the largest improvement amongst the treatment groups. In addition, we hypothesize that a correlation would exist between the biomechanical properties of the healed tendons and the relative gene expression of the collagen genes relevant to the tendon wound healing mechanism (i.e., types 1 and 3), with a higher expression of type 1 collagen genes.

Animal Model:

We chose to use male Lewis rats as the model organism of our study. The Lewis rat strain is an inbred strain of laboratory rat which allowed for a high level of genetic similarity between the subjects. In this study, we prepared the PRP and MSC biologic treatments from the harvested material of one subject to implant into a different subject. If an outbred strain of rat were used in an allograft approach of transplantation, there would be a risk of allograft rejection. The major issue in the outbred allograft approach arises from the PRP treatments. The platelets in the PRP treatments could be recognized by the host immune response and could lead to rejection (Xu2 et al., 2006; Kirk et al., 2008). Alternatively, an autograft approach could be considered. It is possible to readily harvest and prepare PRP treatments from a single subject and administer the treatment to the subject as an autograft transplant (Yuksel et al. 2016). It is also possible to obtain and culture adult MSCs from several adult tissues (Atoui et al., 2008) for use in an autograft transplantation on an individual basis, such as in a case study by Case et al. (2013). In this study, they were able to harvest and re-introduce autologous bone marrow MSCs to the strained calcaneal tendon of a Border Collie along with a custom dynamic orthosis for movement, resulted in a 92% recovery of vertical force output from the lame limb (Case et al., 2013).

For the sample size used in our current study, each individual subject in a treatment group receiving an MSC injection would need to be isolated, cultured, passaged, and the capacity for the cells to differentiate would need to be evaluated to ensure the stem cell properties were present in the treatment. With the procedure we used in the current study, the time between the initial sample harvesting of bone marrow to the re-introduction of third passage MSCs the subjects would be in the magnitude of months for each individual subject. Additionally, this scenario assumes that the MSCs are able to demonstrate the ability to differentiate through the differentiation assay from a single bone marrow harvest, which may not be the case. Complications during cell culturing, such as an unknown source of contamination or death of the cultures due to unknown factors, are always possible. In which case, several harvests may be required until the MSCs demonstrate the ability to differentiate. Therefore, for the sample size used in our current study, an autograft approach would not have been feasible to complete in a timely manner for each individual subject.

Thus, an approach utilizing a syngeneic strain of inbred rats offered the most ideal approach when selecting a model organism to investigate the effects of PRP, MSCs, and a combination of both using a collagen scaffold/carrier. The syngeneic, inbred rat strain posed minimal risk for allograft rejections or host-versus-graft reactions to any of the biologic treatments in the recipient rats during healing as well as providing key advantages over alternative approaches.

Phase 1 – Preparation and Characterization of the Biological Treatments:

We designed a four-phase approach to the study (**Figure 1**). The main goal of the first phase was to establish an easy to access supply of the biologics used as treatments and ensuring

that the biologics possessed the necessary characteristics for our study. CollaTape came ready-to-use and allowed multiple strips to be cut from one pre-packaged strand. CollaTape is a soft, pliable sponge-like material consisting of bovine Type I collagen (Heffner et al., 2012; Mahesh et al., 2015). This material was ideal for our purposes as it provided ease of use for our collagen scaffold, requiring minimal pre-surgical preparation and it was easy to wrap the CollaTape around the tendons after the repair.

Establishing a supply of PRP required more consideration. The platelets were harvested from blood collected when rats were sacrificed, following surgery and recovery. PRP provides a source of growth factors and cytokines which result from an enriched concentration of platelets releasing their α granule stores. Previous studies have attempted to define what determines the quality of a PRP preparation (Lei et al., 2009). However, there is a lack of standardization which defines PRP quality in several areas, such as platelet concentration, exact composition, or preparation methods. Systems of classification have been proposed to assess PRP quality, such as leukocyte and fibrin content in the final PRP product (Dohan Ehrenfest et al., 2009; Dhurat and Sukesh, 2014; Pavlovic et al., 2016). However, reports of data using different classifications of PRP (such as pure PRP vs leukocyte rich PRP) on tissue healing has yielded conflicting results (Bielecki et al., 2008; Dragoo et al., 2012) and warrants further research into their biology and potential uses (Dohan Ehrenfest et al., 2009). Although commercial PRP preparation kits exist, they are often not as economically advantageous as “in-house” PRP preparations and can vary regarding the final leukocyte counts within the final PRP product (Dohan Ehrenfest et al., 2009; Dhurat and Sukesh, 2014). Furthermore, due to the lack of a standardized preparation protocol, there exists a large degree of methodological variation between studies using “in-house” protocols. This makes an accurate evaluation of their PRP product difficult, in terms of the exact composition of the PRP (Dohan Ehrenfest et al., 2009).

We were interested in defining the quality of our PRP preparations based upon a reproducible platelet count. Our primary concern was that the platelet concentrations were sufficiently higher than physiological levels found in blood and that the PRP preparation was consistent with each preparation. To test this, we performed a platelet count on three different PRP samples. There is no clear description of the minimal concentration of platelets in PRP described in the literature. PRP, by definition, is plasma enriched with platelets to levels greater than physiological concentrations, typically 2.0 x 10^5 $\frac{platelets}{mL}$. We established a target platelet concentration range of 6.0x10^7 – 1.5x10^9 $\frac{platelets}{mL}$ from previous studies which used platelet concentrates (Anitua et al. 2006, Aspenberg & Virchenko, 2004). The analysis of our platelet counts show that, not only did our PRP preparations far exceed the physiological concentration of platelets, but also confirm that the platelet dosages were consistent when preparing the PRP preparations.

In our study, we did not assess leukocyte content in our PRP preparation. However, we did not observe white blood cells when doing PRP counts and feel that the PRP which we produced could be considered a pure PRP preparation, meaning that our PRP contained only platelets with minimal contaminants such as leukocytes, erythrocytes, or fibrin. We employed a commonly used two-centrifugation procedure, modified from the method performed by Maekawa et al. (2003). This method excluded the leukocyte containing buffy coat layer after the first centrifugation. This method closely resembles a similar PRP preparation procedure described in a study by Amable et al. (2013) which aimed to optimize the two-centrifugation method of preparing PRP and also examined the content of blood-derived contaminants (i.e, red blood cells and leukocytes) in the preparation. They demonstrated that the preparation method reduced erythrocyte and leukocyte contaminants to below 0.3% after the first centrifugation

and showed a similar reduction after the second centrifugation, yielding a highly pure PRP product, nearly free of other blood derived contaminants (Amable et al., 2003). Without further examination of our PRP product, we cannot say with certainty the quantity of blood-derived contaminants our PRP preparation contained. Further analysis of the PRP product should be an area to consider in future studies.

Establishing a supply of the MSCs requires isolating the cells from the original tissues and careful cell culture. To assure that the MSCs retain their proliferative and differentiation capabilities, we used a commonly employed bone marrow isolation method to obtain our MSCs for this study. The method is a straight-forward method of obtaining initial MSC cultures, while remaining relatively fast and cost effective in comparison to other methods (Karaoz et al., 2011; Ridzuan et al., 2016). However, the percentage of MSCs present in bone marrow is low, ranging from between 0.001% to 0.01% (Dai et al., 2005; Sisakhtnezhad et al., 2017). Thus, expansion of the cultures to enrich the MSC content was necessary to achieve a viable number of MSCs. When extracted directly from bone marrow, the aspirate also contains a number of contaminating cells, such as lymphocytes and macrophages (Javazon et al., 2004). The important properties of MSCs, such as their rate of proliferation and differentiation capacity, are greatly influenced by their microenvironment when cultured *in-vitro*. Passaging the MSC cultures by removing the adherent cells using trypsin and EDTA, then plating at a lower density, serves as both an expansion method for the cell cultures, and also as a method to purify the MSC cells in culture by eliminating contamination (Javazon et al. 2004). MSCs are the predominant cell remaining when the cells are expanded in this manner, as other cells do not continue to proliferate. However, excessive passaging of MSC cultures to obtain higher purity cultures can be detrimental to the potential stem cell properties of MSCs. Moreover, conditions in the cell culturing process such as plating density, culture media, and the plastic cell culturing flask used

can also affect the properties of the MSCs (Sisakhtnezhad et al., 2017). Therefore, it was essential for us to optimize the cell culturing conditions for passaging of our harvested MSCs.

Several studies investigating MSC culture conditions and the effect of passaging have previously been conducted. Bonab and coworkers examined the effect of long term, or high passaged, MSC culture on the cell's ability to proliferate and differentiate, as well as examining changes in telomere length and cell morphology. They found that the MSC cultures which had undergone 6 or more passages had decreased differentiation potential, shortening of the telomeres, and a decrease in proliferation which they attribute to the MSCs entering into senescence (Bonab et al., 2006). Madeira and coworkers (Madeira et al., 2012) used two-dimensional gel electrophoresis to perform a quantitative proteomic analysis, comparing third passage MSC cultures to seventh passage cultures. In this study, they examined proteins involved in apoptosis (i.e., the annexin protein family), cell structure (i.e., actin), energy metabolism (i.e., mitochondrial citrate synthase), cell cycle regulation and aging (i.e., eukaryotic translation initiation factor f subunit), and stress-response proteins (i.e., heat-shock protein 9), among others. They reported higher expression of proteins involved in cell cycle regulation, metabolic energy production, and apoptosis in the seventh passaged cultures, when compared to the third passage cultures, indicating the occurrence of senescence in these late passage cultures. They also observed similar results to those reported by Bonab et al. (2006), showing a 22.5% reduction in telomere length in MSC cultures at higher passages. These studies indicate that MSCs should be used after the third passage, as was performed in the current study.

Though the exact mechanism of MSCs acting as an immunomodulator remains to be answered, it has been hypothesized that this property of MSCs can also be affected by high passage cultures. As reviewed by Javazon and coworkers, the common MSCs culture method in which the cells are grown in media containing fetal bovine serum (FBS) can result in proteins

from the FBS binding to MSC class I MHC in high passage cultures. The FBS proteins bound to MHC can induce T cells to proliferate, leading to a mixed lymphocyte reaction (Javazon et al., 2004) when the MSCs are injected into a host. The mixed lymphocyte reaction may cause MSC death. However, these consequences can be avoided in low (early) passage cultures.

Madeira et al. (2012), also recorded that the maximum growth rate of the cultures was seen at the second and third passage, with the rate declining thereafter. Furthermore, this rate of expansion is enhanced in human and rat bone marrow derived MSCs cultures if the plating density is low (Javazon et al., 2001). Bonab et al. (2006) were able to achieve successful differentiation to osteogenic and adipogenic lineages in all cultures up to 4 passages, prior to seeing a reduction in later passages. A study by Dai et al. (2005), examined the effects of MSC transplantation on myocardial infarction in a rat model, and demonstrated that third passage MSCs were able to retain their capacity to differentiate after transplantation and survived as long as 6 months post transplantation. These studies demonstrate a clear advantage of utilizing early passage MSC cultures, such as second or third passages. In fact, early passage MSCs have been the most frequently used in current research with clinical relevance, as it allows for expansion of a usable number of cells in an acceptable length of time (Javazon et al., 2001; Ringden et al., 2006; Madeira et al, 2012). For these reasons, we used third-passaged MSC cultures in the current study for the purpose of obtaining an enriched, proliferating MSC culture of higher purity while retaining the differentiation capabilities of the MSCs. The cultures were allowed to grow to 80% confluence prior to passage to avoid cell-to-cell interactions which might result in differentiation of the cells.

A previous study from our lab by Thywill Ettey was conducted to determine the optimal thawing times and culturing conditions for the mesenchymal stromal cells which allowed for retention of stem cell characteristics (Ettey 2019). Third passage Mesenchymal stromal cells

were counted, plated in T-25 and T-75 cell culturing flasks, trypsinized either on day 1 or day 2, then visualized and counted again to determine the percentage of cells recovered. It was determined that plating 5 x $10^5 \frac{cells}{mL}$ on T-75 cell culturing flasks resulted in better recovery than plating in T25 flasks. We hypothesized that the larger flask size allowed for more abundant nutrient availability to the cells while also minimizing the probability of pre-mature differentiation of the Mesenchymal stromal cells by minimizing the direct cell-to-cell contact in the cultures (Ettey 2019). It was also determined that thawing the cells and plating them in culture media one day prior to use in a treatment injection would allow for optimal performance of the MSCs.

We sought to determine the differentiation capacity of our Mesenchymal stromal cells needed for determining stem cell characteristics, as outlined by the International Society for Cell & Gene Therapy (ISCT) (Dominici et al. 2006). These cells, in an undifferentiated state, should have a spindle-shaped morphology and be plastic adherent in standard complete cell culture medium. When specific growth factors are introduced *in vitro*, differentiation to other cell lineages can be induced (Dominici et al. 2006, Horwitz et al. 2006). During cell culture and passage procedures, the cells were regularly visualized prior to replenishing the cultures with fresh media. When visualizing the cells incubated in normal culture media, we were able to see that the cells being passaged were indeed plastic adherent and displayed a spindle shaped morphology (panels B and D in **Fig. 3**, **Fig. 4**, and **Fig. 5**). The cell morphology observed here was seen to be similar to the fibroblast-like MSC cells originating from bone marrow first described by Friedenstein et al. (1970). In accordance with the requirements set forth by the International Society for Cellular Therapy (ISCT), this plastic adherence satisfies the first requirement to classify our mesenchymal stromal cells as mesenchymal stem cells (Dominici et al., 2006). To satisfy the second requirement, it was necessary to confirm that our MSCs had the capacity to

differentiate *in-vitro*. Therefore, a differentiation assay was performed two times, with samples plated in triplicate. These results can be seen in panels A and C of **Fig. 3**, **Fig. 4**, and **Fig. 5**.

Alizarin red S is a versatile dye that can be used to assess mineralization in cell cultures, such as assessing calcium-rich deposits from osteoblasts (Gregory et al., 2004). In the differentiation of MSCs to an osteogenic lineage, the differentiated MSCs form aggregated nodules which accumulate calcium within the extracellular matrix. It is this accumulation of calcium which is stained by the Alizarin red S stain (Vater et al., 2011). We were able to observe a morphological change in the cells to a more cuboidal shape (panel C of **Figure 3**), and though the staining is faint, we also observed the reddish-brown staining (panel A of **Figure 3**). This faint staining may be due to the timing of when we stained the cells. Newly differentiated osteoblasts initially produce an extracellular matrix which consists of type I collagen before forming the aggregated nodules (Vater et al., 2011). However, by staining with the Alizarin red S stain, we can distinguish these cells as osteogenic cells rather than chondrogenic cells, as chondrocytes do not produce the calcium rich deposits that osteoblasts do.

When MSCs are differentiated to adipocytes, the MSCs lose their fibroblast-like shape and become more spherical as intercellular lipid-rich vacuoles are formed within the newly differentiated cell. Oil red O stains the neutral triglycerides and lipids within these lipid-rich organelles (Vater et al., 2011). We were able to see both the morphological changes of the cells (panel C of **Figure 4**) and the positive, red staining of the intercellular lipids (panel A of **Figure 4**).

Alcean blue stain was used to identify chondrogenic differentiation of the MSCs, as it binds to the glycosaminoglycan of all collagen types (Vader et al. 2011). The cells that form cartilage tissue arise from the chondrogenic cell lineage. All forms of cartilage tissues are abundant in collagen fibers as they produce collagen to form the ground substance which

surrounds the chondrocyte. The staining which we observed demonstrates the high level of collagen deposition (panel A of **Figure 5**). Visually, the cell clusters we observed bear a resemblance to sections from tissues and pellet cultures. In three-dimensional pellet cultures or tissues, such as those seen in hyaline or elastic cartilage tissues, these cells are arranged within lacunae and form isogenous groups as they replicate. These isogenous groups can be seen arranged in two-cell clusters with distinct, darker staining territorial matrices (Mainil-Varlet et al., 2003; Bosnakovski et al., 2004; Yu et al., 2012; Lach et al., 2019). In our cultures, we can observe the similar staining of the collagen rich territorial matrix deposited by the chondrocytes. Therefore, in each assay, we were able to confirm that the MSCs we isolated from rat bone marrow had indeed retained their ability to differentiate down chondrogenic, osteogenic, and adipogenic cell lineages. When taken together, this satisfies the second requirement that defines a successful isolation of mesenchymal stem cells.

The third requirement for classifying the MSCs as stem cells required analysis of cell surface markers of the unstimulated, undifferentiated MSCs (Dominici et al., 2006). In our current study, due to a lack of clarity concerning rat MSC surface antigens, we did not conduct this analysis. The recommended defining criteria for classifying the MSCs as stem cells outlined by the ISCT applies only to human MSCs (Dominici et al., 2006). In MSCs harvested and cultured from non-human species, gene expression of MSC surface antigens are currently not as well characterized as they are in human models (Tropel et al., 2004, Wang et al., 2018). There currently remains no known universal cell surface antigen phenotype unique to MSCs amongst all species (Horwitz et al., 2006; Da Silva Meirelles, Caplan, and Nardi, 2008). For rat MSCs, there remains a lack of a defined minimum criteria for classification in the current state of the literature and requires further investigation, as it remains unknown (Suto et al., 2017). As such, the ISCT recognizes that the surface Ag profile recommendation for defining MSCs may not apply to non-human models,

such as the rat model used in this study (Dominici et al., 2006). Instead, in our rat model, characterization of the MSCs weighs more heavily on the functional characteristics of plastic adherence (Caplan 1991), and their *in-vitro* differentiation capacity (Javazon et al., 2004; Dominici et al., 2006; Horwitz et al., 2006).

Phase 2 – Rupture Simulation and Sample Storage:

The second phase of the study centered around surgically simulating Achilles tendon rupture and repair to generate the samples needed for analysis in the following phases. There are inherent differences between a "naturally occurring" complete Achilles tendon rupture, such as a rupture experienced during a strenuous sport activity, and a surgically simulated rupture prior to repair. One difference is that in "natural" ruptures, the tendon is most often torn in multiple regions, as if the tendon has been shredded and is rarely the clean, uniform rupture created in our study (Leppilahti and Orava, 1998). Despite this difference, simple end-to-end suturing repair methods similar to the one employed in the current study are most commonly employed in early surgical repairs (Leppilahti and Orava, 1998).

Though the exact healing mechanisms are not fully understood (Schneider et al., 2018), we suspect that the type of wound healing (i.e., healing by first or second intent) in our simulated tendon rupture would be similar to that in "natural" tendon ruptures repaired by open surgical procedures. "Natural" ruptures occur in a manner where the site of repair is not exposed to the external environment, minimizing the risk of external contamination of the wound edges (tendon ends) until an open surgical repair is performed to approximate the edges and close the incision, allowing for healing by first intent to occur in the tendon tissue (Ehrlich and Krummel, 1996; Leppilahti and Orava, 1998; Enoch and Leaper, 2005; Singh et al., 2017).

Several previous studies of Achilles tendon repair and healing using rat models (Bolt et al., 2007; Yuksel et al., 2016; Dietrich et al., 2017) used nearly identical methods for simulating a complete calcaneal tendon rupture to the one used in the current study. The rupture was simulated via an aseptic surgical laceration of the tendon which was approximated during the repair before closing the wound, closely resembling the conditions and repair of "natural" ruptures but representing a best-case scenario in terms of the times between rupture, repair, and treatment.

After harvesting the repaired tendon samples, they were frozen either by flash freezing for RNA analysis or by storing at -20°C wrapped in PBS-soaked gauze for biomechanical testing. To determine the relative expression of the collagen genes among the samples, preserving the mRNA transcripts from the tendon tissues was vital, therefore we chose a flash freezing method. Flash freezing methods offer a high degree of cellular preservation, as well as inactivating endogenous RNase activity within the cells. This allows for high quality preservation of the otherwise the highly fragile mRNA transcripts at temperatures above -80°C (Micke et al., 2006; Medeiros et al., 2007; Najafi and Salehi, 2014).

There have been conflicting results in the literature regarding the preservation of the biomechanical properties of ligaments and tendons extracted post-mortem which have been frozen as a means of storage (Woo et al., 1986; Clavert et al., 2001). Woo and his colleagues (1986) attribute these inconsistencies in the results to a failure to differentiate the structural and mechanical properties of the tissues. They conducted a study using freshly dissected rabbit medial collateral ligaments (MCL), which showed comparable structural and mechanical properties between fresh tendons and rabbit tendons frozen at -20°C for 3 months. They observed no significant differences between the biomechanical properties of the groups, as long as the tissues were kept hydrated and stored properly (Woo et al., 1986). Retention of the mechanical properties of frozen and thawed tissues is further supported by the current methods

for processing musculoskeletal tissue allografts for use in clinical transplant applications. Jung and his coworkers (2011) drew attention to the fact that donated tissues can undergo up to 4 freeze-thaw cycles prior to being used clinically and conducted a study investigating the effect of multiple freeze-thaw cycles on the biomechanical properties of human patellar tendons. Even though their experimental design included a group representing a worst-case scenario of 8 freeze thaw cycles, their data indicated that there was no significant difference among the groups. In the current study, we stored our tendon samples wrapped in PBS-soaked gauze to maintain hydration of the tissues and minimized the number of freeze-thaw cycles by only thawing the samples to be tested that day. Therefore, the mechanical properties of our tendon samples should not have been affected. The samples generated from the second phase of the study were used in the third and fourth phases of our study.

Phase 3 - Biomechanical Properties of Treated Tendons:

The third phase of the study determines the biomechanical tensile properties of the repaired tendon samples and compares the efficacy of the treatments used. In the initial stages of our study conducted by Ettey (2019), only the groups receiving CollaTape with PRP, MSC or both (groups 1 – 4, **Table 2**) were investigated, with the CollaTape only treatment group serving as the control group. When calculated as raw data (**Figure 10**), they could not determine any significant differences in the mechanical properties of the treated tendons (Ettey, 2019). However, the raw data calculations of our initial study did not account for inherent differences between the subjects, such as the size of the animal subjects, possible differences in strength of the animal, and the differences in tendon maturity within the groups. In the current study, we present a normalization of the raw mechanical testing data as a percentage of the unoperated

control tendon from the same animal (**Figure 11**). By normalizing the data from the initial study by Ettey (2019), we were able to show that one week after repair, the strain at failure and at the ultimate tensile strength (which determines the ductility of a material) significantly improved in tendons that received Col + MSC and Col + MSC + PRP treatments. However, in the initial portion of this study (Ettey, et al., 2019) all of the treatments were compared to the CollaTape only group, as it was used as a vehicle control. In terms of the tensile strength of the tendon tissue, the CollaTape material itself has no direct influence on the strength of the tissue and would not affect the results of the tensile testing (Heffner et al., 2012). However, the Collatape vehicle, when used by itself, can be viewed as a treatment as well. From this perspective, it was uncertain whether the CollaTape vehicle was acting to improve the healing of the tendon and possibly causing an improvement in the tensile strength of the tendon. To address this, we included a surgical control group which received no additional treatment outside of approximating the tendon ends, similar to the current open repair methods to treat a complete Achilles tendon rupture. When all treated groups (including the Col only group) were compared to the pure surgical control group, we found that all groups that received treatment had a significant improvement in the ultimate tensile strength, as well as the strain at failure when normalized as a percentage of the unoperated tendon.

A previous study from this lab investigated the effect of these biologics used in combination on abdominal fascial repairs (Heffner et al., 2012). That study had similar results to those found in the current study, with the use of all three biologics in combination resulting a significant improvement in the tensile strength of the repaired abdominal fascia, when compared to the pure surgical controls and those that received CollaTape + PRP at both 4- and 8-weeks after the repair (Heffner et al., 2012). Though, our current study differs slightly from the previous study in the post-repair recovery times and in the healing of Achilles tendons, the

major changes were seen earlier, occurring within the first two weeks. According to a previous study, it is within these initial two weeks where we would expect to see these major changes in calcaneal tendon healing using a rat model (Müller et al., 2016). Although Heffner et al. (2012) did not include a Col only group or a group which received Col + MSCs without PRP, our results that the combination of the biologics improve the tensile strength of the repaired tissue agree with this previous study.

Our study also found that the treatment which used CollaTape + MSCs only marginally outperformed the treatment which used CollaTape + PRP only in terms of the ultimate tensile strength. However, both treatments showed significant improvement in the biomechanical properties of the tendons when compared to the surgical controls (**Figure 11**). A study by Yuksel et al. (2016) comparing the effects of PRP and MSCs alone on Achilles tendon repair in rats showed similar results when testing the tensile strength of the repaired tissue. Although this study did not utilize any form of scaffolding, they too found that the MSC treatment allowed for a slight, although insignificant, improvement over the PRP treatment in ultimate tensile force, but both provided a significant improvement over their surgical control group (Yuksel et al., 2016). However, we have shown that when a collagen scaffold is used, even by itself, the mechanical properties are dramatically improved (**Figure 11**). There have been several previous studies which investigated using scaffolds of various materials, but a study conducted by Müller et al. (2016) investigating the use of a commercially available type I collagen sponge in rat Achilles tendon repairs most accurately reflects the results obtained in the current study. Similar to our current study, they found that just including a type I collagen sponge acting as a scaffold significantly accelerated the healing of the tendon nearly to the point of obtaining the mechanical properties of a naïve, uninjured tendon (Müller et al., 2016).

We believe that the biologics used in the study serve a functional role in healing a ruptured Achilles tendon and that the treatments, when used together, build off of each other to further improve healing. The CollaTape acts as the carrier to which the other injected biologics (i.e, PRP only, MSC only, or both PRP and MSCs) would be able to infiltrate and localize at the injury site. The collagen alone may be providing substrate for tissue remodeling. The collagen matrix of the CollaTape also allows for the *in-situ* activation of platelets in the PRP when injected at the site of the injury. The α2β1 integrin and glycoprotein IV receptors expressed on the surface of the platelets directly bind to the type I collagen triple helical structure (Farndale, 2006). Once activated, the platelets are able to release granules containing proteins and growth factors that are necessary for wound healing. These proteins are trapped and held within the collagen matrix substrate for continued function (Gelse et al., 2003; Pavlovic et al., 2016). The macroporous structure of the collagen scaffold serves to allow the infiltration of cells, such as the MSCs, and to retain them at the site of the calcaneal tendon in need of repair (Heffner et al., 2012). Functionally, this is similar to the role of the type III collagen scaffold formed during the tendon wound healing process (Schneider et al, 2018; Zabrynski et al. 2018). Once adhered to the collagen scaffold, the growth factors released from the activated platelets can influence MSC differentiation *in-vivo*. MSCs also provide cytokines important in would healing and blood vessel formation (Wu et al., 2007) as they have a paracrine effect (Caplan and Dennis, 2006; Chaudhury 2012; Guevara-Alverez et al., 2014).

Phase 4 – Collagen Analysis:

In the fourth, and final phase of our study, we extracted the RNA from the injured portion of the repaired tendon and used a semi-quantitative RT-PCR approach to compare the

relative expression of type I and type III collagen among the groups. We sought to examine the relative collagen expression as it could provide insight on the healing, regeneration, and recovery of the tendon by giving a rough indication of how far into the tendon healing process the samples were at the time of harvest (Chen et al., 2011). However, due to time constraints, we were only able to perform the collagen analysis on two samples from each group. This sample size is not sufficient to determine if statistically significant differences exist between the groups. However, when comparing the data from the treatment groups to the surgical control, a few observable trends were able to be identified. We observed that the amount of extractable RNA (expressed in nanograms) per milligram of the starting tendon tissue segment was higher in all but the MSC groups of those which had received treatment when compared to the surgical control group if the samples were expressed as a ng RNA per mg of tissue (**Figure 12**). This implies that a higher level of gene expression may have occurred in tendons that received CollaTape, PRP or all additives. However, Collatape plus MSC actually appeared to decrease RNA synthesis. When the data was normalized as percent of total RNA extracted (**Figure 13**), it appeared that all treatments increased the amount of RNA produced with CollaTape + PRP + MSC resulting in the highest amount of RNA synthesis. However, without the necessary statistical power needed to determine if the treatment groups differ significantly, we can only speculate why this trend was observed.

One possibility which may explain this trend may involve the entrapment of materials and migrating cells by the CollaTape scaffold, localizing them to the site of injury, and increasing the overall cellularity of the area. Though tendons are poorly vascularized, they are not entirely avascular, and the surgical laceration procedure severs the small blood vessels which supply the tendon, permitting platelets from the blood to be introduced to the wound area. The platelets may then be absorbed and activated through their interaction with the type I collagen provided

by the CollaTape and the existing collagen exposed at the wound site (Ferndale 2006; Singh et al., 2017). Once activated, the platelets release intercellular stores of granules containing growth factors such as VEGF, TGF-β, PDGF, bFGF, and IGF-1, aiding in the early healing process to repair the tissue (Andia et al., 2010; Kaux et al., 2012). These growth factors, among others, are known to influence the processes which affect the tissue cellularity by stimulating angiogenesis, increasing vascular permeability, and promoting fibroblast proliferation leading to increased migration to the wound area. This can result in an increase in localized cell population at the site (Dhanaraj et al. 2004; Heffner et al., 2012; Pavlovic et al., 2016; Schneider et al., 2018). Together, the increased migration coupled with the greater entrapment of cells migrating to the site of repair by the CollaTape, may serve a role in increasing the local cellularity of the tendon tissue, and therefore increasing the amount of extractable RNA from the tissue. A histological analysis of the repaired tendons in future studies should be considered in order to confirm the difference in cellularity of the treated tendons in comparison to the surgical controls.

The samples which received PRP as component of the treatment showed the largest increase in extracted RNA when expressed as percent of ng tendon tissue (**Figure 13**). In addition to the platelets being absorbed and localized to the wound area by the CollaTape scaffold, the growth factors released by the platelets in PRP are known to stimulate gene expression for the synthesis of extracellular matrix components (Molloy et al., 2003; Kaux et al., 2012). This was demonstrated in study conducted by Schnabel et al. (2007). In this study, they examined the dose-dependent effects on gene expression patterns on horse flexor digitorum superficialis tendon explants cultured in media containing different blood products, such as whole blood, bone marrow aspirates, PPP, physiological plasma, and PRP. They showed that the explants cultured in media containing the highest concentration of PRP yielded a greater level of

gene expression of Col1a1, Col3a1, and cartilage oligomeric matrix, when compared the other blood products tested (Schnabel et al., 2007). Cartilage oligomeric matrix protein is proposed to aid in collagen fibrillogenesis and is abundant in tendons. These results were further supported by Kaux et al. (2012) who found similar results when treating transected calcaneal tendons using PRP as an additive in a rat surgical model. Additionally, they also showed that PRP increases the expression of tenomodulin. Tenomodulin is a tendon specific gene that aids in collagen fibril maturation, recruitment of MSCs, stimulation of MSCs to differentiate down a tenocyte lineage, and regulates tenocyte proliferation (Kaux et al., 2012). Our current investigation did not include additional genes as described in the previously mentioned studies. However, the results obtained from previous studies may provide a possible explanation for why we observed the trend in the treatments which received PRP as part of the treatment. Future studies examining the expression of genes that contribute to formation of the extracellular matrix and other tendon-specific genes such as tenomodulin would need to be performed would need to determine the validity of this hypothesis for our experimental groups.

The primers used to amplify the extracted mRNA from the tendon tissues were selected due to their success in a previous study (Heinemeier et al., 2007) and have been used in an earlier investigation from our lab conducted by Mike Kelly (2017) which examined how MSCs contribute to collagen synthesis using MSC and fibroblast cell cultures. The primer sets used by Heinemeier et al. (2007) for Col1a1, Col3a1, and GAPDH (**Table 5**) were evaluated for use in standard PCR and non-quantitative RT-PCR applications for the cell cultures under various conditions (Kelly, 2017). The evaluation showed mixed results in both types of PCR reactions where PCR product bands were found in the standard PCR for amplifying DNA, but no product was seen in the RT-PCR reactions for which these primers were originally designed for. This was attributed to impurities in the extraction products such as organic compounds (i.e., phenol) and

salts, DNA contamination in the RNA, and rapid degradation of the less stable RNA extraction product).

Though speculative, we suspect that these results may have been due to the RNA extraction method used in the previous study for a number of reasons. The description of the RiboZol method used in Kelly's study did not include a DNase treatment step prior to the RT-PCR (Kelly, 2017), thus allowing DNA contamination to be present in the RNA extraction product. Also, the extent of how dry the pelleted RNA was prior to being resuspending can affect the solubility of RNA, possibly influencing the final RNA yield (RiboZol™ RNA Extraction Reagents, 2017). Furthermore, due to the fragile nature of RNA, air drying the RNA may have allowed oxidative degradation to occur. Finally, as Kelly (2017) had critiqued while discussing his results, the RiboZol method uses organic solvents which could introduce contaminants to the final RNA product if the solvents are not removed completely during the extraction process (RiboZol™ RNA Extraction Reagents, 2017).

Due to the results found by Kelly (2017) and the nature of our starting material as whole tissue, we used a different method for extracting RNA in our current study. Unlike the previous study which used an organic solvent based RiboZol method for extracting RNA, we used a RNeasy Fibrous Tissue Mini Kit (Qiagen) to extract the RNA from our tendon tissue samples based on its successful use of extracting RNA from tendon tissues (De Oliveira et al., 2019). The Qiagen kit used in the current study is a guanidinium thiocyanate-based kit designed for fibrous tissues, includes a DNase treatment as part of the protocol, and does not involve any drying steps (RNeasy Fibrous Tissue Mini Handbook, 2020). This method circumvents the issues which we suspect influenced the results in the previous study (Kelly 2017), allowing us to obtain an RNA product with less contaminants that negatively affect downstream RT-PCR reactions. As a result, not only were we able to observe visible bands of the RT-PCR products (**Figure 15**, **Figure**

17, **Figure 18**), but also the observed bands were comparable to the predicted product size determined through a Primer-BLAST search using the NCBI database (**Figure 16**).

Additionally, we wanted to confirm that the bands observed from the RT-PCR were not a result of amplifying DNA contaminants from our RNA extraction product. A standard PCR reaction was conducted using the same primer sets on DNA obtained from a control, unoperated tendon from our surgical control group (sample #96^{a}) (**Figure 21**). From this, we were able to obtain distinguishable bands from each primer set in similar size to the standard DNA PCR products initially found in the previous study (Kelly, 2017). Additionally, when using the primer sets against DNA, our results follow the same trend in regard to the size of the products predicted through a Primer-BLAST search for a standard DNA PCR reaction (with Col3a1 being the largest and GAPDH being the smallest) (**Figure 22**). Finally, when comparing the products from both types of PCR reactions, the results from our Col1a1 and Col3a1 RT-PCR (**Figure 17** and **Figure 18**) and standard PCR (**Figure 21**) reactions using the primer sets show a clear, noticeable difference in product size between the RT-PCR and PCR reactions where the amplified mRNA transcripts were shorter than the amplified DNA transcripts.

When tendons are repaired without additional treatments, such as our surgical controls, type III collagen is the first to be produced initially in the late inflammatory phase and early proliferative phase. During the later proliferative phase and the entirety of the remodeling phase, the production of type III collagen is completely replaced by the production of collagen type I (Schneider et al, 2018; Zabrynski et al. 2018). In our surgical controls, we would expect to see a high level of type III collagen expression in the repaired tendon. However, we would not expect type III collagen expression in any of the unoperated tendons as they did not sustain damage, and therefore, have no need to form this temporary scaffold for healing. In the groups that received treatment, however, we might expect to see a lower expression of type III collagen

if the treatments expedite the transition from producing type III collagen to synthesizing type I collagen. In all of our treatment groups, the CollaTape performs the same relevant functions as the type III collagen scaffold – trapping migrating cells, such as MSCs, and localizing them to the area of damage. In the previous study by Heffner et al. (2012), they attribute their success in accelerating abdominal fascia healing to a rapid transition to the proliferative phase by shortening the inflammatory phase. Due to their ability to modulate the levels of MMPs, superior rate of collagen deposition, and the anti-inflammatory characteristics of MSCs (both naturally invading and those that are applied for treatment), they assert that these aid in shortening the inflammatory phase, while reducing the need to recreate the local tissue architecture (Heffner et al., 2012). By progressing through the inflammatory phase faster, the time period of type III collagen production is reduced, thereby accelerating the transition to producing type I collagen in the treated tendons. In the unoperated tendons of all groups the tendons experienced mechanical loading, as the rat were allowed to move throughout the cage during recovery. It is possible that the rat may compensate, or alter its gait, to keep weight off of the injured limb and thereby apply slightly greater load to the tendon than normal. Mechanical loading has been shown to stimulate the synthesis and deposition of type I collagen by tenocytes (Xu et al., 2018), so we might expect to see some expression in all unoperated tendons though the expression, albeit relatively low in comparison to the repaired tendons that receive treatment. However, the repaired surgical control tendons have to progress through the full duration of the inflammatory phase, depositing the type III collagen scaffold, and slowing the progression through the healing process. Thus, we would expect little to no expression of type I collagen from the operated surgical control tendons.

With these predictions of how expression of the Col1a1 and Col3a1 would behave, we would expect that the treated tendons would be farther into the healing process than that of

the surgical control. Although subjective and not a conclusive method of determining the level of gene expression, evaluating the brightness of the observed bands can give some insight into their activity. A brighter band following RT-PCR indicates a more abundant presence of the transcript within the original tissue than that of a less bright band. This was most clearly demonstrated in the surgical control group (none) by the samples from subject #103. The repaired tendons show a clear but dim band using the Col1a1 primers (**Figure A3*a***) and a much more vibrant band using the Col3a1 primers (**Figure A4*a***). However, both samples have no bands from the unoperated control tendons. In the CollaTape only group (Col), the results from subject #104 show a brighter band for Col1a1 (**Fig A3*a***) than the Col3a1 (**Fig A4*a***) and only type I collagen was present but no type III collagen in the unoperated tendon. This trend continued in tendons receiving CollaTape with PRP (Col + PRP) seen from sample #108 (**Figure A3*b*** and **Figure A4*b***). A faint but visible type III collagen band was seen in the unoperated tendon of subject #111 (Col+MSC) (**Figure 18**). This can be explained in the context of healing microtears. If microtears occurred as a result of the rat compensating to remove weight from the repaired tendon, healing of these microtears could explain why type III collagen was expressed. However, the type I collagen band in both tendons were far brighter for subject #111 (**Figure 17**), indicating a greater expression of the type I collagen than the type III collagen. Although we were not able to obtain RNA from the unoperated tendons for either of the subjects receiving all three biologics, we were able to perform the RT-PCR on both operated tendons, which are our primary interest. The samples from subject #114 (Col + PRP + MSC) show a brighter type I collagen band (**Figure A3*b***) than the faint type III collagen band we observed (**Figure A4*b***). Thus, from an initial visual observation and comparison between the Col1a1 and Col3a1 gels, the bands we were able to obtain seem largely consistent with these predictions for the RT-PCR products using the Col1a1 and Col3a1 primer sets, in that more Col1a1 would be expected in the

treated tendons due to accelerated healing. However, this is only a subjective observation and a means of confirming these observations in a quantifiable manner is required. The comparison of the results from only the collagen genes should also not be considered conclusive without a comparison with GAPDH expression (a housekeeping gene whose expression should be stable and correct for loading errors).

Reliable RT-PCR results were not obtained when using the GAPDH primer sets. One reason for this is the poor separation of bands in the RT-PCR gels when run on 1% agarose gels. Samples showed better band separation in 1% agarose gels when using a 30-second extension time during RT-PCR than were seen when using a 6-minute extension (such as sample #115). However, this was not seen for all samples (such as all samples from subject #111) (**Figure 19**). For those samples which did not show improved band separation with the shorter extension time, we could not distinguish if the observed band was a result of amplified GAPDH mRNA transcripts or if they were primer dimers. Therefore, assessing the brightness of the bands would not be reliable. To achieve better band separation the electrophoresis could be performed on a gel with a higher agarose percentage, as was done using a 2% agarose gel (**Figure 15**). However, in the higher percentage gel bands were observed in samples receiving no reverse transcriptase enzyme during the cDNA synthesis (**Figure 15**). This suggests that the RNA extracted from the tendon segments contained some form of unknown contaminant. Thus, the results when using the GAPDH primer sets were inconclusive.

Though we can only speculate about the source of this contamination, one possibility that can be considered could be that an outside source of contamination was introduced at some point prior to cDNA synthesis. Even across species, the GAPDH gene codes for an important metabolic enzyme that converts glyceraldehyde 3-phosphate to 1,3-bisphosphoglycerate during glycolysis and is highly conserved. Relative to humans, GAPDH shares between 94 to 96%

identity across mammals and can even reach up to 65% homology in microorganisms (Seidler, 2012). Only when the GAPDH primer sets were used did we observe bands from the samples which received no reverse transcriptase during cDNA synthesis. If the source of contamination originated from bacterial cells, for example, they can express the GAPDH gene but cannot express either of the collagen genes tested here. In this scenario, there would be contaminating genetic material which coding for GAPDH in the reverse transcriptase control sample, but no nucleic acid material that codes for either collagen types we tested. If this occurred, it provides a probable explanation for the results we observed. Alternatively, an explanation may lie with the primer sets for GAPDH themselves. Though we have shown that they are able to bind and amplify GAPDH transcripts for both RT-PCR and standard DNA PCR reactions, we cannot be certain that they bind specifically to those from rats. A solution for future studies may be to target the portion of the GAPDH gene which codes for the N-terminus of the enzyme as this region often shows variability across diverse species (Seidler, 2012). Nevertheless, because we were unable to obtain reliable results when using the GAPDH primer sets, we do not have a constitutively expressed gene to compare the results obtained from the Col1a1 and Col3a1 RT-PCR reactions. Thus, we were not able to verify the relative expression of the collagen genes and the results from our collagen analysis remain inconclusive.

Summary:

The purpose of our current study was to examine the effect PRP and MSCs on a type I collagen scaffold has on the repair of a simulated complete calcaneal tendon rupture and to compare them to a surgical control. Determining an exact mechanism for how CollaTape, PRP, and MSCs as treatments interact in the repair ruptured Achilles tendons *in-vivo* is beyond the

scope of our current study. However, based on the current state of literature and previous studies conducted from our lab, we suspect that the combination of biologics serves a functional role in healing a ruptured Achilles tendon and work synergistically to further improve healing in the rat model. The CollaTape acts as the carrier to which the other injected biologics (i.e, PRP only, MSC only, or both PRP and MSCs) would be able to infiltrate and localize at the injury site (Marie et al., 2010; Heffner et al., 2012). Once absorbed into the collagen scaffold and localized to the wound area, the MSCs and the growth factors released by the activated platelets in PRP may influence the tendon healing, both as individual treatments (Yuksel et al., 2016) and synergistically with each other (Heffner et al., 2012).

The type I collagen matrix of the CollaTape allows for the *in-situ* activation of platelets in PRP when injected at the site of the injury. This is due to the α2β1 integrin and glycoprotein IV receptors that are expressed on the surface of the platelets which allow for direct binding to specific structural motifs found in the type I collagen triple helical structure (Ferndale, 2006). Once activated, the platelets are able to release their granules containing proteins and growth factors that are necessary for wound healing, which are then also trapped and held within the collagen matrix substrate (Gelse et al., 2003; Pavlovic et al., 2016). Even without the use of a scaffold, PRP has been shown to improve both the mechanical and histological properties in rat Achilles tendon healing with only a single localized injection and are known to aid in processes such as tissue regeneration, angiogenesis, and promoting cell migration (Aspenberg and Virchenko, 2004; Rozman and Bolta, 2007; Parafioriti et al., 2011). It has been shown that among these migrating cells are leukocytes and other immune cells (Smith and Roukis, 2009) which may aid in debridement of the tendon edges. Though some of the released growth factors are also released by MSCs as paracrine factors (i.e., VEGF), in PRP the number of platelets present determines the biological effect. A high platelet count can yield a higher concentration

of growth factors released in a dose-dependent manner (Gruber et al., 2004; Han et al., 2007; Qian et al., 2017).

The macroporous structure of the CollaTape also serves to allow the infiltration of cells, such as the MSCs, and to retain them at the site of the calcaneal tendon in need of repair (Marie et al., 2010; Heffner et al., 2012), functioning similarly to the type III collagen scaffold formed during natural tendon wound healing process (Schneider et al, 2018; Zabrynski et al. 2018). Entrapment of the cells ensures that the MSCs remain localized at the wound site and increases the cellularity of the wound site. The use of MSCs is known to assist healing in ruptured tendons by potentially differentiating directly into tenocytes to aid in tissue regeneration and by displaying paracrine effects which aid in healing (reviewed in Caplan and Dennis, 2006; Chaudhury 2012; Guevara-Alverez et al., 2014). In a previous study, the paracrine properties of bone marrow MSCs have also been shown to contribute to neovascularization in wounds, expressing a high level of VEGF (Wu et al., 2007). Additionally, the collagen matrix of the CollaTape may also serve to enhance MSC differentiation down a tenogenic lineage. Previous studies have shown that bone marrow derived MSCs may preferentially differentiate toward a tenogenic lineage when in the presence of collagen *in-vitro*, and when the tendon tissue microenvironment is replicated, the collagen matrix enhances the differentiation of MSCs toward the formation of tenocytes (Sharma and Snedeker, 2010; Tong et al., 2012).

When combined, the enriched concentration of platelets, providing enhanced levels of growth factors in physiologic ratios, along with the MSCs acting as “replacement parts” for temporary vascular components and tenocytes, should provide an ideal environment which supports wound healing in tendons. The high localized growth factor concentrations of PDGF, IGF-1, TGF-β, VEGF, and FGF may expedite processes such as angiogenesis and cell migration, increasing the vascularity to the otherwise poorly vascularized tissue (Pavlovic et al., 2016;

Schneider et al, 2018). Additionally, PRP has been previously shown to be mitogenic for rat bone marrow MSCs (Oprea et al., 2003), further contributing to their proliferation and the cellularity of the recovering tendon tissue. In combination with the collagen scaffold and native collagen from the tendon, it may also be possible that the growth factors may influence the actions of MSC *in-vivo* (Tong et al., 2012). The growth factors originating from the activated platelets may assist the function of MSCs by promoting cell proliferation, differentiation toward a tenocyte lineage, and allowing earlier deposition of types I and III collagen to the ECM in tendons (Zhang and Wang, 2010; Gulotta et al., 2011; Heffner et al., 2012; Qian et al., 2017). Together, these combined actions may serve to shorten the duration of the inflammatory phase, allow for an early transition to the proliferative phase, and ultimately provide a faster rate of recovery.

From the results of our biomechanical testing, we were able to determine that the groups which received any of the treatment biologics improved significantly in the ultimate tensile strength and the strain at failure in comparison to the surgical controls (**Figure 11**). Common among those treatments is that all treatments included a Collatape scaffold. We are unsure if this improvement is due to the CollaTape scaffold being incorporated into the healed portion of the tendons or if it was degraded and replaced by endogenously produced collagen. This was also unknown in the previous study from our lab conducted by Heffner et al. (2012). In their study, they performed a histological evaluation of the collagen abundance in the abdominal fascia. They found that the group receiving all three biologics as the current study in combination displayed a greater abundance of collagen compared to the group which received CollaTape + PRP, supporting the formation of newly produced collagen in the wound (Heffner et al., 2012). However, in the current study on Achilles tendons, we did not perform a histological analysis. Though we also suspect that the CollaTape scaffold was not incorporated into the tendon and that the production of endogenous collagen is better supported by the mechanical

testing of the tendons. If type III collagen is incorporated in the healed tendon, it causes a stiffer tendon. CollaTape is composed of the more elastic type I collagen. If incorporation of the CollaTape scaffold occurred, we would expect to see a more elastic tendon. However, though we found that the strength and ductility of the tissues significantly improved, there was no significant improvement in the modulus of elasticity. Therefore, we suspect that incorporation of the CollaTape seems less likely, though future studies are required to confirm these suspicions.

In our current study, there is the existence of intrinsic limitations. To our knowledge, there currently is no animal model which accurately represents tendon healing in humans. Additionally, the exact tendon healing process in humans is not completely understood and requires additional research. The results presented here should be interpreted with caution in the context of treatment of tendon injuries in humans. Another limitation lies with the method of creating the simulated rupture. As stated previously, the time between laceration/rupture and repair of the tendon represents a best-case scenario which may be a more accurate representation of instances of iatrogenic tendon damage obtained during an ankle surgery. However, simulating a complete calcaneal tendon rupture in this manner does not accurately reflect a “natural” rupture which may be the result from several underlying clinical conditions such as age, nutritional deficiencies, or degenerative conditions such as tendinitis. The recovery periods in our study were intended to represent healing at early timepoints after injury. Testing at later time points after repair would be required to determine the long-term performance of these treatments. Finally, as the tensile testing of the treated tendons were conducted exclusively by Brittany Austin and the testing of the surgical controls were tested by a separate group of mechanical engineering students, this may have introduced some variability in the methods which should be considered when interpreting these results.

The major limitation of our current study lies with the processing of samples for collagen analysis. We have demonstrated with the collagen primer sets that the methodology used here is indeed viable for extracting mRNA transcripts from tendon samples and performing an RT-PCR process. However, processing an individual sample from tissue to amplified cDNA was a time-consuming process due to manual grinding of the frozen tissue in liquid nitrogen. As a result, we were unable to process the samples from the three subjects in each group, and therefore not able to determine any statistical relevance from the data. Due to the time constraints, we also were not able to prepare gels with a higher percentage of agarose, which should have provided better band separation of the GAPDH bands. The 1% agarose gels available allowed acceptable band separation in the collagen samples due to their larger size. The culmination of these circumstances, in addition to the possible presence of contaminants in our GAPDH samples, ultimately led to inconclusive results in determining the relative expression of the collagen genes from our samples and our interpretation of these results are speculative. However, we were able to observe trends amongst the RNA extraction data. For each group, when the data was normalized as the averaged total amount of RNA extracted per milligram of the starting tendon tissue with the operated tendons expressed as a percentage of the unoperated tendons from the same animals in the group, we observed that all treatment groups increased the amount of RNA produced in comparison to the surgical control group, with CollaTape + PRP + MSC showing the highest amount of RNA synthesis in relation to their control, unoperated tendons (**Figure 13**).

In future studies the collagen analysis should be repeated. The use of a tissue homogenizer instead of the mortar and pestle would potentially reduce the sample processing time. Histologic analysis of the repaired tendons should be conducted which evaluates parameters such as vascularization and cellularity of the tissues, as well as the amount and

organization of collagen fibers within the tissues. Examination of these parameters would provide further insight in regard to the tendon healing process and allow for a more thorough explanation of the biomechanical testing results. The leukocyte content in our PRP preparation should be determined as there is no consensus in the current literature regarding their effects on wound healing in tendons. Performing this analysis may contribute to knowledge of the effects of PRP. An attempt to explore an alternative “epoxy-box” lower fixture method for tensile testing five surgical control tendons (results not shown), though for consistency of testing methods within the current study we elected not to include those results in the current study. Exploration and comparison of alternate fixturing methods in future studies should be conducted to fully establish the consistency of our tendon-vise fixturing method.

In conclusion, the purpose of the current study was to examine the effect of combining three promising biologics – platelet rich plasma, bone marrow derived mesenchymal stromal/stem cells, and a collagen carrier/scaffold in the form of CollaTape - for use as an additive treatment in a rat model of surgical repair of a calcaneal tendon rupture. The cells extracted and purified from the tibias and fibula of Lewis rats were demonstrated to be mesenchymal stem cells by their ability to differentiate toward osteogenic, chondrogenic, and adipogenic cell lineages. The method of preparing platelet-rich plasma was shown to produce a product sufficiently above physiologic platelet levels and with consistent platelet numbers in separate preparations. When normalized as a percentage of the control tendon, a trend was observed with the amount of extracted RNA per milligram of the tendon tissue segment was higher in all groups which received treatment when compared to the surgical control group. These results suggest that a higher level of gene expression may have occurred in tendons that received additional biologics treatments. However, due to the sample size being insufficient for statistical analysis significance could not be determined. Data from biomechanical tensile tests,

when normalized as a percentage of the unoperated tendon from the same animal, showed significant improvement in the strain (deformation) tolerated at failure and the ultimate tensile strength of the tendon when compared to the surgical control group. The group which received treatment utilizing all three biologics in combination (Col + MSC + PRP) also showed significant improvement over all other conditions at one week of recovery. These results support our hypothesis that applying a combination of MSCs and PRP on a CollaTape scaffold yields significantly improved mechanical properties in the repaired tendons.

Rupture of the calcaneal tendon remains a common, debilitating injury which requires long recovery periods and poses a heightened chance of re-rupture after healing. This study shows that applying MSCs, PRP, and CollaTape in combination produces an increase in the mechanical properties of the repaired calcaneal tendons. This improvement in the mechanical properties implies that the tendons treated in this manner exhibit an accelerated rate of healing and may be less prone to re-rupture after healing. In people who lead physically active lifestyles or whose occupation involves a great degree of physical labor, musculoskeletal injuries can have a dramatic impact on their quality of life. Continued research in this field may lead to improved medical treatments in the fields of orthopedics and podiatry, and ultimately lead to more effective care for the patients.

References:

2017. RiboZol™ RNA Extraction Reagents. Amresco, LLC. Protocol. https://www.amrescoinc.com/media.acux?path=/media/products/dfu/dfu-N580.pdf.

2018, GoTaq Hot Start Green Master Mix, Promega, Standard application (for a 25µL reaction volume), https://www.promega.com/-/media/files/resources/protocols/product-information-sheets/g/gotaq-hot-start-green-master-mix-protocol.pdf?la=en, April 2018

2019, RNeasy Mini Handbook, Qiagen, Disruption using a mortar and pestle, https://www.qiagen.com/us/resources/resourcedetail?id=14e7cf6e-521a-4cf7-8cbc-bf9f6fa33e24&lang=en , October 2019

2019, RNeasy Mini Handbook, Qiagen, Homogenization using a syringe and needle, https://www.qiagen.com/us/resources/resourcedetail?id=14e7cf6e-521a-4cf7-8cbc-bf9f6fa33e24&lang=en , October 2019

2020, RNeasy Fibrous Tissue Mini Handbook, Qiagen, Purification of Total RNA using the RNeasy Fibrous Tissue Mini Kit, https://www.qiagen.com/us/resources/resourcedetail?id=f6843b49-3b43-42c5-9f6d-ad5ddc4a9427&lang=en , February 2020

2019, Wizard Genomic DNA Purification Kit Technical Manual, Promega, Isolating Genomic DNA from Tissue Culture and Animal Tissue, https://www.promega.com/-/media/files/resources/protocols/technical-manuals/0/wizard-genomic-dna-purification-kit-protocol.pdf?la=en, March 2019

2020, Protoscript II cDNA FirstStrand synthesis kit instruction manual, New England BioLabs, Standard Protocol, https://www.neb.com/-/media/nebus/files/manuals/manuale6560.pdf?rev=c10bd92965f74f94b60789d9c88353d4&hash=E2D8FF9DE3DB6CE347D7142C3012D3AB, March 2020

Akino, Kozo, et al. “Early Cellular Changes of Human Mesenchymal Stem Cells and Their Interaction with Other Cells.” Wound Repair and Regeneration, vol. 13, no. 4, 2005, pp. 434–440., doi:10.1111/j.1067-1927.2005.130411.x.

Aktas E, Chamberlain CS et al., (2016) Immune Modulation With Primed Mesenchymal Stem Cells Delivered Via Biodegradable Scaffold to Repair an Achilles Tendon Segmental Defect. Journal of Orthopaedic Research 35(2):269-280

Al-Ani, Mohanad Kh, et al. “Study of Bone Marrow Mesenchymal and Tendon-Derived Stem Cells Transplantation on the Regenerating Effect of Achilles Tendon Ruptures in Rats.” Stem Cells International, vol. 2015, 2015, pp. 1–11., doi:10.1155/2015/984146.

Amable PR, Carias RB, Teixeira MV, da Cruz Pacheco I, Corrêa do Amaral RJ, Granjeiro JM, et al. Platelet-rich plasma preparation for regenerative medicine: Optimization and quantification of cytokines and growth factors. Stem Cell Res Ther 2013;4:67.

Andia, Isabel, et al. “Tendon Healing and Platelet-Rich Plasma Therapies.” Expert Opinion on Biological Therapy, vol. 10, no. 10, 2010, pp. 1415–1426., doi:10.1517/14712598.2010.514603.

Anitua, Eduardo, et al. “New Insights into and Novel Applications for Platelet-Rich Fibrin Therapies.” Trends in Biotechnology, vol. 24, no. 5, 2006, pp. 227–234., https://doi.org/10.1016/j.tibtech.2006.02.010.

Aspenberg P (2007) Stimulation of tendon repair: mechanical loading, GDFs and platelets. A mini-review. Int Orthop 31: 783-789

Aspenberg, Per, and Olena Virchenko. (2004) Platelet Concentrate Injection Improves Achilles Tendon Repair in Rats. Acta Orthopaedica Scandinavica, 75(1):93–99., doi:10.1080/00016470410001708190.

Atoui, Rony, et al. “Myocardial Regenerative Therapy: Immunologic Basis for the Potential ‘Universal Donor Cells.’” The Annals of Thoracic Surgery, vol. 86, no. 1, 2008, pp. 327–334., doi:10.1016/j.athoracsur.2008.03.038.

Austin B.L., *A Biomechanical Investigation of Collagen, Platelet-rich Plasma, and Mesenchymal Stromal Cells on the Achilles Tendon in a Rat Model.* M.S. Thesis. Youngstown State University, Youngstown, 2019. Electronic.

Badiavas, Evangelos V., et al. “Participation of Bone Marrow Derived Cells in Cutaneous Wound Healing.” *Journal of Cellular Physiology*, vol. 196, no. 2, 2003, pp. 245–250., doi:10.1002/jcp.10260.

Bielecki T, Gazdzik TS, Szczepanski T. Benefit of percutaneous injection of autologous platelet-leukocyte-rich gel in patients with delayed union and nonunion. Eur Surg Res 2008;40:289–96.

Bolt, Patrick, et al. “BMP-14 Gene Therapy Increases Tendon Tensile Strength in a Rat Model of Achilles Tendon Injury.” The Journal of Bone & Joint Surgery, vol. 89, no. 6, 2007, pp. 1315–1320., https://doi.org/10.2106/jbjs.f.00257.

Bonab, Mandana Mohyeddin, et al. “Aging of Mesenchymal Stem Cell in Vitro.” BMC Cell Biology, vol. 7, no. 1, 2006, https://doi.org/10.1186/1471-2121-7-14.

Bosnakovski, Darko, et al. “Chondrogenic Differentiation of Bovine Bone Marrow Mesenchymal Stem Cells in Pellet Cultural System.” Experimental Hematology, vol. 32, no. 5, 2004, pp. 502–509., https://doi.org/10.1016/j.exphem.2004.02.009.

Brinchmann, Jan E. “Expanding Autologous Multipotent Mesenchymal Bone Marrow Stromal Cells.” *Journal of the Neurological Sciences*, vol. 265, no. 1-2, 2008, pp. 127–130., doi:10.1016/j.jns.2007.05.006.

Caplan AI. Mesenchymal stem cells. J Orthop Res 1991;9:641 – 50.

Caplan, Arnold I., and James E. Dennis. “Mesenchymal Stem Cells as Trophic Mediators.” Journal of Cellular Biochemistry, vol. 98, no. 5, 2006, pp. 1076–1084., https://doi.org/10.1002/jcb.20886.

Case, J. Brad, et al. “Gastrocnemius Tendon Strain in a Dog Treated With Autologous Mesenchymal Stem Cells and a Custom Orthosis.” Veterinary Surgery, vol. 42, no. 4, 2013, pp. 355–360., doi:10.1111/j.1532-950x.2013.12007.x.

Chaudhury S. “Mesenchymal stem cell applications to tendon healing.” Muscles, Ligaments and Tendons Journal 2012; 2 (3): 222-229

Chen, Ming-Yan, et al. “Endothelial Differentiation of Wharton's Jelly–Derived Mesenchymal Stem Cells in Comparison with Bone Marrow–Derived Mesenchymal Stem Cells.” Experimental Hematology, vol. 37, no. 5, 2009, pp. 629–640., https://doi.org/10.1016/j.exphem.2009.02.003.

Chen, Lei, et al. “Synergy of TENDON Stem Cells and Platelet-Rich Plasma in TENDON HEALING.” Journal of Orthopaedic Research, vol. 30, no. 6, 2011, pp. 991–997., doi:10.1002/jor.22033.

Chen, Siwei, et al. “Interleukin-6 Promotes Proliferation but Inhibits Tenogenic Differentiation via the Janus Kinase/Signal Transducers and Activators of Transcription 3 (JAK/STAT3) Pathway in Tendon-Derived Stem Cells.” Medical Science Monitor, vol. 24, 2018, pp. 1567–1573., doi:10.12659/msm.908802.

Chiodo CP and Wilson MG (2006) Current concepts review: acute ruptures of the Achilles tendon. Foot Ankle Int 27:305-313.

Chong AK, Ang AD et al., (2007) Bone marrow-derived mesenchymal stem cells influence early tendon-healing in a rabbit Achilles tendon model. J Bone Joint Surg Am 89:74-81

Clavert, P., et al. “Effects of Freezing/Thawing on the Biomechanical Properties of Human Tendons.” Surgical and Radiologic Anatomy, vol. 23, no. 4, 2001, pp. 259–262., doi:10.1007/s00276-001-0259-8.

Cury DP, Dias FJ, Miglino MA, Wantabe li-s (2016) structural and ultrastructural characteristics of bone-tendon junction of the calcaneal tendon of adult wistar rats. PLoS ONE 11(4): e0153568. Doi:10.1371/journal. pone.0153586

Da Silva Meirelles, Lindolfo, et al. “In Search of the in Vivo Identity of Mesenchymal Stem Cells.” Stem Cells, vol. 26, no. 9, 2008, pp. 2287–2299., doi:10.1634/stemcells.2007-1122.

Dai W, SL Hale, BJ Martin, J-Q Kuang, JS Dow, LE Wold, and RA Kloner. 2005. Allogeneic mesenchymal stem cell transplantation in postinfarcted rat myocardium: Shortand long-term effects. Circulation 112:214-223

De Oliveira, Anderson Rodrigues, et al. “Effect of Photobiomodulation and Exercise on Early Remodeling of the Achilles Tendon in Streptozotocin-Induced Diabetic Rats.” PLOS ONE, vol. 14, no. 2, 2019, https://doi.org/10.1371/journal.pone.0211643.

Dhanaraj S, Mukhopadhyay K, Fung R, et al. 2004. Stimulation of cell proliferation and cell migration by platelet rich plasma (PRP). Trans 50th Ann Mtg ORS 29: 35.

Dhurat R, and Sukesh MS. “Principles and Methods of Preparation of Platelet-Rich Plasma: A Review and Author’s Perspective.” Journal of Cutaneous and Aesthetic Surgery, vol. 7, no. 4, 2014, p. 189., https://doi.org/10.4103/0974-2077.150734.

Dietrich, Franciele, et al. “Effect of Platelet-Rich Plasma on Rat Achilles Tendon Healing Is Related to Microbiota.” Acta Orthopaedica, vol. 88, no. 4, 2017, pp. 416–421., doi:10.1080/17453674.2017.1293447.

Dohan Ehrenfest DM, Rasmusson L, Albrektsson T. Classification of platelet concentrates: From pure platelet-rich plasma (P-PRP) to leucocyte- and platelet-rich fibrin (L-PRF). Trends Biotechnol 2009;27:158-67.

Dominici M, Le Blanc K, Mueller I, et al. Minimal criteria for defining multipotent mesenchymal stromal cells. The International Society for Cellular Therapy position statement. Cytotherapy. 2006; 8:315–317. [PubMed: 16923606]

Dragoo, Jason L., et al. “Comparison of the Acute Inflammatory Response of Two Commercial Platelet-Rich Plasma Systems in Healthy Rabbit Tendons.” The American Journal of Sports Medicine, vol. 40, no. 6, 2012, pp. 1274–1281., https://doi.org/10.1177/0363546512442334.

Edwards LC, Dunphy JE. Wound healing: injury and abnormal repair. N Engl J Med 1958;259 :275-80.

Ehrlich, H. Paul, and Thomas M. Krummel. “Regulation of Wound Healing from a Connective Tissue Perspective.” Wound Repair and Regeneration, vol. 4, no. 2, 1996, pp. 203–210., doi:10.1046/j.1524-475x.1996.40206.x.

Eliasson, Pernilla, et al. “Influence of a Single Loading Episode on Gene Expression in Healing Rat Achilles Tendons.” Journal of Applied Physiology, vol. 112, no. 2, 2012, pp. 279–288., doi:10.1152/japplphysiol.00858.2011.

Enoch, Stuart, and David John Leaper. “Basic Science of Wound Healing.” Surgery (Oxford), vol. 23, no. 2, 2005, pp. 37–42., doi:10.1383/surg.23.2.37.60352.

Ettey T., *An Investigation of Collagen, Platelet-Rich Plasma and Bone Marrow Derived Mesenchymal Stem Cells on Achilles Tendon Repair in a Rat Model.* M.S. Thesis. Youngstown State University, Youngstown, 2019. Electronic.

Farndale, Richard W. “Collagen-Induced Platelet Activation.” Blood Cells, Molecules, and Diseases, vol. 36, no. 2, 2006, pp. 162–165., doi:10.1016/j.bcmd.2005.12.016.

Fedato, Rosangela Alquieri, et al. “Stem Cells and Platelet-Rich Plasma Enhance the Healing Process of Tendinitis in Mice.” Stem Cells International, vol. 2019, 2019, pp. 1–9., doi:10.1155/2019/1497898.

Friedenstein AJ, Chailakhjan RK, Lalykina KS. The development of fibroblast colonies in monolayer cultures of guinea-pig bone marrow and spleen cells. Cell Tissue Kinet 1970;3:393–403.

Gelse K et al. (2003) collagens- structure, function, and biosynthesis. Advanced drug delivery reviews. 55 (2003) p 1531 – 1546. Doi: 10.1016/jaddr.2003.08.002

Gregory A. Carl, Gunn G. Grady et al., (2004) An Alizarin red-based assay of mineralization by adherent cells in culture: comparison with cetylpyridinium chloride extraction. Analytical Biochemistry, 329(1): 77-84.

Gruber R, Karreth F, Kandler B, Fuerst G, Rot A, Fischer MB, Watzek G (2004) Platelet-released supernatants increase migration and proliferation, and decrease osteogenic differentiation of bone marrow-derived mesenchymal progenitor cells under in vitro conditions. Platelets 15, 29–35.

Guevara-Alvarez, Alberto. “Growth Factor Delivery Vehicles for Tendon Injuries: Mesenchymal Stem Cells and Platelet Rich Plasma.” Muscles, Ligaments and Tendons Journal, 2014, https://doi.org/10.11138/mltj/2014.4.3.378.

Han, J., et al. “The Effect of Different Platelet-Rich Plasma Concentrations on Proliferation and Differentiation of Human Periodontal Ligament Cells in Vitro.” Cell Proliferation, vol. 40, no. 2, 2007, pp. 241–252., https://doi.org/10.1111/j.1365-2184.2007.00430.x.

Heffner, J. J., et al. “Bone Marrow-Derived Mesenchymal Stromal Cells and Platelet-Rich Plasma on a Collagen Matrix to Improve Fascial Healing.” Hernia, vol. 16, no. 6, 2012, pp. 677–687., https://doi.org/10.1007/s10029-012-0941-2.

Heinemeier, K. M., et al. “Expression of Collagen and Related Growth Factors in Rat Tendon and Skeletal Muscle in Response to Specific Contraction Types.” The Journal of Physiology, vol. 582, no. 3, 2007, pp. 1303–1316., doi:10.1113/jphysiol.2007.127639.

Henriksen, N. A., et al. “Connective Tissue Alteration in Abdominal Wall Hernia.” British Journal of Surgery, vol. 98, no. 2, 2010, pp. 210–219., doi:10.1002/bjs.7339.

Horwitz et al. “Mesenchymal Stromal Cells.” Current Opinion in Hematology, vol. 13, no. 6, 2006, pp. 419–425., doi:10.1097/01.moh.0000245697.54887.6f.

Javazon E, Colter D et al., (2001). Rat marrow stromal cells are more sensitive to plating density and expand more rapidly from single-cell-derived colonies than human bone marrow stromal cells. Stem Cells 19: 219-225.

Javazon EH, Beggs KJ et al. (2004) Mesenchymal stem cells: Paradoxes of passaging. Experimental Hematology 32:414–425

Jung, Ho-Joong, et al. “The Effects of Multiple Freeze–Thaw Cycles on the Biomechanical Properties of the Human Bone-Patellar Tendon-Bone Allograft.” Journal of Orthopaedic Research, vol. 29, no. 8, 2011, pp. 1193–1198., doi:10.1002/jor.21373.

Kadler KE, Baldock C et al., (2007) Collagens at a glance, Journal of Cell Science 120:1955-1958

Kadler KE, Hill A, Canty-Laird GC (2008) collagen fibrillogenesis: fibronectin, integrins, and minor collagens as organizers and nucleators. Current opinion in cell biology 20: 495 – 501. Doi: 10.1016/j.ceb.2008.06.008.

Kanchanatawan, Wichan, et al. “Hybrid Achilles Tendon Repair.” Arthroscopy Techniques, vol. 7, no. 6, 2018, doi:10.1016/j.eats.2018.02.011.

Karaöz, Erdal, et al. “A Comprehensive Characterization Study of Human Bone Marrow Mscs with an Emphasis on Molecular and Ultrastructural Properties.” Journal of Cellular Physiology, vol. 226, no. 5, 2011, pp. 1367–1382., doi:10.1002/jcp.22468.

Kaux, Jean-François, et al. “Effects of Platelet-Rich Plasma (PRP) on the Healing of Achilles Tendons of Rats.” Wound Repair and Regeneration, vol. 20, no. 5, 2012, pp. 748–756., doi:10.1111/j.1524-475x.2012.00826.x.

Kelly M.C., *Using Phage Display to Determine Mesenchymal Stem Cell Contribution to Collagen Synthesis.* M.S. Thesis. Youngstown State University, Youngstown, 2017. Electronic.

Kirk, A. D., et al. “Platelets Influence Vascularized Organ Transplants from Start to Finish.” American Journal of Transplantation, vol. 9, no. 1, 2008, pp. 14–22., doi:10.1111/j.1600-6143.2008.02473.x.

Kostrominova, Tatiana Y., and Susan V. Brooks. “Age-Related Changes in Structure and Extracellular Matrix Protein Expression Levels in Rat Tendons.” Age, vol. 35, no. 6, 2013, pp. 2203–2214., doi:10.1007/s11357-013-9514-2.

Lach, Michał Stefan, et al. “Chondrogenic Differentiation of Pluripotent Stem Cells under Controllable Serum-Free Conditions.” International Journal of Molecular Sciences, vol. 20, no. 11, 2019, p. 2711., https://doi.org/10.3390/ijms20112711.

Lei, Hua, et al. “The Effect of Anticoagulants on the Quality and Biological Efficacy of Platelet-Rich Plasma.” Clinical Biochemistry, vol. 42, no. 13-14, 2009, pp. 1452–1460., https://doi.org/10.1016/j.clinbiochem.2009.06.012.

Leppilahti, Juhana, and Sakari Orava. “Total Achilles Tendon Rupture.” Sports Medicine, vol. 25, no. 2, 1998, pp. 79–100., doi:10.2165/00007256-199825020-00002.

Madden, John W., and Erle E. Peacock. “Studies on the Biology of Collagen During Wound Healing.” Annals of Surgery, vol. 174, no. 3, 1971, pp. 511–520., doi:10.1097/00000658-197109000-00017.

Madeira A, Silva CL et al., (2012) Human Mesenchymal Stem Cell Expression Program upon Extended Ex-Vivo Cultivation, as Revealed by 2-DE-Based Quantitative Proteomics. PLoS ONE 7(8): e43523.

Mahesh L, Kurtzman GM et al., (2015) Regeneration in Periodontics: Collagen—A Review of Its Properties and Applications in Dentistry, Compendium 36:5

Mainil-Varlet P., et al. “Histological Assessment of Cartilage Repair.” The Journal of Bone and Joint Surgery-American Volume, vol. 85, 2003, pp. 45–57., https://doi.org/10.2106/00004623-200300002-00007.

Marie H, Zhang Y, Heffner J et al (2010) Biomechanical and elastographic analysis of mesenchymal stromal cell treated tissue following surgery. J Biomech Eng 132:074503

Medeiros F, Rigl CT, Anderson GG, Becker SH, Halling KC (2007) Tissue handling for genome-wide expression analysis: a review of the issues, evidence, and opportunities. Arch Pathol Lab Med 131: 1805-1816.

Micke, Patrick, et al. “Biobanking of Fresh Frozen Tissue: Rna Is Stable in Nonfixed Surgical Specimens.” Laboratory Investigation, vol. 86, no. 2, 2006, pp. 202–211., doi:10.1038/labinvest.3700372.

Mishra, Allan, et al. “Treatment of Tendon and Muscle Using Platelet-Rich Plasma.” Clinics in Sports Medicine, vol. 28, no. 1, 2009, pp. 113–125., doi:10.1016/j.csm.2008.08.007.

Najafi M, Salehi Z. “RNA Preservation and Stabilization.” Biochemistry & Physiology: Open Access, vol. 03, no. 01, 2014, doi:10.4172/2168-9652.1000126.

Moller M, Movin T, Granhed H, Lind K, Faxen E, and Karlsson J. “acute rupture of tendo Achillis: a prospective randomized study of camparison between surgical and non-surgical treatment” J. Bone Joint Surg Br. 2001;83(6):843-848.

Molloy, Timothy, et al. “The Roles of Growth Factors in Tendon and Ligament Healing.” Sports Medicine, vol. 33, no. 5, 2003, pp. 381–394., doi:10.2165/00007256-200333050-00004.

Müller, Sebastian A., et al. “Effect of a Simple Collagen Type I Sponge for Achilles Tendon Repair in a Rat Model.” The American Journal of Sports Medicine, vol. 44, no. 8, 2016, pp. 1998–2004., https://doi.org/10.1177/0363546516641942.

Oprea WE, Karp JM, Hosseini MM, Davies JE (2003) Effect of platelet releasate on bone cell migration and recruitment in vitro. J. Craniofac Surg. 14, 292–300.

Parafioriti A, Armiraglio E, Del Bianco S, Tibalt E, Oliva F, BerardiAC.Single injection of platelet-rich plasma in a rat Achilles tendon tear model. Muscles Ligaments Tendons J. 2011;1:41-47.

Pavlovic V, Ciric M, Jovanovic V, and Stojanovic P. “Platelet Rich Plasma: a Short Overview of Certain Bioactive Components.” Open Medicine, vol. 11, no. 1, 2016, pp. 242–247., doi:10.1515/med-2016-0048.

Pittenger, M. F. “Multilineage Potential of Adult Human Mesenchymal Stem Cells.” Science, vol. 284, no. 5411, 1999, pp. 143–147., doi:10.1126/science.284.5411.143.

Qian, Yun, et al. “Platelet-Rich Plasma Derived Growth Factors Contribute to Stem Cell Differentiation in Musculoskeletal Regeneration.” Frontiers in Chemistry, vol. 5, 2017, https://doi.org/10.3389/fchem.2017.00089.

Ridzuan, Noridzzaida, et al. “Characterization and Expression of Senescence Marker in Prolonged Passages of Rat Bone Marrow-Derived Mesenchymal Stem Cells.” Stem Cells International, vol. 2016, 2016, pp. 1–14., doi:10.1155/2016/8487264.

Ringdén, Olle, et al. “Mesenchymal Stem Cells for Treatment of Therapy-Resistant Graft-versus-Host Disease.” Transplantation, vol. 81, no. 10, 2006, pp. 1390–1397., https://doi.org/10.1097/01.tp.0000214462.63943.14.

Rozman P, Bolta Z. Use of platelet rich growth factors in treating wounds and soft-tissue injuries. Acta Dermatovenerol Alp Panonica Adriat. 2007;16;156-165

Schnabel, Lauren V., et al. “Platelet Rich Plasma (PRP) Enhances Anabolic Gene Expression Patterns in Flexor DIGITORUM SUPERFICIALIS TENDONS.” Journal of Orthopaedic Research, vol. 25, no. 2, 2007, pp. 230–240., doi:10.1002/jor.20278.

Schneider, Magdalena, et al. “Rescue Plan for Achilles: Therapeutics Steering the Fate and Functions of Stem Cells in Tendon Wound Healing.” Advanced Drug Delivery Reviews, vol. 129, 2018, pp. 352–375., doi:10.1016/j.addr.2017.12.016.

Seidler, Norbert W. “Basic Biology of GAPDH.” GAPDH: Biological Properties and Diversity, 2012, pp. 1–36., https://doi.org/10.1007/978-94-007-4716-6_1.

Shamrock, Alan G. “Achilles Tendon Ruptures.” StatPearls [Internet]., U.S. National Library of Medicine, 20 Jan. 2020, www.ncbi.nlm.nih.gov/books/NBK430844/.

Sharma RI, Snedeker JG. “Biochemical and biomechanical gradients for directed bone marrow stromal cell differentiation toward tendon and bone.” Biomaterials 2010;31:7695-7704.

Singh S, et al. “The Physiology of Wound Healing.” Surgery (Oxford), vol. 35, no. 9, 2017, pp. 473–477., doi:10.1016/j.mpsur.2017.06.004.

Sisakhtnezhad, Sajjad, et al. “External Factors Influencing Mesenchymal Stem Cell Fate in Vitro.” European Journal of Cell Biology, vol. 96, no. 1, 2017, pp. 13–33., https://doi.org/10.1016/j.ejcb.2016.11.003.

Smith SE, Roukis TS (2009) Bone and wound healing augmentation with platelet-rich plasma. Clin Podiatric Msd Surg 26:559-588

Suto, Eriko Grace, et al. “Prospectively Isolated Mesenchymal Stem/Stromal Cells Are Enriched in the cd73+ Population and Exhibit Efficacy after Transplantation.” Scientific Reports, vol. 7, no. 1, 2017, doi:10.1038/s41598-017-05099-1.

Tong, Wing Yin, et al. “Functional Replication of the Tendon Tissue Microenvironment by a Bioimprinted Substrate and the Support of Tenocytic Differentiation of Mesenchymal Stem Cells.” Biomaterials, vol. 33, no. 31, 2012, pp. 7686–7698., https://doi.org/10.1016/j.biomaterials.2012.07.002.

Tropel, Philippe, et al. “Isolation and Characterisation of Mesenchymal Stem Cells from Adult Mouse Bone Marrow.” Experimental Cell Research, vol. 295, no. 2, 2004, pp. 395–406., doi:10.1016/j.yexcr.2003.12.030.

Vater C, Kasten P, Stiehler M. Culture media for the differentiation of mesenchymal stem cells. Acta Biomaterialia. 2011; 7: 463-477

Wang, Xiaoyi, et al. “Simultaneous Isolation of Mesenchymal Stem Cells and Endothelial Progenitor Cells Derived from Murine Bone Marrow.” Experimental and Therapeutic Medicine, 2018, doi:10.3892/etm.2018.6844.

Woo, Savio L.-Y., et al. “Effects of Postmortem Storage by Freezing on Ligament Tensile Behavior.” Journal of Biomechanics, vol. 19, no. 5, 1986, pp. 399–404., doi:10.1016/0021-9290(86)90016-3.

Wu, Yaojiong, et al. “Mesenchymal Stem Cells Enhance Wound Healing Through Differentiation and Angiogenesis.” *Stem Cells*, vol. 25, no. 10, 2007, pp. 2648–2659., doi:10.1634/stemcells.2007-0226.

Xu, Shao-Yong, et al. “Intensity-Dependent Effect of Treadmill Running on Rat Achilles Tendon.” *Experimental and Therapeutic Medicine*, 2018, doi:10.3892/etm.2018.6084.

Xu1, Shao-Yong, et al. “Response of Decorin to Different Intensity Treadmill Running.” Molecular Medicine Reports, 2018, doi:10.3892/mmr.2018.8802.

Xu2, H. “Platelet-Derived or Soluble CD154 Induces Vascularized Allograft Rejection Independent of Cell-Bound CD154.” Journal of Clinical Investigation, vol. 116, no. 3, 2006, pp. 769–774., doi:10.1172/jci27155.

Yang X., et al. “Management of Acute Achilles Tendon Ruptures” : Bone Joint Res 2018;7:561–569. doi: 10.1302/2046-3758.710.

Yuchi Maekawa, Kyouko Yagi, Ayako Nonomura, Rie Kuraoku, Emi Nishiura, Emi Uchibori, and Kikuko Takeuchi. 2003. A Tetrazolium-based colorimetric assay for metabolic activity of stored blood platelets. Thrombosis Research 109:307-314.

Yu, Da-Ae, et al. “Stimulation of Chondrogenic Differentiation of Mesenchymal Stem Cells.” International Journal of Stem Cells, vol. 5, no. 1, 2012, pp. 16–22., https://doi.org/10.15283/ijsc.2012.5.1.16.

Yuksel S, et al. Comparison of the early period effects of bone marrow-derived mesenchymal stem cells and platelet-rich plasma on the Achilles tendon ruptures in rats. Connect Tissue Res. 2016; 57(5):360-373.

Zabrzyński, J., et al. “Tendon — Function-Related Structure, Simple Healing Process and Mysterious Ageing.” Folia Morphologica, vol. 77, no. 3, 2018, pp. 416–427., doi:10.5603/fm.a2018.0006.

Zhang Jianying, and James H.-C. Wang. “Platelet-Rich Plasma Releasate Promotes Differentiation of Tendon Stem Cells into Active Tenocytes.” The American Journal of Sports Medicine, vol. 38, no. 12, 2010, pp. 2477–2486., https://doi.org/10.1177/0363546510376750.

Appendix:

Table A1: RNA extraction results.

Treatment	Sample	Code	Elution [a]	RNA conc. (ng/uL)	A260/ A280	A260/ A230
None	A101	101	2	21.7	1.96	2.31
		101c	1	34.8	1.57	0.65
	A103	103	2	46.7	1.8	0.71
		103c	1	32.5	1.54	0.6
Col	A104	104	2	34.1	1.9	1.17
		104c	1	34	1.6	0.66
	A106	106	2	50.4	2	1.15
		106c	1	25.2	1.85	1.2
Col + PRP	A108	108	2	62.3	1.67	0.97
		108c	1	22.3	1.54	0.59
	A109	109	3	22.5	1.97	2.08
		109c	2	18.4	1.5	0.66
Col + MSC	A111	111	1	57.9	1.6	0.69
		111c	1	38.8	1.56	0.61
	A112	112	2	19.1	2.05	2.16
Col + MSC + PRP	A114	114	1	98.2	1.73	0.92
	A115	115	2	88.5	2.03	2.2

[a] Multiple elutions with 30µL of RNase-Free water were performed, separately, to clear the RNA from the column or until the RNA concentration was determined to be below the minimum RNA concentration of 16.67 $^{ng}/_{\mu L}$ necessary to achieve a 100ng of RNA for cDNA synthesis. The separate elutions were not combined to avoid diluting the RNA concentration.

[b] cDNA synthesis was done on elutions which were above the minimum RNA concentration of 16.67 $^{ng}/_{\mu L}$ necessary to achieve a 100ng of RNA for synthesis. Elutions with a concentration above 100 $^{ng}/_{\mu L}$ did not proceed to cDNA synthesis, but were instead stored at -80°C.

[c] Sample 112c was the first attempt at extracting the RNA from the 4mm tendon segments. As such, we used an 80µL elution volume of RNase-free water as recommended by the manufacturer. However, by using this volume, this resulted in a diluted the RNA concentration of the eluate and causing us to adopt a 30µL elution volume approach.

Table A2: **Mass of the 4mm tendon tissue sample at the time of harvest prior to flash freezing**.

Sample Mass (mg)				
Treatment	None			
Sample	**101**	**103**	**Avg.**	**SD**
Test	65	38	51.50	19.09
Control	20	20	20.00	0.00
Treatment	Col			
Sample	**104**	**106**	**Avg.**	**SD**
Test	64	16	40.00	33.94
Control	17	20	18.50	2.12
Treatment	Col + PRP			
Sample	**108**	**109**	**Avg.**	**SD**
Test	5	76	40.50	50.20
Control	9	32	20.50	16.26
Treatment	Col + MSC			
Sample	**111**	**112**	**Avg.**	**SD**
Test	61	34	47.50	19.09
Control	15	15	15.00	0.00
Treatment	Col + MSC + PRP			
Sample	**114**	**115**	**Avg.**	**SD**
Test	96	58	77.00	26.87
Control	24	27	25.50	2.12

[a] The RNA extraction procedure was not performed on samples 102 (surgical control), 105 (CollaTape only), 107 (Col + PRP), 110 (Col + MSC), and 113 (Col + PRP + MSC) and are not included in the Table.

Table A3: **Calculated total amount of RNA extracted from each tendon tissue sample.**

Total RNA Extracted (ng)				
Treatment	None			
Sample	101	103	Avg.	SD
Test	9999	6336	8167.50	2590.13
Control	1224	1350	1287.00	89.10
Treatment	Col			
Sample	104	106	Avg.	SD
Test	5802	11967	8884.50	4359.31
Control	1038	1155	1096.50	82.73
Treatment	Col + PRP			
Sample	108	109	Avg.	SD
Test	5208	13947	9577.50	6179.41
Control	897	846	871.50	36.06
Treatment	Col + MSC			
Sample	111	112	Avg.	SD
Test	1914	2358	2136.00	313.96
Control	1347	112	729.50	873.28
Treatment	Col + MSC + PRP			
Sample	114	115	Avg.	SD
Test	8250	24351	16300.50	11385.13
Control	264	1173	718.50	642.76

[a] The RNA extraction procedure was not performed on samples 102 (surgical control), 105 (CollaTape only), 107 (Col + PRP), 110 (Col + MSC), and 113 (Col + PRP + MSC) and are not included in the Table.

[b] Amount of RNA was calculated by multiplying the concentration of RNA ($\frac{ng}{\mu L}$) by the elution volume (µL) for each elution to determine the amount of RNA (ng) in each elution. For each sample, the amount of RNA in each elution were added together to obtain the total amount extracted

Table A4: **Normalized RNA extraction result expressed as amount of RNA extracted per mg of tendon tissue.**

ng RNA/mg Tissue				
Treatment	None			
Sample	101	103	Avg.	SD
Test	153.83	166.74	160.28	9.13
Control	61.20	67.50	64.35	4.45
Treatment	Col			
Sample	104	106	Avg.	SD
Test	90.66	747.94	419.30	464.77
Control	61.06	57.75	59.40	2.34
Treatment	Col + PRP			
Sample	108	109	Avg.	SD
Test	1041.60	183.51	612.56	606.76
Control	99.67	26.44	63.05	51.78
Treatment	Col + MSC			
Sample	111	112	Avg.	SD
Test	31.38	69.35	50.36	26.85
Control	89.80	7.47	48.63	58.22
Treatment	Col + MSC + PRP			
Sample	114	115	Avg.	SD
Test	85.94	419.84	252.89	236.11
Control	11.00	43.44	27.22	22.94

[a] The RNA extraction procedure was not performed on samples 102 (surgical control), 105 (CollaTape only), 107 (Col + PRP), 110 (Col + MSC), and 113 (Col + PRP + MSC) and are not included in the Table.

[b] The normalized amount of RNA extracted from the tissue was calculated by dividing the total amount of RNA extracted from the sample by the original mass of the tendon tissue sample.

Table A5: Total RNA extracted expressed as a percent of unoperated tendon [(operated tendon/unoperated tendon) x 100].

Total Extracted RNA				
treat.	None			
sample	**101**	**103**	avg	SD
test	9999	6336	8167.5	2590.132
control	1224	1350	1287	89.09545
% control	816.9118	469.3333	643.1225	245.7751
treat.	col			
sample	**104**	**106**	avg	SD
test	5802	11967	8884.5	4359.313
control	1038	1155	1096.5	82.73149
% control	558.9595	1036.104	797.5317	337.392
treat.	col+PRP			
sample	**108**	**109**	avg	SD
test	5208	13947	9577.5	6179.406
control	897	846	871.5	36.06245
% control	580.602	1648.582	1114.592	755.1756
treat.	col+MSC			
sample	**111**	**112**	avg	SD
test	1914	2358	2136	313.9554
control	1347	112	729.5	873.2769
% control	142.0935	2105.357	1123.725	1388.237
treat.	col+Both			
sample	**114**	**115**	avg	SD
test	8250	24351	16300.5	11385.13
control	264	1173	718.5	642.7601
% control	3125	2075.959	2600.48	741.7839

Table A6: **Amount of RNA extracted per mass of tendon tissue expressed as a a percent of unoperated tendon [(operated tendon/unoperated tendon) x 100].**

ng RNA/mg tissue				
treat.	none			
sample	**101**	**103**	avg	SD
test	153.8308	166.7368	160.2838	9.125972
control	61.2	67.5	64.35	4.454773
% control	251.3575	247.0175	249.1875	3.068788
treat.	col			
sample	**104**	**106**	avg	SD
test	90.65625	747.9375	419.2969	464.768
control	61.05882	57.75	59.40441	2.339692
% control	148.4736	1295.13	721.8017	810.8084
treat.	col+PRP			
sample	**108**	**109**	avg	SD
test	1041.6	183.5132	612.5566	606.759
control	99.66667	26.4375	63.05208	51.78084
% control	1045.084	694.1396	869.6116	248.1549
treat.	col+MSC			
sample	**111**	**112**	avg	SD
test	31.37705	69.35294	50.365	26.85301
control	89.8	7.466667	48.63333	58.21846
% control	34.94103	928.834	481.8875	632.0778
treat.	col+Both			
sample	**114**	**115**	avg	SD
test	85.9375	419.8448	252.8912	236.1081
control	11	43.44444	27.22222	22.94169
% control	781.25	966.3947	873.8224	130.9171

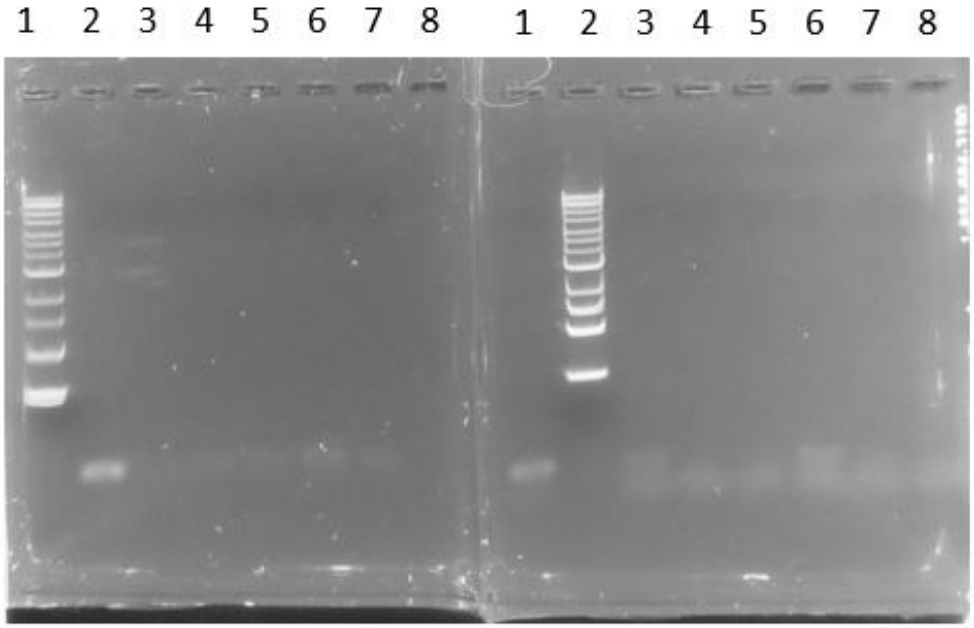

Lane (left)	1	2	3	4	5	6	7	8
Sample	**1 kb ladder**	**108** (Col + PRP)	**X108** (Col + PRP)	**108c** (Col + PRP)	**X108c** (Col + PRP)	**112** (Col + MSC)	**X112** (Col + MSC)	**Blank**
Lane (right)	**1**	**2**	**3**	**4**	**5**	**6**	**7**	**8**
Sample	**109** (Col + PRP)	**1 kb ladder**	**X109** (Col + PRP)	**109c** (Col + PRP)	**X109c** (Col + PRP)	**114** (Col + PRP + MSC)	**X114** (Col + PRP + MSC)	**Water control**

<u>Figure A1:</u> Initial RT-PCR results for gels using GAPDH Primer set with 6-minute extension time. Electrophoresis set-up two results running two 8-well 1% agarose gels with each gel being loaded according to the accompanying table below the image. Left gel is considered the first gel (above black line in table) and the right is considered the second gel (below black line in table).

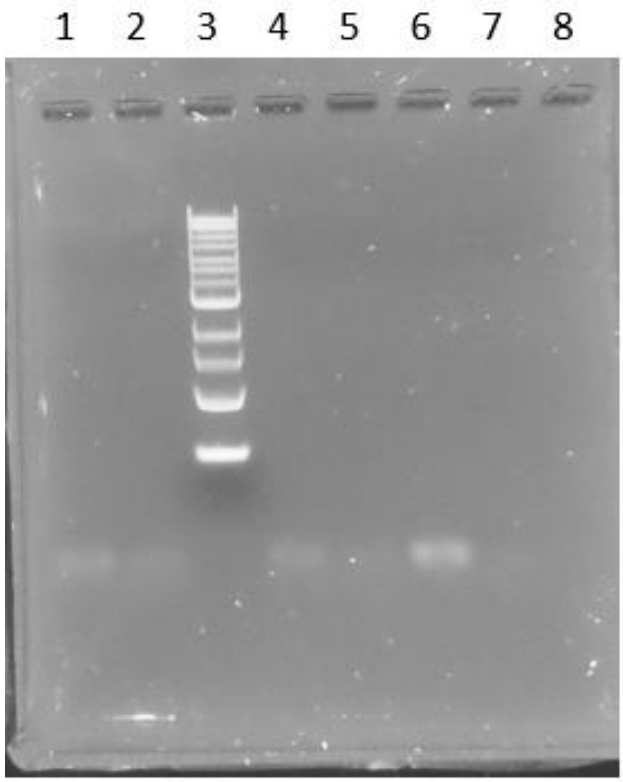

Lane	1	2	3	4	5	6	7	8
Sample	**111** (Col + MSC)	**X111** (Col + MSC)	**1 kb ladder**	**111c** (Col + MSC)	**X111c** (Col + MSC)	**115** (Col + PRP + MSC)	**X115** (Col + PRP + MSC)	**Blank**

<u>Figure A2:</u> Initial RT-PCR results for gels using GAPDH Primer set with 6-minute extension time. Electrophoresis set-up three running one 8-well 1% agarose gel. The lanes were loaded according to the accompanying table below the imaged gel.

a)

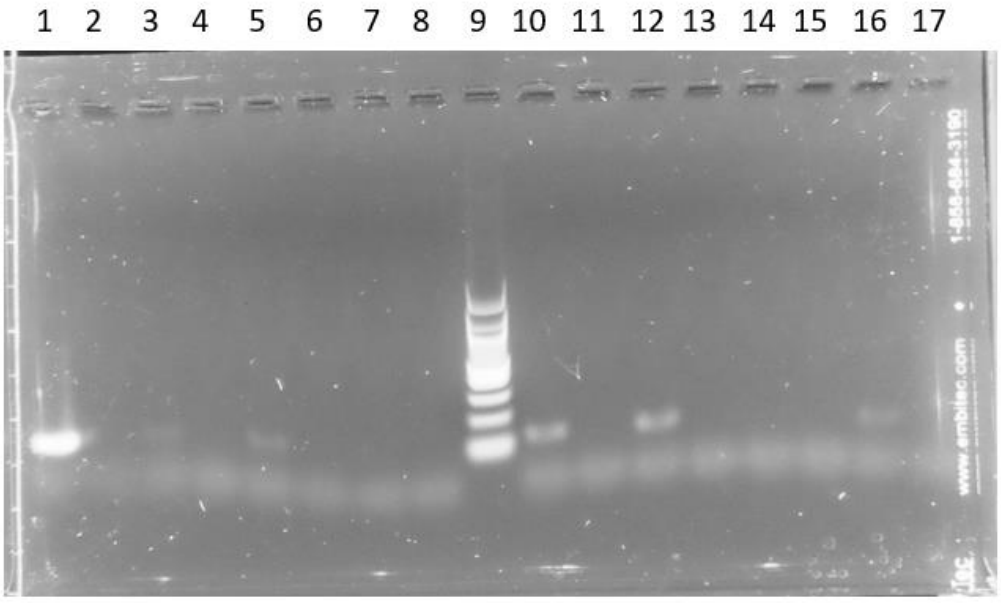

Lane	1	2	3	4	5	6	7	8	9
Sample	**101** (none)	**X101** (none)	**101c** (none)	**X101c** (none)	**103** (none)	**X103** (none)	**103c** (none)	**X103c** (none)	**100 bp ladder**
Lane	**10**	**11**	**12**	**13**	**14**	**15**	**16**	**17**	
Sample	**104** (Col)	**X104** (Col)	**104c** (Col)	**X104c** (Col)	**106** (Col)	**X106** (Col)	**106c** (Col)	**X106c** (Col)	

b)

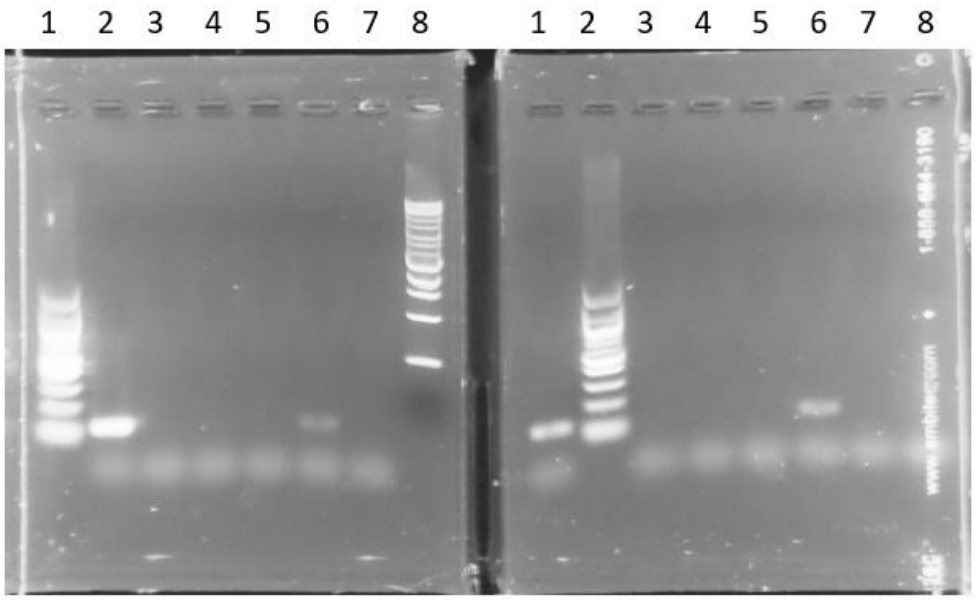

Lane (left)	1	2	3	4	5	6	7	8
Sample	**100 bp ladder**	**108** (Col + PRP)	**X108** (Col + PRP)	**108c** (Col + PRP)	**X108c** (Col + PRP)	**112** (Col + MSC)	**X112** (Col + MSC)	**1 kb ladder**

Lane (right)	1	2	3	4	5	6	7	8
Sample	**109** (Col + PRP)	**100 bp ladder**	**X109** (Col + PRP)	**109c** (Col + PRP)	**X109c** (Col + PRP)	**114** (Col + PRP + MSC)	**X114** (Col + PRP + MSC)	**Water control**

<u>Figure A3:</u> Col1a1 Primer set RT-PCR results for 1% agarose gel set-ups one and two amplified with a 30-second extension time. The predicted PCR product of the PCR reaction using the Col1a1 primer set was determined by a Primer-BLAST search to be 128 bp. *a)* electrophoresis set-up one results on a 17-well gel. The lanes were loaded according to the accompanying table *b)* electrophoresis set-up two results on two 8-well gels with each gel being loaded according to the accompanying table. The left gel is considered the first gel (above black line in the table) and the right gel is considered the second gel (below black line in the table).

a)

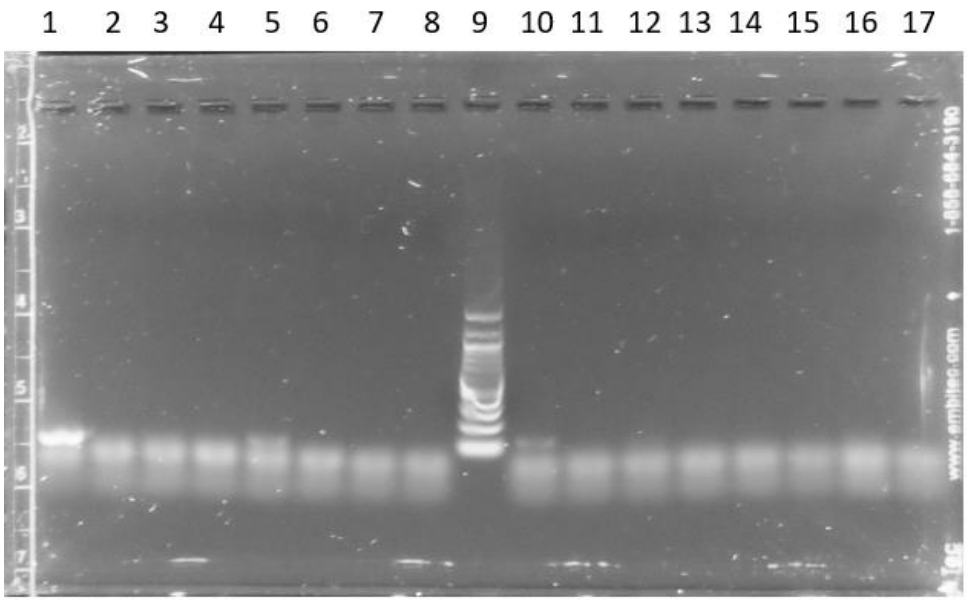

Lane	1	2	3	4	5	6	7	8	9
Sample	**101** (none)	**X101** (none)	**101c** (none)	**X101c** (none)	**103** (none)	**X103** (none)	**103c** (none)	**X103c** (none)	**100 bp ladder**
Lane	**10**	**11**	**12**	**13**	**14**	**15**	**16**	**17**	
Sample	**104** (Col)	**X104** (Col)	**104c** (Col)	**X104c** (Col)	**106** (Col)	**X106** (Col)	**106c** (Col)	**X106c** (Col)	

b)

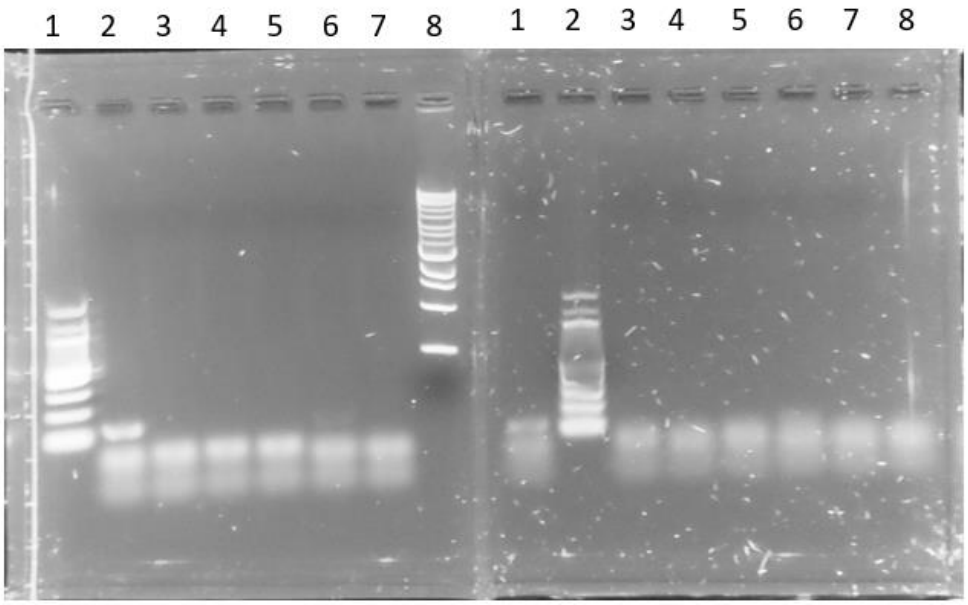

Lane (left)	1	2	3	4	5	6	7	8
Sample	**100 bp ladder**	**108** (Col + PRP)	**X108** (Col + PRP)	**108c** (Col + PRP)	**X108c** (Col + PRP)	**112** (Col + MSC)	**X112** (Col + MSC)	**1 kb ladder**

Lane (right)	1	2	3	4	5	6	7	8
Sample	**109** (Col + PRP)	**100 bp ladder**	**X109** (Col + PRP)	**109c** (Col + PRP)	**X109c** (Col + PRP)	**114** (Col + PRP + MSC)	**X114** (Col + PRP + MSC)	**Water control**

<u>Figure A4:</u> Col3a1 Primer set RT-PCR results for 1% agarose gel set-ups one and two amplified with a 30-second extension time. The predicted PCR product of the PCR reaction using the Col3a1 primer set was determined by a Primer-BLAST search to be 143 bp. *a)* Electrophoresis set-up one results on a 17-well gel. The lanes were loaded according to the accompanying table. *b)* Electrophoresis set-up two results on two 8-well gels with each gel being loaded according to the accompanying table. The left gel is considered the first gel (above black line in the table) and the right gel is considered the second gel (below black line in the table).

Table A7: Genomic DNA extraction yield from 13.4 mg of sample tendon #96c[a].

Test	Concentration ($^{ng}/_{\mu L}$) [a]	$^{A260}/_{A280}$ [a]	$^{A260}/_{A230}$ [a]
1	39.5	1.83	0.52
2	39.5	1.84	0.52
3	38.8	1.82	0.52
Average [b]	***39.2***	***1.83***	***0.52***

[a] These results were determined using NanoDrop and conducted in triplicate from the same sample.

[b] The average of the three results from the NanoDrop was calculated for the concentration, A260/A280 ratio, and the A260/A230 ratios.

IACUC Approval

YOUNGSTOWN STATE UNIVERSITY

One University Plaza, Youngstown, Ohio 44555
Office of Research
330.941.2377

November 7, 2018

Dr. Diana Fagan
Department of Biological Sciences
UNIVERSITY

Re: **IACUC Protocol, 06-18**
Title: An investigation of collegan, platlet-rich plasma, and bone marrow derived mesenchymal stem cells on the Achilles tendon in a rat model

Dear Dr. Fagan:

The Institutional Animal Care and Use Committee of Youngstown State University has reviewed the aforementioned protocol you submitted for consideration and determined it should be unconditionally approved for the period of August 14, 2018 through its expiration date of August 14, 2021.

This protocol is approved for a period of three years; however, it must be updated yearly via the submission of an Annual Review-Request to Use Animals form. These Annual Review forms must be submitted to the IACUC at least thirty days *prior* to the protocol's yearly anniversary dates of August 14, 2019 and August 14, 2020. If you do not submit the forms as requested, this protocol will be immediately suspended. You must adhere to the procedures described in your approved request; any modification of your project must first be authorized by the Institutional Animal Care and Use Committee.

Good luck with your research!

Sincerely,

Dr. Gregory Dillon
Interim Associate Vice President for Research
Authorized Institutional Official

GD:dks

C: Dr. Stanley Dannemiller, Consulting Veterinarian, NEOMED
Dawn Amoisch, Animal Tech., Biological Sciences